Contribution to the study and minimizing the impact of electromagnetic waves on the human body : Application in the field of mobile telephony

Najat Nasser

Thèse de doctorat

Université de Limoges

Université de Limoges

École Doctorale 610 – Sciences et Ingénierie des Systèmes, Mathématiques, Informatique (SISMI)

Faculté des Sciences et Techniques - XLIM - Axis RF Systems - Team Aerials & Signal

Thèse pour obtenir le grade de

Docteur de l'Université de Limoges

Discipline : Electronique des Hautes Fréquences, Photonique et Systèmes

Présentée et soutenue par

Najat Nasser

Le 14 décembre 2018

Contribution to the study and minimization of the impact of electromagnetic waves on the human body. Application in the field of mobile telephony.

Thèse dirigée par Patrick Vaudon et co-dirigée par Mohammad Rammal

JURY :

Rapporteurs :

Mr. Tchanguiz RAZBAN	**Professeur des Universités** Université de Nantes-Polytech'Nantes, Institut d'Electronique, de Télécommunications-Rennes UMR 6164
Mr. Najib FADLALLAH	**Professeur des Universités** Université Libanaise- Institut Universitaire de Technologie Saida - Equipe RADIOCOM

Examinateurs :

Mr.Francis DENANOT	**Professeur des Universités** Docteur de l'Université de Limoges-XLIM – Axe Systèmes RF-Equipe « CEM & Diffraction»
Mr. Mohamed RAMMAL	**Professeur des Universités** Université Libanaise- Institut Universitaire de Technologie Saida - Equipe RADIOCOM
Mr. Patrick VAUDON	**Professeur des Universités** Emérite Université de Limoges- XLIM – Axe Systèmes RF- Equipe « Antennes & Signaux »

Acknowledgement

First of all I am deeply indebted to the God who gave me the opportunity to complete this thesis. Also, I am truly indebted to several people for their guidance and valuable support throughout this PhD work.

I am grateful to Prof. Dr. Patrick Vaudon, for his constant encouragement and concern for my research. I also wish to thank him for his valuable suggestions and exposure that he offered during the course of my research.

I would like to express my sincere gratitude to my supervising guide, Prof. Dr. Mohammad Rammal, for his guidance, encouragement and the timely care that he rendered to me during my research period. His imminent way of thinking has helped me to explore my research abilities and encouraged in implementing the ideas with absolute satisfaction. I was able to successfully complete this research work and deliver this thesis because of his able guidance and immense patience.

My sincere thanks to Dr. Dina Serhal for all the support, advice and encouragement she has given me throughout this work.

My appreciation also extends to my friends and colleagues who kept pushing me forward with their constant motivation and encouragement and created a better and joyful environment to endorse my studies.

My most sincere goes to my parents and family for their prayer, patience, understanding and encouragement throughout this work. Finally, I express my special thanks to my beloved husband Dr. Abd El Salam, who has filled my life with happiness and always there to share the good times, making my life enjoyable. His endless love, support and understanding are very much appreciated. Special thanks to my kids Lea and Yara for being patient during my research period.

Last but not least, I would like to thank all the staff in Lebanese university-Faculty of technology that leaded by Prof. Dr. Mohammad Hajjar, for all the support, advice and encouragement they have given me throughout this work. Also thanks to all staff in Limoges University-Faculty of science and Technology (XLIM Lab)-France.

Table of Contents

Table of Figures

List of Table

General Introduction

General Introduction

The use of mobile phones has grown exponentially in the last decade, and now it becomes an essential part of life. Currently, the number of mobile phone users is estimated to be about 4.77 billion globally, and expected to reach up to 5 billion in 2019 [1]. This in turn, will lead to an unprecedented increase in traffic on the mobile networks, which requires the deployment of additional radio towers. As a result, people will be exposed to massive amounts of electromagnetic radiation. Many concerns have been focused on the interaction between mobile phone and the human head, as the latter is usually in the reactive near field of mobile phone, and also on the interaction between cell towers and human body, as it occurs in the far field region.

It is estimated that the mobile phone antenna transmits a power between 1 and 2 Watts in all communication frequency bands, in which the radiation is considered low. Besides, there are several factors correlated with the mobile phone use, such as call duration, distinct situations of usage and users' physiology, and the quantity of the electromagnetic wave being absorbed within biological tissue [2]. These factors are the main concentration of the continued realization of biological health effects of mobile phone [3]. On the other hand, cell tower antenna transmits power in the frequency range of 869 - 894 MHz (CDMA band), 935 - 960 MHz (GSM900 band), 1810 – 1880 MHz (GSM1800 band), 2110 - 2170 MHz (3G); 2450 MHz is approximately the center frequency of Wi-Fi, WLAN, Bluetooth, Microwave, and (5G). Mobile phone must be able to transmit and receive sufficient signal for suitable communication up to a few kilo-meters, this depends on a way the base station and its transmitting power are designed. Cell tower antenna conveys radiation permanently, thus people who are living at a distance within 10's of meters far from the tower will receive 10^3 to 10^6 times sturdier signal than desired for mobile communication [2], which in turn leads to severe health effects. Thus, the distance between human body and the cell tower, transmitting power and the gain of transmitting antenna are the main factors in determining the radiated power density of cell tower that has great effect on human health.

An important part of the electromagnetic wave radiation is that coming from mobile antenna as well as cell tower antenna toward human body. These waves can be transmitted, reflected, refracted, scattered, or absorbed by the human body tissue as human body behaves as lossy dielectric material [4]. The absorbed electromagnetic wave radiation resulting from either mobile phone antenna or cell towers antenna can lead to several biological effects that can be classified as: thermal or non-thermal [5]. SAR (Specific Absorption Rate), and the power density, are the

fundamental parameters that quantify the thermal power absorbed by the human body when exposed to mobile phone and cell tower antennas. The current studies show that there are no adverse health effects coming from the radiation of mobile phones and cell towers, when operated in accordance with the standard and guidelines from ICNIRP, IEEE, USA, and FCC [6]. Moreover, SAR parameter might not be suitable for characterizing the absorption of electromagnetic waves in the body when discussing non-thermal effects [7]. On the other hand, there is no other standard to follow for measuring this non-thermal biological effect, and still not well defined, but several studies show that such kind of effect are 3 to 4 times much harmful than the thermal effect [8], and can lead to salivary gland tumors, behavioural problems, and migraines. These risks have been shown to be higher in people who have used cell phones for at least ten years [2], and who are living in the vicinity of cell towers.

Our thesis is divided into two parts. The first part consists of proposing new safety mobile antenna structures that are able to minimize the SAR without affecting antenna performance. Most of antenna structures that were proposed in the literature to reduce the effect of electromagnetic wave radiation on human head are either complex, or affecting the antenna performance in terms of radiation pattern. Our proposed structure is based on reducing the SAR without affecting the antenna performance. This is done by simply reshaping the ground plane of mobile antennas so that surface currents along the ground plane that are responsible of increasing the SAR in the human head are reduced dramatically. The proposed method consists of adding U, L, and V-shape edge-groove structure at each corner of the ground plane. Three cases are considered: single band, dual band, and tri-band mobile phone antenna operation. Two studied scenarios were done: First one, when the U-shape edge-groove is inserted below each corner of ground plane. In this scenario, three situations were examined: first one, when the U-shape edge-groove is made of PEC (perfect electric conductor). Second one, when the U-shape edge-groove is made of liquid material (salty water) that is considered as a combination between dielectric and conductor in the sake of further reducing the SAR, as liquid material has shown promising results in terms of radiation pattern [9]. Third one, when the U-shape edge-groove is filled with liquid material (salty water) in the sake of predicting the best design in terms of SAR and performance of antenna. Second scenario, when the U-shape edge-groove is inserted above each corner of ground plane for preserving height of antenna. Our study involves head modelling, computer simulation. The SAR spatial distributions and values are evaluated and analysed by simulation using CST (Computer Simulation Technology) Microwave Studio.

The second part of this thesis aims to design a base station safety tower antenna that provides constant power density with uniform coverage over certain surface area. Literature studies show only the harmful biological effects caused by cell towers [2], without indicating any idea about designing a safety antenna that aims to prevent these hazardous effects. Our main goal in this part is to design a desired radiation pattern of antenna that achieves constant field strength with uniform coverage, in order to limit the biological effects caused by radiation emissions, and this will depend on the studied site whether it is urban, sub-urban, rural, open area, etc.. In this part, we synthesize the proposed radiation pattern of safety antenna using SARA (Synthesis of Array of Antenna) software [10], [11]. After that, a wide-band printed dipole antenna having omnidirectional array is designed and simulated using CST software. Then, the synthesized proposed pattern is simulated over certain surface area in a dense urban area using Atoll software.

The thesis is organized as follows:

Chapter 1 describes the types of electromagnetic radiation and its interaction with the human body with short explanation of the electric properties of human tissues, and the properties of the EMW during its propagation toward human tissues. Theoretical explanation of SAR, and power density were presented. Then, the biological and health effects of electromagnetic fields were discussed. The standards, exposure limits for the computation of SAR and power density were explained. Finally, several studied techniques on reducing the distribution of SAR on human head were shown.

Chapter 2 illustrates the investigation to SAR reduction. The beginning of this chapter exhibits the determination of SAR of the mobile handset either numerical or measurement. After that, simulation results of several antennas (half-wavelength dipole, an array of half-wavelength dipole, patch, and PIFA antennas) operating at GSM 1800 band in the vicinity of human head were presented for investigating the value of SAR. After that, simulation results of single band PIFA antenna (GSM1800) with certain geometrical structures made of water in its ground plane in the vicinity of human head were compared and shown for predicting best structures in terms of SAR and performance of antenna.

Chapter 3 presents our proposed methods for reducing SAR. At first, theoretical explanation of our proposed idea was discussed. Then, simulation results of our proposed single-band PIFA antenna operating at GSM 1800 band, where a comparison is done between U, L, and V-shape edge-groove that are made of PEC, and are inserted below each corner of ground plane are presented. Then, simulation results of conventional and proposed dual-band and tri-band antennas operating at (GSM

900, and GSM 1800 bands), and (GSM 900, GSM 1800, and GSM 2400 bands) in the vicinity of human head were exhibited, respectively. After that, two methods for liquid antennas were examined: first one, U-edges groove made of water. Second one, U-edges groove filled with water for the single-band and dual band. After that, simulation results of single band and tri-band PIFA antennas with U-shape edge-groove made of PEC above each corner of ground plane were presented.

Chapter 4 illustrates our proposed base station safety antenna design for achieving constant field strength with uniform coverage along certain covered area. In this scenario, COST231-WI (NLOS) path loss model that is comparable to an equivalent cosecant beam was studied. The desired pattern of proposed safety antenna is synthesized using SARA software. After that, we propose a wide-band printed dipole antenna having omnidirectional array that is designed and simulated using CST software. At the end, the proposed pattern is simulated using Atoll software.

Chapter I :
Electromagnetic radiation and its interaction with the human body

I.1. Introduction

The rapid increase in the use of mobile phones and the number of cell towers has raised public concern on the interaction between human body and the mobile phone antenna as well as the cell tower antenna. The electromagnetic wave is being absorbed by human body tissue rather than being radiated over the air [12]. This occurs at both sides of the mobile communication: at the mobile phone antenna level where the human head is considered to be in the reactive near field region of antenna, and at the tower antenna level where the human body is in the far field region of antenna. The amount of electromagnetic wave being absorbed by human body tissue is mainly caused by both the internal electric and the magnetic fields that are induced into human body causing either thermal effect or non-thermal effect [13].

In order to examine and protect humans from the possible adverse biological effects due to the exposition of Radio frequency (RF) either from mobile phone antenna or cell tower antenna, a number of national and international organizations have contrived guidelines on exposure levels. In near field region, the exposure limits are defined as Specific Absorption rate (SAR) that can be defined as a metric system for quantifying the amount of energy being absorbed by the biological tissues during exposition to mobile phone utilizing radio frequency. Moreover, this amount of energy that is transmitted and absorbed in the human head tissue depends on the frequency of the energy source, the distance from the antenna, the field polarization, the orientation of handset, the amount of power delivered, the time of exposure, the shape and size of the human head and the dielectric properties of the exposed tissues [14]. On the other hand, in far field region, the exposure limits are defined as the radiated power density which is the quantity of flow of electromagnetic energy per unit area utilized to measure the amount of electromagnetic radiation at a given point from a conveying antenna [15].This amount of power density depends on the power and gain from transmitters, and also on the distance from transmission cell tower to a human body at ground level.

The aim of this chapter is to present a short review on the types of electromagnetic radiations, and the interaction between electromagnetic fields and the human body. Brief information about SAR as well as power density metrics and their regulation standards and limits are presented. In addition to that, literature review on SAR reduction and safety power density are also presented.

I.2. Types of Electromagnetic Radiation

The electromagnetic radiation can be classified as either ionizing or non-ionizing depending on the amount of energy carried by radiation. Electromagnetic wave radiation is considered as non-ionizing when the frequency is below 10^{15} Hz, and as ionizing when the frequency is above 10^{15} Hz as presented in (Figure 1) [16].

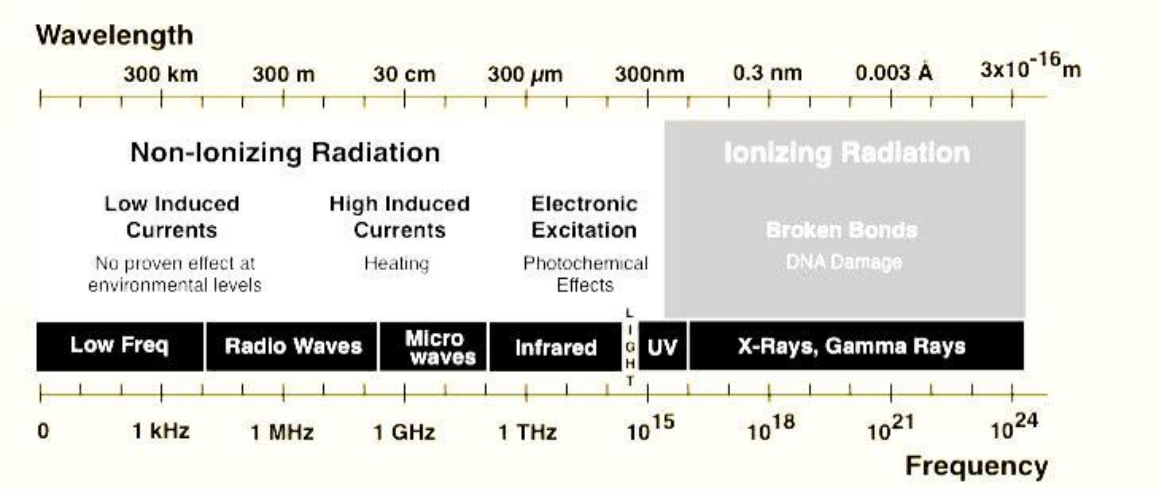

Figure 1 Types of Electromagnetic Radiation

I.2.1. Ionized Radiation

Radiation that has sufficient energy to knock off tightly bound electrons from the orbit of an atom, thus generating ionized atom is referred to as "Ionized Radiation". Ultra violet, X-ray, Nuclear and Gamma rays fall under this type of radiation that will affect biological health [17], [18].

I.2.2. Non-Ionized Radiation

Non-Ionized radiation doesn't carry enough energy to ionize atoms or molecules; instead it can possess enough energy to excite electrons, thus, pushing them into a higher energy state causing some heating effect. Low frequency waves, Radio waves, microwaves, infrared light, and visible light are considered as non-ionizing radiations that will cause heating tissue effect or as known "Thermal effect" [19], [20]. Many studies show that this type of radiation is not directly interfering with DNA but it can increase the biological tissue temperature at high exposition to RF-electromagnetic waves [21].

I.3. Impact of electromagnetic radiation on the human body

I.3.1. Interaction between electromagnetic radiation and the human body

The user of a mobile phone can be deemed as a portion of the radiating system, as the nearby human tissue has a great impact on the electromagnetic fields produced by the device. Thus, the effect of the user must be taken into consideration for designing mobile antennas with appropriate performance and convenient SAR value.

When the electromagnetic waves propagate in the human tissue, they induce internal electric and magnetic fields in the biological systems as shown in (Figure 2) [17], which interact with cells and tissues in several ways, based on the frequency, intensity of the induced fields and the energy absorbed in the biological systems. The frictional forces between the particles that begin to transfer cause losses due to the effect of electric field, which results in an absorption of energy, leading to heating effect in the human tissue. On the other hand, the effect of magnetic field in the interaction between electromagnetic wave and human tissue is not notable as the human tissue is considered as non-magnetic. It is well known how these fields inside a dielectric material interact with the material, but it is complex to some extent as the interaction procedure is affected by the regulation techniques such as respiration, circulation, and perspiration [22]. Moreover, the interaction between the original external fields and the produced internal fields is still an object of studies.

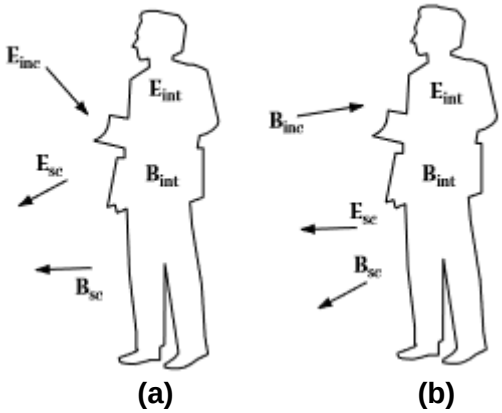

Figure 2 The internal and scattered electric and magnetic fields due to an incident electric field (a), and due to an incident magnetic field (b).

Since the performance of antenna when placed in the vicinity of human body is sturdily influenced by the power absorbed by the user, SAR demands, i.e., the subject of energy absorbing techniques in human body tissue is essential not solely because of the SAR limits but also from the antenna performance point of view. Thus, for an antenna designer, it would be extremely beneficial

to identify and understand these techniques and therefore to have the ability to expect the tendency of bandwidth, efficiency and SAR.

I.3.2. Properties of electromagnetic wave in the human tissue

As the wave propagates through the lossy tissue, an amount of radiating power will be absorbed by the human tissue causing loss to the propagating wave due to the current density generated where $J = \sigma E$. Thus, part of the power in the electromagnetic field is converted into heat.

The dielectric properties of a material characterized by its complex permittivity can be defined as follow [17]:

$$\varepsilon = \varepsilon_0 \varepsilon_r = \varepsilon_0 (\varepsilon'_r - \mathrm{j}\varepsilon''_r) \qquad \text{equation I-1}$$

$$\varepsilon_r = \varepsilon'_r - \mathrm{j}\left(\frac{\sigma_{eff}}{\omega \varepsilon_0}\right) = \varepsilon'_r \left(1 - j\frac{\varepsilon''_r}{\varepsilon'_r}\right) = \varepsilon'_r (1 - j tan\delta) \qquad \text{equation I-2}$$

where ε_0 is the free space permittivity, $\varepsilon'_r$the real part of complex permittivity, ε''_r the imaginary part of complex permittivity and $\omega = 2\pi f$ the angular frequency, and tan δ is the loss tangent.

The imaginary part of the real permittivity ($Im\,(\varepsilon_r) = \frac{\sigma_{eff}}{\omega \varepsilon_0}$) represents all losses in the material, where σ_{eff}described all the conductivity and dielectric losses.

An important parameter in bio-electromagnetic field is the attenuation constant (α) that depends on the conductivity; the permittivity of a studied tissue, as well as the operating frequency and it is given by the following equation:

$$\alpha = \omega \sqrt{\frac{\mu' \varepsilon'}{2} \left(\sqrt{1 + \left(\frac{\sigma_{eff}}{\omega \varepsilon'}\right)^2} - 1 \right)} \qquad \text{equation I-3}$$

It can be noticed from (equation I-3) that either by increasing the frequency or the effective conductive current, the attenuation increases. Moreover, the attenuation parameter can be used for determining the skin depth which is given by 1/α, it is very small for high frequencies and high conductivity.

On the other hand, loss tangent (tan δ) plays an essential role in indicating how much loss in the human tissue will be considered. When the loss tangent parameter is small, this indicates that the tissue has a very low loss. On the other hand, when the loss tangent is large, this means that the tissue is very lossy.

During propagation of the wave toward human body, the peak magnitude of this wave diminishes exponentially as a function of distance travelled as presented in (Figure 3) [17], where the field inside the human body can be found from $E_0\, e^{-\alpha z}$, where E_0 is the incident field just inside

the surface of the body, and z is the propagation distance that represents how far the field has penetrated into the body.

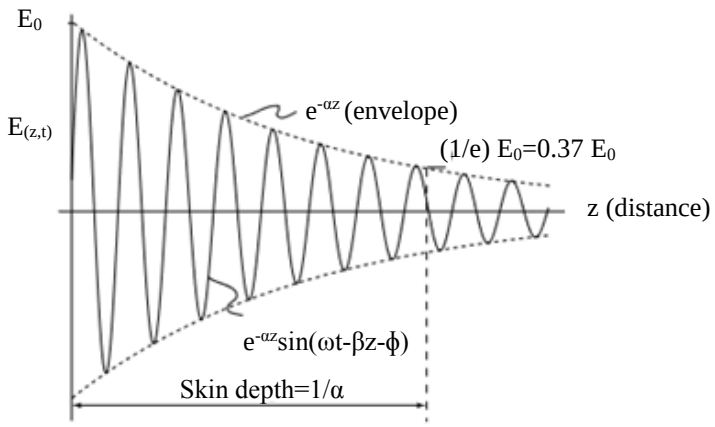

Figure 3 Propagating wave having the form: $E(z,t)=Eoe^{-\alpha z\sin(\omega t-\beta z-\phi)}$ taken at one instant of time.

The propagation constant (β) is given by:

$$\beta = \omega\sqrt{\frac{\mu'\varepsilon'}{2}\left(\sqrt{1+\left(\frac{\sigma_{eff}}{\omega\varepsilon'}\right)^2}+1\right)} \qquad \text{equation I-4}$$

It reflects how much the wave will be phase shifted during its propagation. It also depends on the conductivity, the permittivity of a studied tissue, as well as the operating frequency.

I.3.3. Electrical properties of the human body

The electrical properties of human tissues (relative permittivity ε'_r and conductivity σ_{eff}) control the propagation, reflection, attenuation, and other behaviour of electromagnetic fields in the body. Human tissues can be treated as a mixture of insulators and conductors since they are made up of water and various salts and organic synthesis. Muscle and organs can be considered as good conductor tissues having high salinity, high water content, high $\varepsilon'_r$and σ_{eff}, and smaller skin depth, in contrast to the fat and bones that are estimated as poor conductor having lower water content, low $\varepsilon'_r$and σ_{eff} and larger skin depth. At low frequency, the conductivity of the human tissue dominates the behaviour of the field in contrast to high frequency situation where the relative permittivity tends to dominate [17]. Values of the dielectric properties of human head at each studied frequency will be presented in the following chapters.

I.3.4. Media boundaries for lossy tissue material

An interface between two different media shall be contented by both normal and tangential component of the electric field. These conditions are derived from Maxwell's equations where the following equations must be satisfied at the boundary:

$$E_{t1} = E_{t2} \qquad \text{equation I-5}$$

$$\varepsilon_{complex1} E_{n1} = \varepsilon_{complex2} E_{n2} \qquad \text{equation I-6}$$

The above equations show that the tangential component of the electric field across the boundaries of two media must be equal, whereas the normal component depends on the properties of the tissue. As the permittivity of the dielectric material increases, the directions of the electric fields inside this material are required to become more parallel to the surface of this material, and the electric field perpendicular to the surface of dielectric material becomes more attenuated at the boundary. Thus, when the permittivity of the dielectric material is high, the strength of the electric field penetrates hardly through it, and this was verified by simulation results studied in [23].

If we substitute $\varepsilon_{complex} = (\varepsilon' - j\varepsilon'') = \varepsilon_0(\varepsilon'_r - j\varepsilon''_r)$ in (equation I-6) we get the following:

$$(\sigma_{eff1} + j\omega\varepsilon'_1)E_{n1} = (\sigma_{eff2} + j\omega\varepsilon'_2)E_{n2} \qquad \text{equation I-7}$$

$$J_{c,eff\,n1} + J_{displacement\,n1} = J_{c,eff\,n2} + J_{displacement\,n2} \qquad \text{equation I-8}$$

(Equation I-8) predicts that the normal effective conduction current density across the boundaries between two different media must be equal as well as the normal displacement current [17].

I.4. Specific Absorption Rate (SAR)

Traditionally, mobile phone antenna is placed in the vicinity of human head, mainly in the near field zone of the antenna. This zone is divided into two regions: the reactive near field region and the radiating near field region.

To protect humans from the possible adverse biological effects due to the exposition of Radio frequency (RF), specific Absorption rate (SAR) was hipped since the1970s by A.W. Guy, and raised in public mainly through the work of Gandhi and Durney from the University of Utah [24].

I.4.1. Definition

SAR measured in Watt per kilogram, can be defined as a metric parameter for quantifying the actual amount of electromagnetic energy that is absorbed or dissipated per mass of human tissue

when discussing thermal effects [25]. It is usually averaged either over the whole body, or over a specific organ, or over small volume of mass tissue containing 1g or 10g, the higher is the value of SAR, the more radiation absorbed per mass of the human tissue will occur.

Mathematically, SAR can be defined by IEEE standard C95.3 [26] as the time derivative of the incremental energy (∂W measured in joule) absorbed in an incremental mass (∂m measured in kg). It is given by the following equation:

$$SAR = \frac{\partial}{\partial t}\frac{\partial W}{\partial m} \qquad \text{equation I-9}$$

Since mass is related to the mass density (ρ measured in Kg/m^3) and the volume (V measured in m^3), where ρ is assuming constant, then (equation I-9) is equivalent to:

$$SAR = \frac{d}{dt}\frac{dW}{\rho dV} = \frac{dP}{\rho dV} \qquad \text{equation I-10}$$

Where the time derivative of the incremental energy is equal to power density (P). On the other hand, the power per unit area is equal to the power density (S).The magnitude of the power density [27] is given by:

$$|S| = \frac{|E|^2}{Z} \qquad \text{equation I-11}$$

From (equation I-10), and (equation I-11), it can then be written that:

$$SAR = \frac{dP}{\rho dV} = \frac{dP}{\rho dA dl} = \frac{1}{\rho dl}\frac{dP}{dA} = \frac{1}{\rho dl}\frac{|E|^2}{Z} \qquad \text{equation I-12}$$

Moreover, the conductivity can be defined as the inverse of resistivity per unit length [28], So SAR can be written as:

$$SAR = \frac{1}{\rho dl}\frac{|E|^2}{Z} = \sigma\frac{|E|^2}{\rho} \qquad \text{equation I-13}$$

Since the current density (J) measured in A/m^2 is given by:

$$J = \sigma E \qquad \text{equation I-14}$$

Then, the local SAR can be derived from (equation I-13) and (equation I-14) as follows:

$$SAR = \sigma\frac{|E|^2}{\rho} = \frac{J^2}{\sigma\rho} \qquad \text{equation I-15}$$

SAR metric is classified into three terms due to the variation in the amount of energy absorbed into different parts of the human body [29], namely: whole-body averaged SAR, organ-specific averaged SAR and peak-spatial averaged SAR [30].

Whole-body averaged SAR

It can be defined as a ratio of the total amount of power absorbed by the human body tissue to the mass of the whole body, averaged over a period around 6 minutes as per regulatory acquiescence. It can be expressed as follows:

$$\mathrm{SAR(Whole\ body)} = \frac{1}{M}\int_{R} \mathrm{SAR}\,dm = \frac{1}{M}\int_{R} \sigma\frac{|E|^2}{\rho}(\rho dV) = \frac{1}{M}\int_{R} \sigma|E|^2 dV \qquad \text{equation I-16}$$

where M, R, E, σ, ρ, V denote respectively the total mass of the body, the region of the body, the rms electric field, conductivity of the tissue, density of the body, and the total volume of the body tissue.

Organ-specific averaged SAR

It can be defined as an average mass of SAR in a particular organ in the body. This term describes how the electromagnetic waves can be absorbed by specific organ of the body. It can be expressed as follows:

$$\mathrm{SAR(specific\ organ)} = \frac{1}{M_{organ}}\int_{Organ} \mathrm{SAR}\,dm = \frac{1}{M_{organ}}\int_{Organ} \sigma\frac{|E|^2}{\rho}(\rho dV) = \frac{1}{M_{organ}}\int_{Organ} \sigma|E|^2 dV \qquad \text{equation I-17}$$

where M denotes the mass of the considered organ.

Peak-spatial averaged SAR

It can be defined as a maximum local SAR averaged over a 10g or 1g of mass tissue within average time around 6 minutes.

The power absorbed by the human tissue during mobile phone operation is converted into heat; this procures another definition of SAR that is related to a rise in temperature as given by the following equation [31]:

$$\mathrm{SAR} = c\frac{dT}{dt} \qquad \text{equation I-18}$$

where c, dT/dt denotes the specific heat of tissue, temperate change over duration of exposure to electromagnetic waves.

I.4.2. Variation of SAR with respect to frequency, polarization and size of the human body

The electromagnetic energy absorbed by the human tissue during electromagnetic wave exposure is mainly a function of frequency, shape, size, and the electrical properties of the studied tissue. In this paragraph, we will present how SAR varies with respect to frequency, and how the polarization and the size of the body can affect SAR.

The frequency band from 30MHz to 3000 MHz is said to be a resonance zone, since the half-wavelength is relative to the dimension of the human body at those frequencies [31]. On the other hand, various parts of the human body have their reign resonance frequencies, as in case of human head in which it resonates at 400MHz [32]. A little perception can be made from the below (Figure 4) [17] that depicts the whole-body SAR radiated by an incident plane wave with a power density of 10W/m^2 as a function of frequency for a block model of an average human being where the electric field is parallel to the linear axis of the human body, in which the coupling between electric and magnetic field is maximum [33].

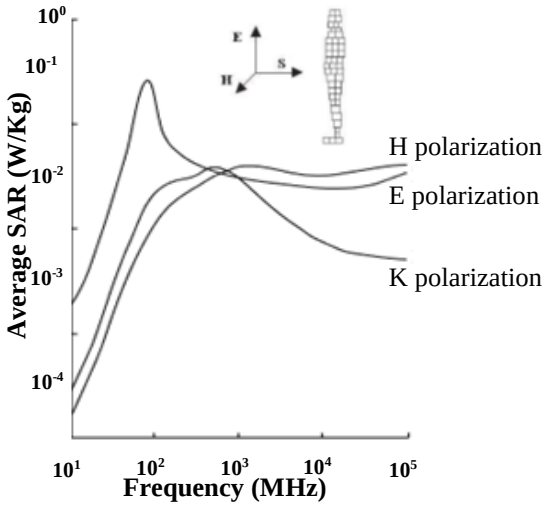

Figure 4 Average radiated by an incident plane wave with a power density of 10W/m^{2}as a function of frequency for a block model of an average human being for three polarizations E, H, and K.

In case of E, H, and K polarizations, we notice that at low frequencies (from 10 MHz and forth), the SAR is approximately proportional to the square of the frequency before reaching the resonant frequency of the whole body that occurs when the length of the human body is about four-tenth of a wavelength. The resonant frequency for the whole human body is considered about 75 MHz in case of ungrounded human body model and about 37.5 MHz in case of grounded human body model where maximum SAR achieves to be roughly half of that of an ungrounded body model [31]. We notice also from (Figure 4), that when the frequency is below the resonant, polarization

has a great impact on SAR, where the SAR varies significantly with it. This impact can be described by two general cases [17]: First case, when the incident electric field E_{inc} is parallel to the linear axis of the body surface, the internal electric field is stronger than when E_{inc} is normal to the axis of the body surface. Second case, when the cross sectional area is larger while being opposed by the incident magnetic field (H_{inc}), then the internal electric field is stronger than that when cross sectional area is smaller while being opposed by the incident magnetic field. In case at low frequency, the electric and magnetic fields are uncoupled, where the internal electric field is the sum of the internal electric field created by both the E_{inc} and the H_{inc}. SAR is highest in case of E-polarization, since the internal fields produced by E_{inc} and H_{inc} are strong, as E_{inc} is parallel to the linear axis of the body surface, and the cross sectional area opposed by H_{inc} is large. On the other hand, SAR is lowest in case of H-polarization since E_{inc} is normal to the linear axis of the body surface, and the cross sectional area opposed by H_{inc} is smaller, this leads to a weaker internal fields produced by both the E_{inc} and the H_{inc}. In case of K-polarization, we notice that SAR is less than that in case of E-polarization, but it is greater than that in case of H-polarization, this is due to the fact that the E_{inc} is normal to the linear axis of the body surface, while the cross sectional area opposed by H_{inc} is large. Thus in case of K-polarization, the internal field produced by E_{inc} is weak, and the internal field produced by H_{inc} is strong [31]. At higher frequencies, the impact of polarization on SAR is somewhat complex due the coupling and strong interaction between electric and magnetic fields. At frequencies above resonance, SAR starts to diminish and it is approximately inversely proportional to the frequency [17].

On the other hand, SAR frequency dependence varies with human body size. For example, the resonant frequency of a child is higher than in case of man, probably because of the smaller dimensions of the child's body [34]. As mentioned before, the resonant frequency occurs when the length of the human body is about four-tenth of a wavelength long. The resonance in child is less evident than in case of man, perhaps because the man is thinner than the child. In case of child's body, at frequencies below resonance SAR is approximately proportional to the square of the frequency, and at frequencies above resonance SAR is approximately inversely proportional to the frequency. Moreover, SAR varies from point to point inside a specific body, and its internal spatial distribution will be quite different as a function of frequency inside two bodies of different sizes, this is due to the difference in the ratio of the human body size to the wavelength. For that, to achieve same internal spatial distribution of SAR for two human bodies of different sizes, they should radiate at a frequency in which the ratio of the human body size to the wavelength is approximately the same. Besides, SAR in a human body can further be influenced by the existence of other objects, such as the resonant frequency is roughly break in half when a human body is

placed on a perfectly conducting plane as compared to resonant frequency in free space, this is probably because the conducting plane has the effect of mirroring the object. Furthermore, the resonant frequency in case of a human body being placed on non-perfecting conducting plane would be lower than that the resonant frequency of the human body in free space, but not half as in case of a perfectly ground plane. Moreover, when any human body wear shoes, the latter would isolate the human body from the ground, which in turn will affect the resonant frequency [17].

I.5. Radiated Power Density

Since the cell tower antenna operates in the proximity of the human body, the electromagnetic waves radiation exposure from such antenna almost occur in the far field region. The electromagnetic exposure in the far-field is generally estimated in terms of power density.

I.5.1. Definition

Power density measured in (W/m^2) can be defined as the amount of energy per unit area normal to the direction of propagation. The rate of this energy depends on the electromagnetic field components. The general expression for the power density having coordinates (r, θ, ϕ) in case of single cell tower for any object being placed at a point on the ground at a distance from the cell tower antenna is given by the equation:

$$P(r,\theta,\varphi) = \frac{P_T \times G(\theta,\varphi)}{4\pi r^2} \qquad \text{equation I-19}$$

Where P_T, G, r, denotes the transmitting power (measured in watt), the gain function of antenna, and the distance from the antenna in meter.

I.6. Biological and health effects of electromagnetic fields

Radio frequency radiation is considered as non-ionized radiation and thus may not directly interfere with DNA, but unfortunately it can increase the biological tissue temperature at high exposition to RF-electromagnetic waves [21]. Besides, the biophysical techniques beyond the tissue heating caused by intense electromagnetic fields are recognized well and the current standard exposure limits are based on them. The potential occurrence of certain adverse non-thermal effects has been under enormous biological studies, but no eventual confirmation has been established [35]. Furthermore, the non-thermal effects produced by frail fields have stayed disputable, but the dangerous thermal effects such as cataracts are not able to be disputed. The human body is made up of 70% of liquid, and the effects are more considerable in body parts that contain more fluid such as brain which constitutes 90% of water [2], eye, heart, in which the movement of fluid is less. If the

rise of temperature along the surface of the brain is not greater than 0.3 degrees, it is recognized that this does not have any physiological indications. As a comparison, an increase around two degrees in temperature during a strenuous physical exercise is excessively mutual, since the plain physiological range is around ±1°C [36]. The amount of data given by enormous research results is considered to be too huge for particular person to search, nevertheless, there are several organizations such as the World Health Organization (WHO) [37], the International Committee for Non-Ionizing Radiation Protection (ICNIRP) [38] and the Finnish Radiation and Nuclear Safety Authority (Säteilyturvakeskus, STUK) [35] that check and outline the conducted studies.

There are numerous biological health effects correlated with mobile phone antenna and cell tower antenna. Some of these are presented in [2], [36].

I.7. Regulation standards for safety RF-electromagnetic wave exposure

During recent years, several national and international safety norms have been created to prevent the RF radiation hazards**.** The most essential ones are the norms that limit the RF-electromagnetic wave coming from mobile handset toward human body. Some of these norms can be established as standards and recommendations covering the electromagnetic fields up to 300GHz in case of exposure limits for local SAR. Nevertheless, parts of these norms are considered as technical documents that can be used as consultative, in which those adjust by the major specialized organizations carry magnificent authority up to this time.

The most essential standards are those limiting the RF-electromagnetic wave coming from mobile handset toward the human body. The specialized international and standardization organizations are presented in [36].

I.7.1. Exposure limits for SAR

The RF-electromagnetic wave exposure from mobile handset of the general public in an uncontrolled environment is regulated by safety limits that differ from those regulated for limiting the exposure of the occupational controlled environment [36].

For 10 MHz-10 GHz frequency range in the controlled environment, the SAR averaged over the whole body shall be 0.4W/Kg over any 6-minute time average (IEEE 1982, IEEE 1992, CENELEC 1995, ICNIRP 1998), and shall be about 0.4W/Kg over 15-minute time average (NRPB), whereas this SAR ought to be less than 0.08W/Kg (according to ICNIRP) and 0.1W/Kg (according to NRBP) in the condition of uncontrolled environment. However, for a short duration of

time, the SAR value can be higher than that indicated above being provided that the 6-minutes time doesn't override the given limits [31].

For preventing the loading of the thermoregulatory system of the human body, the average SAR value shall be 0.4W/Kg. On the other hand, certain tests made on human body that presents the maximum average SAR shall be 1-1.4 W/Kg during relaxation and more than 10 W/Kg during exhausting physical exercise [36]. The exposure limits for local SAR ought to have a higher value than the whole body SAR, since the normal thermoregulatory missions of the body is equal to the temperature rise at local hotspots [31]. Limiting the local SAR value is considered as an essential task in designing mobile handset in which the user during mobile operation is in the near field radiation of antenna where the distribution of SAR is almost specious [35].

The RF-electromagnetic energy exposure limits for the maximum value of local SAR in the head and torso are presented in [36]. It has been noticed that according to international and European recommendations (CENELEC 1995, ICNIRP1996, ICNIRP 1998), the maximum local SAR will not exceed 2 W/Kg being averaged over 10g of mass tissue in the general public, whereas in united states and Finland, the maximum local SAR will not exceed 1.6 W/Kg being averaged over 1g of mass tissue in the general public [31], that is in fact for 6 minutes per day operation. The safety margin for this SAR must not exceed 18 to 24 minutes per day. Nevertheless, this knowledge is not generally recognized to the people, as many people use mobile phones for more than an hour per day without apprehending its related health dangers [2]. The major difference between ICNIRP guidelines [39] and the IEEE standard [40] in SAR limitation is that the first one treats pinnae to be as parts of the head while the second one treats it as extremities. This is precious observing since most of the power absorbed in pinnae where the spatial peak SAR often occurs in it [31]. The US limits appear stricter than its European counterpart, due to its low SAR and high average volume [36], but nowadays IEEE ameliorate its recommendations, to be coordinated with the guidelines of ICNIRP. On the other hand, the exposure limits for local SAR in controlled environment mutates between 8-10 W/Kg [31].

I.7.2. Exposure limits for Power Density

Certain countries such as India choose radiation norms specified by ICNIRP guidelines (1998) for performing safe power density of f (MHz)/200. Thus, the power density is about 4.7W/m^2 for GSM 900 transmitting band, and about 9.2W/ m^2 for GSM 1800. This exposure limit in such country is only used to a single carrier, therefore the exposure radiation level overrides by numerous times than even recommended by ICNIRP guidelines, based upon the overall number of transmitters in that zone, since the ICNIRP guidelines obviously declare that for concurrent

exposure to various frequency fields, the sum of all the energy must be taken into concern. But, ICNIRP guidelines have deemed only the thermal effects of electromagnetic radiation, while scientists all over the world investigate that the electromagnetic radiation can lead to non-thermal effects that take place at level much below these norms, and can cause considerable health effects. On the other hand, the recent USA standard for power density for the electromagnetic radiation coming from cell towers is between 5.8-10 W/m^2, nevertheless they are now thinking for reviewing the norms. Besides, many countries all over the world have taken on much rigorous maximum values of power density between 0.001-0.24 W/m^2 (1/100th to 1/1000th of ICNIRP guidelines), in which the people have studied widely the adverse health effects of cell tower radiation to adopt rigorous radiation norms [2].

According to the National Radiological Protection Board (NRPB) of the UK, the power density limits are 26 W/m^2 - 33 W/m^2 and 100 W/m^2 for the 800 MHz - 900 MHz and 1550 MHz - 3000 MHz frequency ranges, respectively [36]. On the other hand, the limits for power density being averaged over any 20 cm^2 exposed area and $t = 68/f^{1.05}$ minutes (where f denotes the frequency), were adjusted at 50 W/m^2 and 10 W/m^2 for various frequency ranges for occupational and public exposures, respectively as recommended by ICNIRP [29].

The reference level for power density as recommended by several standards is presented in [36] in case of general public and control environment.

I.8. Literature Review

I.8.1. SAR Reduction

There are several studies done on reducing SAR values in the head of the mobile handset user, some of these studies are presented as following:

Andi Hakim Kusuma et.al [41] proposed a novel low SAR dual-band PIFA's structure (Spiral PIFA and U-slot PIFA) operated at 0.9 GHz and 1.8 GHz bands for wireless mobile handset application. He suggested that the reducing exposure of electromagnetic wave radiation coming from mobile –set antenna towards the human head; can be investigated through reducing the back radiation coming from the mobile-set antenna and the ground plane. The SAR reduction is achieved by introducing a thin metallic layer between the ground plane and the antenna. This layer is attached to the ground plane through few posts situated at designated optimum position, thus reducing the flow of the current along the ground plane as shown in (Figure 5a). In addition to that, it has been shown that adding three vertical sidewalls as shown in (Figure 5b) supply further reduction to the electromagnetic wave toward human head, which in turn reduce the SAR values.

The result of the proposed spiral PIFA structure shows that SAR can be reduced by 48.1% at 0.9 GHz and 74% at 1.8 GHz, and also can be reduced by 45.88% at 0.9 GHz and 29% at 1.8 GHz of the proposed U-slot PIFA for maximum 10-g averaged SAR.

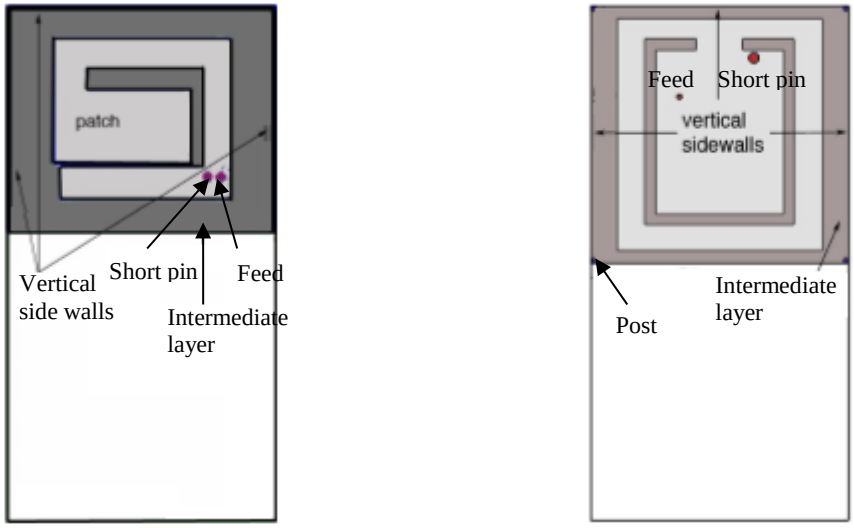

(a) (b)

Figure 5 Top view of propose PIFA's antenna: Spiral (a), and U-slot (b).

T. Anita Jones Mary [42] investigated a dual band slotted PIFA antenna operated at 900 and 1800 MHz band as presented in (Figure 6a). RF shield is located between the human head and antenna as shown in (Figure 6b) for reducing the peak SAR in the human head. Results have been shown that with the introduction of RF shield of thickness 1mm, the peak SAR at the centre frequencies (frequency range of 0.7GHz and 2.16GHz) averaged over 10g mass tissue is reduced up to 7.79% and 11.977% in case of 10 g mass tissue.

(a) (b)

Figure 6 Slotted PIF antenna: without RF shield (a), and with RF shield in the presence of human head (b).

M. R. I. Faruque [43] proposed a new design of square metamaterials (SMMs) as shown in (Figure 7a) for reducing the electromagnetic wave exposure toward the human head. The metamaterial is placed between PIFA antenna operated at 0.9 and 1.8GHz band and the human head as presented in (Figure 7b). Based on FDTD method with lossy-Drude model, various parameters were optimized such as the position, distance, and the size of metamaterial. The results present that

the peak SAR averaged over 10g mass tissue can be reduced up to 53.06% while using such design of metamaterial.

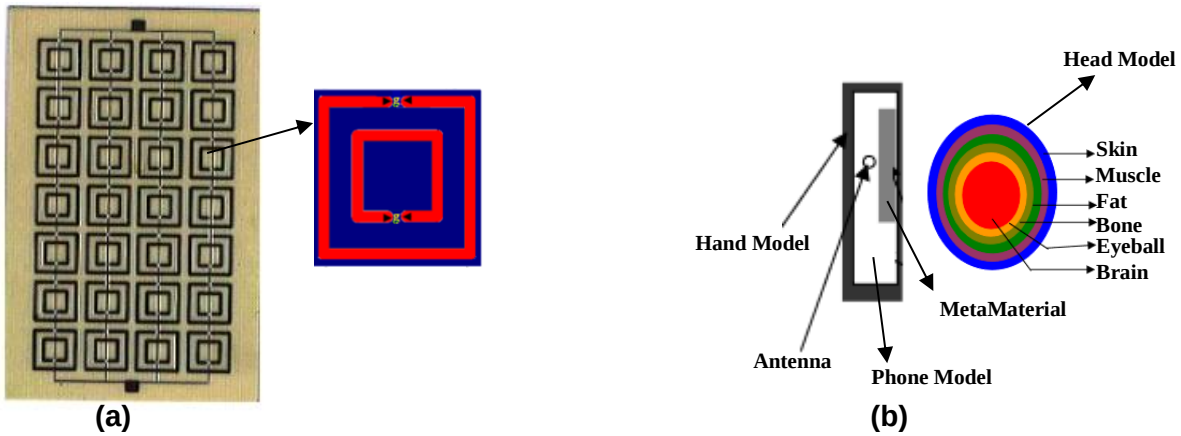

Figure 7 Structure of SRRs array designed on printed circuit board (a), metamaterial placed between PIFA and human head (b).

H.-H. Chou [44] investigated numerically and experimentally the effect of using R-cards on reducing the peak SAR for mobile handset with monopole type antenna established in a helical sense operated at 1800GHz. R-cards are considered as resistive sheets that have the ability for either preventing or attenuating the electromagnetic waves through impedance transformation. The main purpose of this work was to reduce the peak SAR without affecting the radiation pattern of an antenna. The peak SAR values were optimized through optimum values of impedance of the R-cards, where several position for R-cards are optimized in which three cases are taken into consideration: Case A, the R-card wrapped the keypad area as shown in (Figure 8a), Case B, the R-card was linked on top of the LCD display and was prolonged beyond the antenna feed as shown in (Figure 8b), and Case C, where the R-card was connected around the monopole antenna as shown in (Figure 8c). Simulation and experimental results perform the good agreement. Numerical results reveal that R-cards in case A and B weren't affected the radiation pattern of antenna, however case C leads to degradation in the gain of antenna with higher impedance levels. On the other hand, Case B can be considered as a best choice for achieving maximum SAR reduction factor, and due to its simple implementation. Results have been predicted an achievement of a peak SAR reduction of over 60%.

Figure 8 R-card wrapped the keypad area (a), R-card was linked on top of the LCD display (b), R-card was connected around the monopole antenna (c).

M.R.I.Faruque [45] proposed a new design of Dual band PIFA antenna with E-shaped patch to be operated at 0.9GHz and 1.8GHz for reducing the specific absorption rate in the human head. The proposed antenna as presented in (Figure 9) was performed by modifying the conventional ground plane of PIFA antenna using a planar one dimensional metamaterial array (DNG metamaterial) to create a new metamaterial embedded PIFA antenna. SAR values are evaluated in two different hold positions: tilt and cheek. It has been noticed that there exist a good agreement between simulation and measurement in evaluating the SAR. Results reveal that the proposed antenna can reduce significantly the SAR in comparison with the conventional PIFA antenna. On the other hand, during cheek position it has been noticed that at 0.9GHz, the SAR values averaged over 1g mass tissue in case of both conventional and proposed PIFA antennas are very close to each other, while it has been observed a significant reduction in SAR in case of proposed antenna in comparison with the conventional PIFA antenna at 1.8GHz. On the other hand, the SAR values during tilt position was lower than that cheek position, this in fact due to the distance between an antenna and human head. At 0.9GHz, during tilt position both conventional and proposed antennas are similar, while a considerable reduction at 1.8GHz in case of proposed antenna occurs. So, with the proposed antenna during cheek position, the SAR values can be reduced up to 42.33% and66.85% 1gSARand 10g SAR respectively at1.8 GHz, and up to 58.38% and 51.36% during tilt position. Thus, such proposed antenna demonstrates the SAR reduction crucially at 1.8 GHz, due to the metamaterial embedded ground plane.

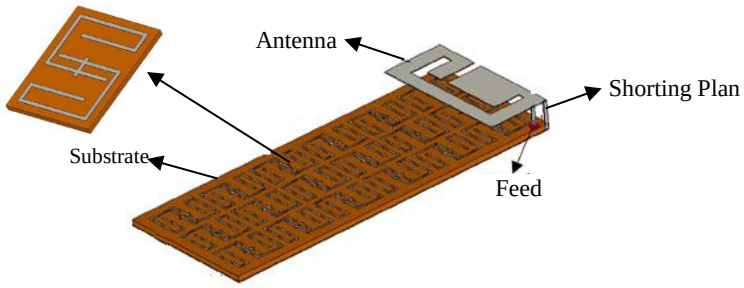

Figure 9 Geometry of the metamaterial embedded PIFA.

Jianqing Wang [46] proposed a ferrite sheet attached to the 1/4- wavelength monopole antenna mounted on a rectangular conducting box operated at 900MHz as shown in (Figure 10) for reducing the spatial peak SAR in a human head . Based on FDTD method in incorporation to human head model, the reduction of SAR depends on the location of ferrite sheet, the size of the sheet, and the material properties. The numerical results have been detected that the ferrite sheet ought to be attached to the location where the maximum surface current exists, and the magnetic loss tangent of the ferrite sheet ought to be considered as large as probable. So, all the previous parameters are chosen to optimize the designing of ferrite sheet with the largest SAR reducing effect for mobile handset.

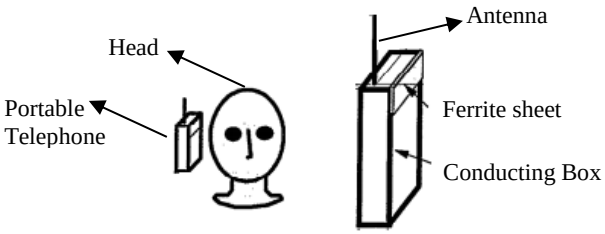

Figure 10 Portable telephone with attached ferrite sheet in the proximity of human head.

Nizar Sghaier [47], proposed a new approach of complementary split ring resonators (CSRRs) PIFA antenna operated at 2.425 GHz for Wireless Local Area Network application to reduce the peak SAR in the homogenous human head model as well as the size of the PIFA antenna. The technique is to combine a single CSRRs cell and a periodic array of CSRRs on the radiating patch. The results have been revealed that introducing CSRR into the radiating patch as shown in (Figure 11) will improve the radiation efficiencies, gains, and power loss density, in addition to a reduction of specific absorption rate up to 17.36% for four CSRRs structure.

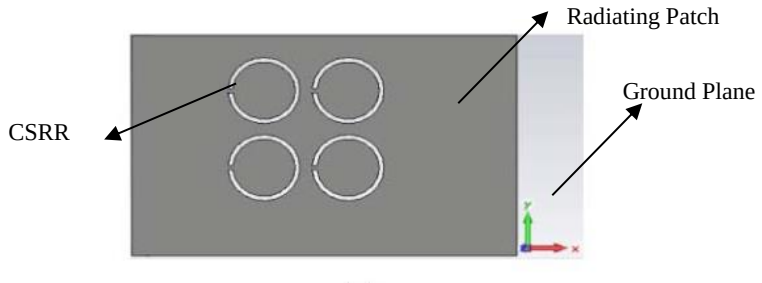

Figure 11 PIFA antenna with an inclusion of four CSRRs.

Mohammad Naser-Moghadasi [48], proposed a novel low SAR printed PIFA antenna as shown in (Figure 12) for ultra-wideband applications. The proposed antenna was designed to operate across the frequency range of 1200-3000 MHz for VSWR less than 2. So, it can cover several wireless standards such as GPS/DCS/GSM1800/PCS/WLAN/Bluetooth/WiMAX/LTE. It has been noticed that the current is distributed in both sides of antenna in the case of proposed antenna, while in case of conventional PIFA antenna the current is focused on one side of the radiator, therefore more current density as well as SAR is focused at limited area, where as in case of proposed antenna the current density is distributed in larger surface, and the SAR dispense in large surface thus producing low SAR , and that result was achieved by dispensing current in the top and bottom layer by introducing two vias. Results also reveal that the proposed antenna have the ability to reduce SAR in human head averaged over 1g mass tissue at 1.8 GHz up to 51% in comparison to conventional PIFA antenna. In addition to that, it has been presented that such design of proposed antenna has more efficiency and gain and low SAR in contrast to other structures of PIFA antenna.

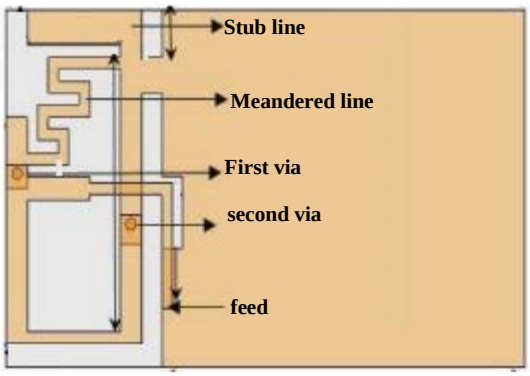

Figure 12 Geometrical structure of the proposed antenna.

Kamel S. Sultan [49] proposed a new structure of mobile antenna that is composed of a planar monopole with inverted L-shape and meander line sections with the addition of a uniplanar EBG structure as shown in (Figure 13) that is positioned between human head and an antenna to supress the surface wave and limit the undesired electromagnetic radiation from the ground plane, which in turns reduce the radiation toward human head, thus reducing the SAR. The proposed

antenna covers the following bands range from (50–1030MHz) and (1.71–7.8GHz). The covered bands are the GSM 900, DCS 1800, PCS 1900, UMTS 2100, and most of the LTE bands. Additionally, it covers the ISM, WiMAX and the WLAN bands. Results show that the reduction of SAR averaged over 10g mass tissue in case of proposed antenna at 0.9GHz, 1.8GHz, and 2.1 GHz was 66.84%, 38.04%, 21.91%.

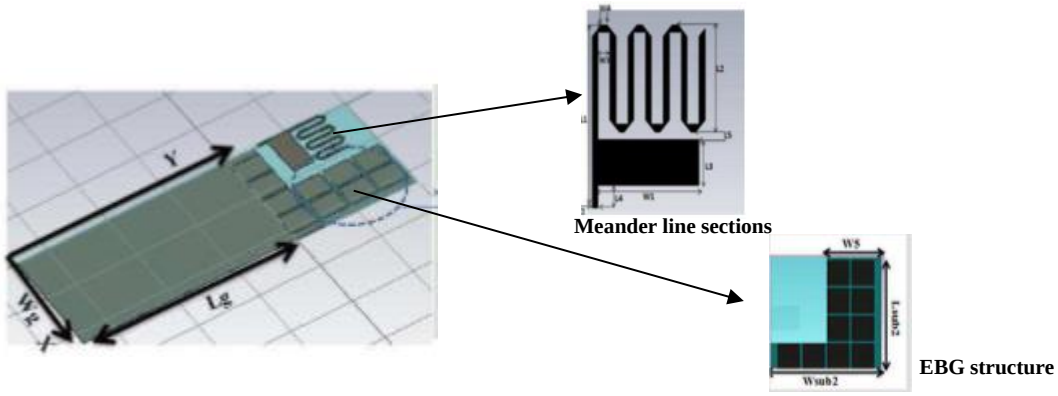

Figure 13 Geometrical structure of the proposed antenna.

Mr. Kamlesh T. Kaharpardeshi [50] investigated the performance of phased array dipole antenna consisting of two identical dipole antennas above circular patch EBG structure operating at frequency band from 3.4 to 3.8GHz for 4G mobile handset application as shown in (Figure 14) to reduce the specific absorption rate in human head.

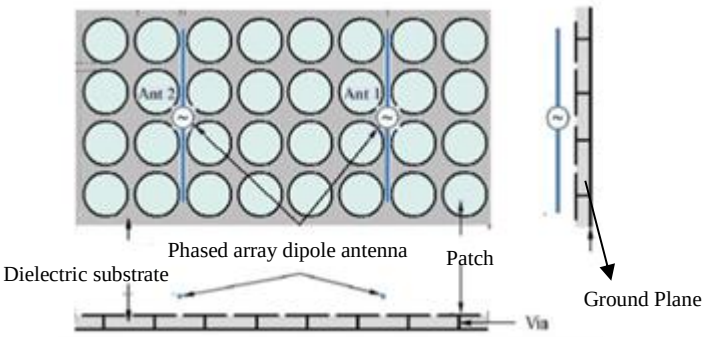

Figure 14 Proposed dipole phased array antenna above circular patch EBG substrate.

A comparison was done between two cases, first one when a conventional rectangular patch EBG structure was used, and second one when proposed circular patch EBG structure was used. It was noticed the SAR distribution depends significantly on the phase difference between the two antennas when phase shift is equal to 0 º, 90 º, 180 º, and 270 º. It has been observed that the SAR hotspot occurs near the location of two dipole antenna. On the other hand, higher value of SAR occurs when the phase shift is 90º, and lower value occurs when the phase shift is 270º. Moreover,

the proposed antenna achieved a lower value of SAR and a reduction over 11% in all cases of phase shift between both antennas in comparison to conventional rectangular patch EBG structure.

C. S. Shin [51], proposed a meander line monopole antenna mounted in folder type phone covering PCS, IMT-2000 and WLAN (2450 GHz) bands as shown in (Figure 15) for reducing SAR in human head. It has been noticed that there was a good harmonization between simulation and measurement. In addition to that, a comparison is done between external and internal monopole antenna while studying two position cases of antenna: when the antenna mounted on the up case and down case of folder type antenna. As a result, internal antenna mounted on the down case of folder type phone gives the lowest SAR, in which the SAR reduction is about 50% in contrast to external monopole antenna. The SAR value for 1 g and 10 g mass tissue of the internal monopole antenna are 0.686 and 0.356 W/kg, while SAR values for 1g and 10g mass tissue of the external monopole antenna are 1.33 and 0.812 W/kg, respectively.

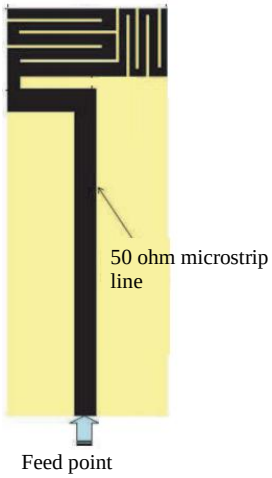

Figure 15 Geometry of the proposed low profile planar monopole antenna.

M. R. I. Faruque [52] investigated a new structure of metamaterials termed as triangular split ring resonators (TSSRs) that is placed between quarter wavelength PIFA antenna operated at 0.9 GHz and 1.8 GHz band and the human head as shown in (Figure 16) for reducing the peak SAR. This metamaterial is based on triangular metamaterials (TMMs) correlation. The FDTD method with lossy-Drude model is investigated in this study. It has been noticed that the position, distance, and the size of new design of metamaterials have an influence on SAR, so they are optimized to achieve the lowest peak SAR value in the human head. Results reveal that this new design of metamaterials reduce the peak SAR up to 45.44% for 1g mass tissue and up to 63.40% for 10g mass tissue.

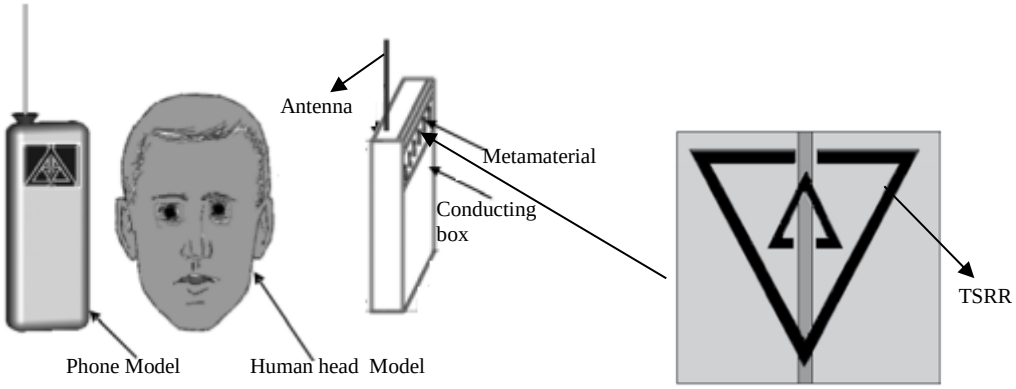

Figure 16 Human head in the vicinity of proposed antenna.

In our thesis work that will be presented in (chapter III), we get a reduction of SAR about 74.5% at GSM1800MHz in case of single band, and about 71.15%, 80.67% at GSM900MHz and GSM1800MHz, respectively in case of dual band, and about 64.37%, 79.92%, and 54.71% at GSM900MHz, GSM1800MHz, and 2400 MHz in case of Tri-band averaged over 10g mass tissue, while using U-edge groove at each corner of ground plane. This is due a reduction of the surface current density along the ground plane that leads in turn to a reduction in current density distribution along the human head. The theortical explanation on how we get the idea on reducing the SAR along the human head was discussed in (chapter III).

I.8.2. Safety Antenna for cell tower

Till now, there is no presented literature on how to design a safety cell tower antenna that provides constant field strength with uniform coverage for preventing humans from the several biological effects. All studies were based on determining safety power density such as in [53], [54]. Thus, the work in this thesis seems to be the first study on designing the safety antenna cell tower.

For this purpose, we will use the antenna array synthesis and optimization in order to build our desired radiation pattern. Then, we will proceeds by designing an elementary omnidirectional antenna and use this element to build the antenna array using CST Microwave studio. After that, we will use Atoll simulation for testing our proposed safety antenna. This part of thesis work will be presented briefly in (chapter IV) showing our idea in designing safety antenna.

I.9. Conclusion

This chapter presented the short review on electromagnetic radiation. The way how the electromagnetic waves can deposit and interact with the human body theoretically was discussed, the electrical properties of human body were presented. Brief explanation of SAR and power

density was discussed. Then, the biological and health effects of electromagnetic fields were shown. An overview for the standards, exposure limits for the computation of SAR and power density were also presented. Finally, a detailed literature review of how to reduce the SAR on human head, and how to determine safety power density of cell tower antenna were presented. In the following chapters, we will present our work on achieving a safety mobile antenna with low SAR, and safety cell tower antenna having constant field with uniform coverage.

Chapter II :
Investigation to Specific Absorption Rate (SAR) Reduction

II.1. Introduction

The use of mobile handsets has become the most prevalent technique of communication across worldwide in the last two decades. It is considered as the most mutual media utilized for facilitating communication between several people. At the same time, the radiation effects resulting from the mobile handsets have raised attentions in the general public, since mobile handsets are operated in the proximity of human head where the exposure to RF-electromagnetic waves occurs in the near field of the antenna, thus part of the power emitted by a mobile handset (normally 10-90%) is being absorbed by the human tissues [31]. For this reason, it is essential to reduce the interaction of electromagnetic wave energy towards human head during mobile handset operation.

In this chapter, the main attention is to investigate the peak SAR value along the human head while using certain types of antenna. Methods for SAR determination were discussed. Then, simulation results of half-wave dipole, an array of half-wave dipole, patch (Linear and circular polarization), and PIFA antennas in the vicinity of human head were presented. After that, several structures made of water were done on the ground plane of PIFA antenna to examine the effect of water that is considered as an absorbing material on the SAR.

II.2. Determining SAR of mobile handsets

SAR of mobile handsets can determined either by measurement method or by numerical methods.

II.2.1. Measurement method

Various standards are followed around the world concerning SAR testing of several wireless equipment [55]; however nowadays all the standards tend to be conjoined. The standards involve allotment for the calibration procedures of the measurement equipment. The measurement system that includes the necessity for the sensitivity, linearity and isotropy of the probe and the report concerning information related to measurement setup shall all be specified [31]. In addition, there should exist a conditions for the environment in the laboratory such as to have an ambient temperature ranging between 15°C to 30°C, and the modulation shall not exceed ± 2°C during the test, and to pay attention if there exist any reflections coming from any sides as: floors, walls in order not to have any influence on SAR measurement [56]. The SAR can be obtained by measuring

the electric field induced in the human tissue or by measuring the increase in temperature in the studied tissue, but usually the latter measurement is limited to the settings of SAR probes [36].

The norm SAR measurement system consists of the physical phantom, mobile handset holder, and the measurement devices in addition to the scanning system such as the one presented in (Figure 17) [57]. Physical phantom can be classified as either heterogeneous or homogenous phantom, where the former is considered as more realistic phantom, but it is difficult to implement, it consists of semi-solid materials in which the measurements have to be implemented in steady holes that distort the electric field, and the latter consists of liquid solution and it is characterized by a great feature that allows the probe to be free in movement for measuring the energy being absorbed. Therefore, it is probable that the standardized SAR tests will be established on measurements being implemented with homogeneous liquid phantoms. The geometry of the head phantom has a great effect on the value of SAR, which means as large as the head phantom will be, the more energy coupling will exist [31], [36]. In 1989, SAM phantom model is an abbreviation of Specific Anthropomorphic Mannequin (SAM) has been sophisticated in terms of shape and size of 90% of large adult male [58]. The dielectric properties of the liquid that filled the SAM phantom are analogous to that of realistic human head [31].

Figure 17 SAR measurement system for mobile phone that involves an E-field probe positioned by a robot in a head phantom exposed to a mobile phone at the right ear.

II.2.2. Numerical methods

Since the analytical calculation of the electromagnetic fields becomes nearly impossible in the more complex cases, then several numerical computational methods are established [31]. The main feature of the numerical methods is their capability to treat complex geometries by breaking it

into mathematical cell, each of which is allocated its own dielectric properties. The fields in each cell are determined by solving the electromagnetic equations for the group of cells. Several numerical methods apply various forms of the equations and utilize various techniques for their solution, but the aim is to detect the fields in several sampled shape over the volume of the model. Numerical methods are considered as enormous tools in resolving many electromagnetic problems and are applied widely in nearly all domain application. The type of simulation method applied depends on the range of frequency, in spite of that the type of simulation can also be determined by the type of phantom model being used and the accuracy with which the source shall be designed [36].

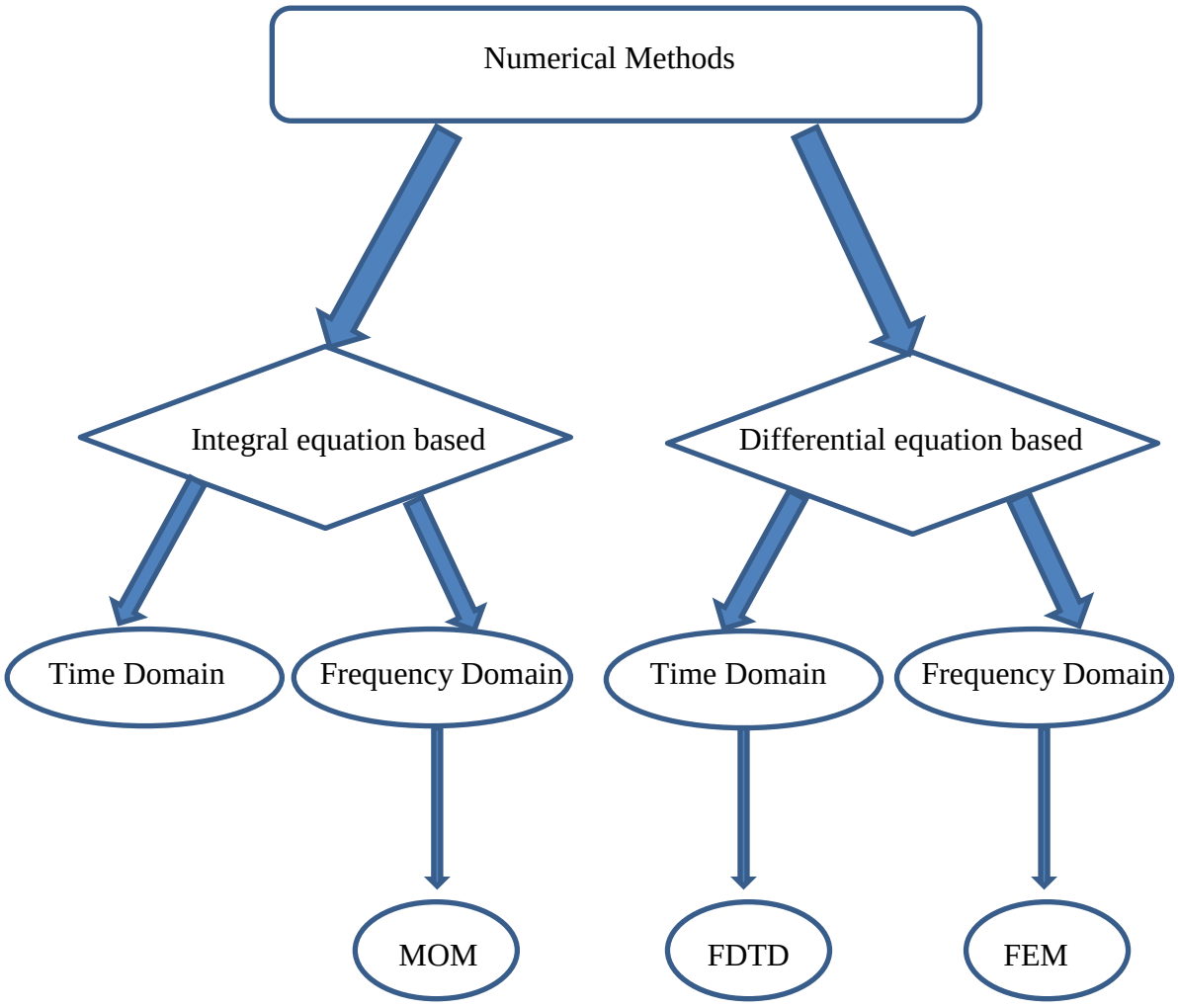

Figure 18 Classes of simulation numerical methods.

Broadly, a large number of small mathematical cells in which the electromagnetic fields can be evaluated with finer resolution shall be needed while simulating a model with more realistic structure, but this requests more computational time as well as more memory capacity in computer. Since the memory capacity and the computational time depend strongly on the number of unknown

fields in the issue space that relies on the electrical bulk of the issue space and the issue resolution, nowadays, there exists a huge capacity of memory for computer such as supercomputers, servers leading to calculate very advanced dosimetry calculations [18].

Some commonly used numerical methods for the objective of antenna design stand out is: the moment method (MoM) [59], finite-element method (FEM) [60], finite-difference time-domain (FDTD) method [61].The section of methods is shown in (Figure 18) [62].

II.3. Dipole and Patch Antennas

Several types of antennas such as: half-wave dipole antenna, an array of two half-wave dipole antenna, patch antenna (linear and circular polarization), are used to investigate the peak SAR values along the human head for examining if such antennas can be utilized in mobile application. We placed each antenna in the vicinity of the Standard Anthropomorphic Model (SAM) phantom which is used as the homogeneous model of the human head that was provided by CST-MWS(Computer Simulation Technology-Microwave Studio). This SAM phantom is composed of two parts: fluid and shell. The outer shell of the head had a constant relative permittivity of 3.5 and constant electrical conductivity of 0.0016 S/m in this simulation [63]. The dielectric properties of the fluid tissue depend on the studied frequency. Since the density of several tissues in the human body is closer to the density of water, then $\rho = 1000 kg/m^3$ was taken in this simulation [64]. During calculation of SAR value in CST, the average method was chosen to be IEEE/IEC 62704-1, and the power to be normalized at 1W.

II.3.1. Design of λ/2 dipole antenna in the vicinity of SAM human head model

The half-wave dipole antenna operated at GSM 1800MHz band in the vicinity of SAM human head model is designed and simulated using CST-MWS. This antenna consists of two wires having radius = lambda/100, and a length= lambda*0.44, and are separated by a gap=lambda/200. This antenna is fed by a discrete port with 50Ω. The half-wave dipole antenna is positioned at a distance 5mm from the SAM human head model as shown in (Figure 19). The dielectric properties of the fluid SAM phantom head at GSM1800MHz band are presented in the following (Table II-1) [64].

Table II-1 Dielectric properties of the fluid of SAM phantom at GSM1800MHz.

	Tissue Type & Frequency	**ε'_r**	**σ_{eff}**
SAM phantom head	**Fluid @ 1800 MHz**	40	1.4

Figure 19 Half-wave dipole antenna in the vicinity of human head: Perspective view (a), Top view (b).

II.3.1.1. Simulation results

The following paragraphs present the simulation results of half-wave dipole antenna when placed in the vicinity of human head.

Return Loss parameter (S_{11})

The simulated reflection characteristic of half-wave dipole antenna in the vicinity of human head is shown in (Figure 20). It is noticed that the antenna is matched at GSM 1800MHz band since S_{11} is less than -10dB.

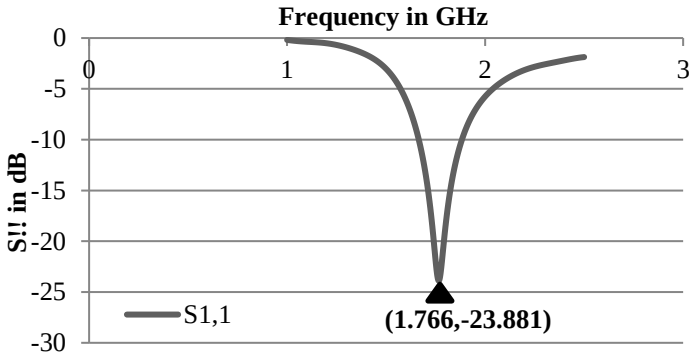

Figure 20 Graphical representation of S_{11} parameter.

3-D Radiation pattern

The three dimensional pattern of the gain of half-wave dipole antenna in the vicinity of human head is presented in (Figure 21). Its gain is equal to 7.66dB.

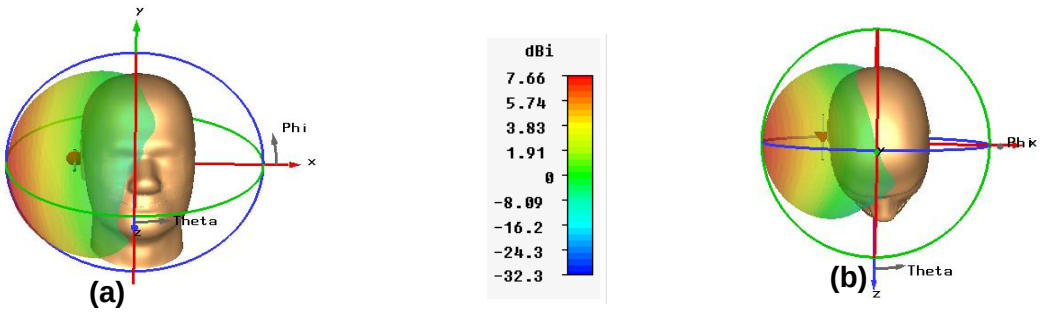

Figure 21 3D-representation of the gain of antenna in the vicinity of human head at 1800 MHz: Perspective view (a), Top view (b).

SAR distribution along the human head

The peak SAR distribution along human head is presented in (Figure 22). It is indicated that the peak SAR is higher than the standard limit value; it is equal to 14.9W/Kg averaged over 10 g mass tissues.

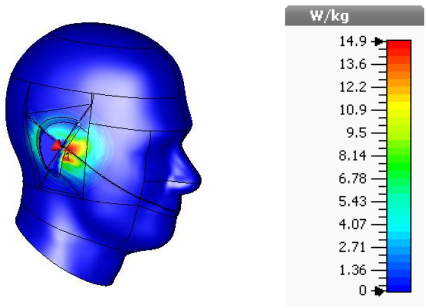

Figure 22 SAR distribution along the human head at 1800 MHz.

II.3.2. Design of λ/2 dipole antenna in the vicinity of SAM human head and human hand models

The above half-wave dipole antenna is positioned at a distance 20mm from the human hand model as shown in (Figure 23) to investigate if the presence of hand can increase or decrease the SAR. The dielectric properties of the human hand model at GSM1800MHz band are presented in (Table II-2) [65].

Figure 23 Half-wave dipole antenna in the vicinity of human head and hand: Perspective view (a), Top view (b).

Table II-2 Dielectric properties of the human hand at GSM 1800MHz.

	Tissue Type & Frequency	**ε'_r**	**σ_{eff}**
Human Hand	**Fluid @ 1800 MHz**	32.6	1.26

II.3.2.1. Simulation results

The following simulation results of half-wave dipole antenna in the vicinity of human head and hand are:

Return Loss parameter (S_{11})

The simulated reflection characteristic of the half-wave dipole antenna in the vicinity of human head and hand models is shown in (Figure 24). It is observed that it is matched at GSM 1800 MHz band.

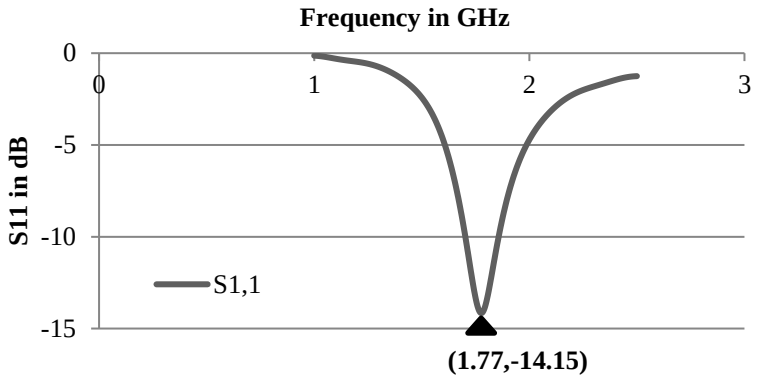

Figure 24 Graphical representation of S_{11} parameter.

3-D Radiation pattern

The three dimensional pattern of the gain of the above antenna is presented in (Figure 25). Its gain is equal to 4.29dB.

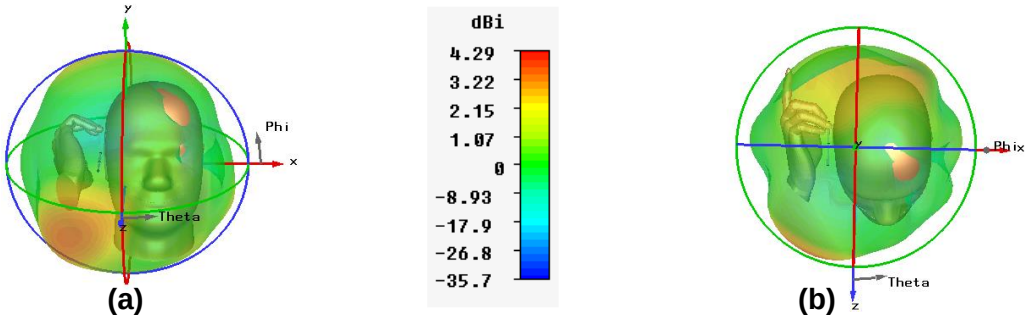

Figure 25 3D-representation of the gain of antenna in the vicinity of human head and hand at 1800 MHz: Perspective view (a), Top view (b).

SAR distribution along the human head

The peak SAR distribution along human head is presented in (Figure 26). It is indicated that the peak SAR is increased from 14.9W/Kg (without hand) to 16.8W/Kg (with hand) averaged over 10 g mass tissues.

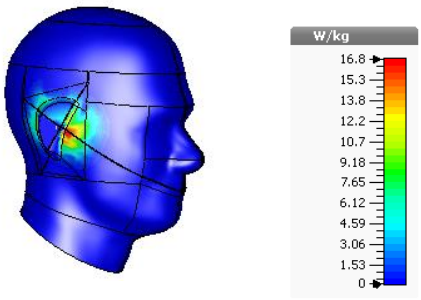

Figure 26 SAR distribution along the human head at 1800 MHz.

From the above indicated results, it is clearly shown that the half-wave dipole antenna cannot be applied in mobile application, as the value of its SAR is above the standard limit when placed in the vicinity of human head and hand.

II.3.3. Design of an array of two λ/2 dipole antenna with phase shift in the vicinity of SAM human head model

An array of two half-wave dipole antennas are positioned at a distance 5mm from the human hand model and are separated by a distance D=0.5λ as shown in (Figure 27).

Figure 27 Array of two half-wave dipole antenna in the vicinity of human head: Perspective view (a), Top view (b).

A comparison chart between SAR and the distance (D) between two dipoles with several phase shifts as shown in (Figure 28) was done. From the Graph below, it is clear indicated that the phase shift 180^0 between the two dipoles gives the lowest value of SAR. After that, the effect of this phase shift on the performance of antenna was examined.

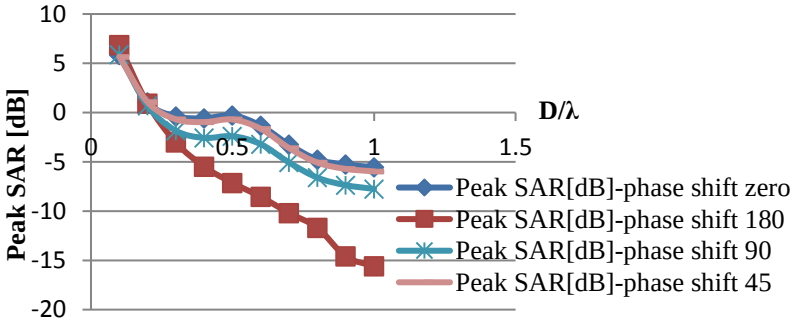

Figure 28 Comparison chart between the phase shifts of two antennas.

II.3.3.1. Simulation results

The following simulation results of an array of two half-wave dipole antennas with phase shift 180^0 in the vicinity of SAM human head model are:

Return Loss parameter (S_{11}), (S_{21})

The simulated reflection characteristic of an array of two half-wave dipole antennas in the vicinity of human head is shown in (Figure 29).

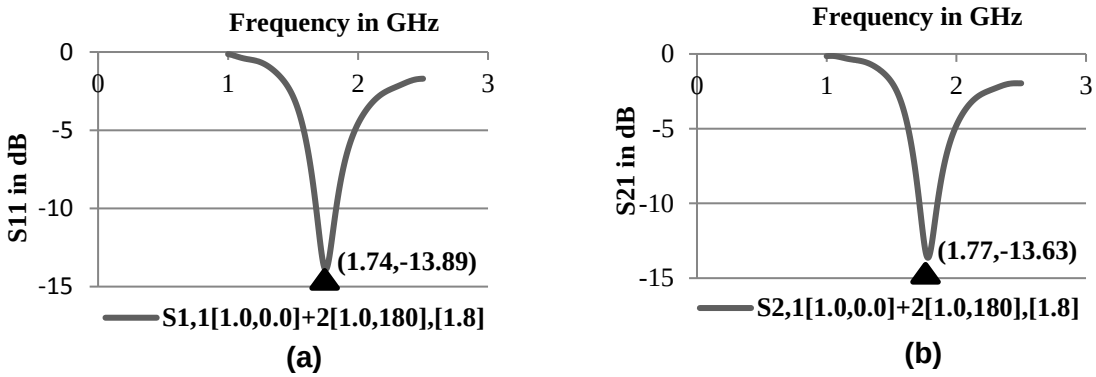

Figure 29 Graphical representation of S_{11} parameter (a), and S_{21} parameter (b).

3-D Radiation pattern

The three dimensional pattern of the gain of studied antenna is presented in (Figure 30). It's equal to 1.55dB

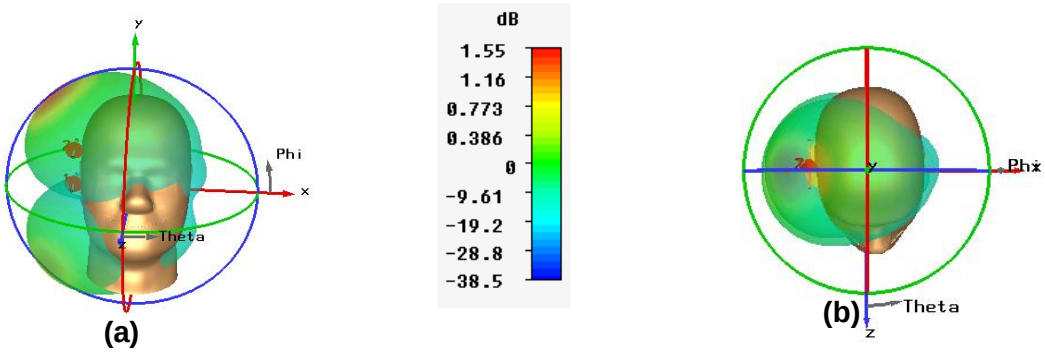

Figure 30 3D-representation of the gain of studied antenna in the vicinity of human head at 1800 MHz: Perspective view (a), Top view (b).

SAR distribution along the human head

The peak SAR distribution along human head is presented in (Figure 31). It is indicated that the peak SAR is decreased to 10.44 W/Kg averaged over 10 g mass tissues, but still higher than the standard limit value.

From the above mentioned results, it was noticed that half wave dipole antenna array cannot be applied in mobile application, as we get SAR values above the standard limit in above studied cases; in addition to that, although the phase shift 180^0 between two antennas reduced the SAR up to 42%, we notice that the radiation is null at certain area and higher at other areas, in addition to a great impact on the gain of antenna.

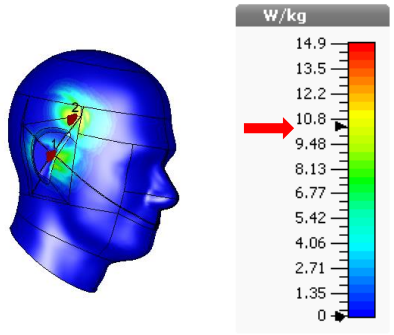

Figure 31 SAR distribution along the human head at 1800 MHz.

II.3.4. Design of patch antennas in the vicinity of SAM human head model

Patch antenna and circular polarized patch antenna in the vicinity of SAM human head model as shown in (Figure 32)are designed and simulated using CST-MWS, and are operated at GSM 1800MHz band. The dimensions of the patch antenna are presented in (Table II-3). The feeding is a coaxial cable having impedance 50Ω, and the substrate is FR-4 with epsilon equal to 4.3. In case of circular polarization; two feeding ports are designed with 90^0 phase shift.

Table II-3 Dimensions of Linear and Circular polarization patch antenna.

Name	Value (mm)	Description
h	3	Height of antenna
lambda	80.32	wavelength
t	0.1	Thickness
Wp	2*Lambda/4.25	Width of patch
Lp	2*Lambda/4.25	Length of patch
W	Lambda	Width of ground plane
L	Lambda	Length of ground plane

Figure 32 Patch antenna and circular polarized patch antenna in the vicinity of human head: Perspective view (a) and (c), Top view (b) and (d).

II.3.4.1. Simulation results

The following simulation results of patch antenna and circular polarized patch antenna in the vicinity of human head are presented as:

Return Loss parameter (S_{11}, and S_{21})

The simulated reflection characteristic of patch antenna and circular polarized patch antenna in the vicinity of human head is shown in (Figure 33).

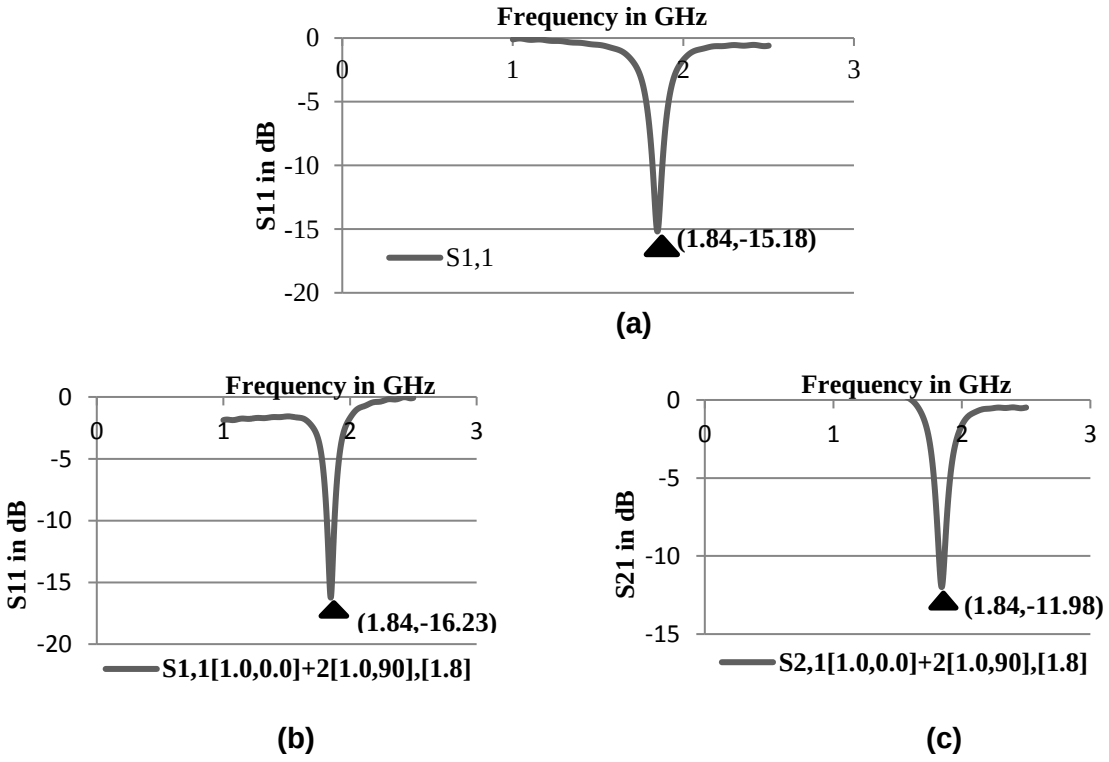

Figure 33 Graphical representation of S_{11} parameter of: patch antenna (a), circular patch antenna (b), and S21 parameter of circular patch antenna (c).

3-D Radiation pattern

The three dimensional patterns of the gain of above antennas are presented in (Figure 34). Its gain is equal to -0.395dB in case of patch antenna, and equal to -0.337dB in case of circular polarization.

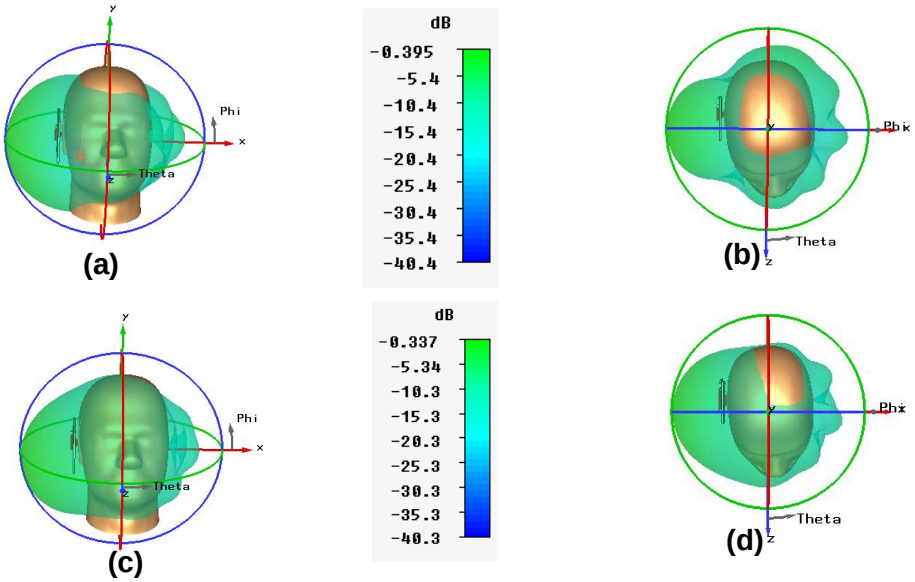

Figure 34 3D-representation of the gain of studied antennas in the vicinity of human head at 1800 MHz: Perspective view (a) and (c), Top view (b) and (d).

SAR distribution along the human head

The peak SAR distribution along human head for patch antenna and circular polarized patch antenna are presented in (Figure 35). It is indicated that in both cases, the peak SAR is higher than the standard limit value; it is equal to 15.3W/Kg in case of linear polarization, and 15W/Kg in case of circular polarization averaged over 10 g mass tissues.

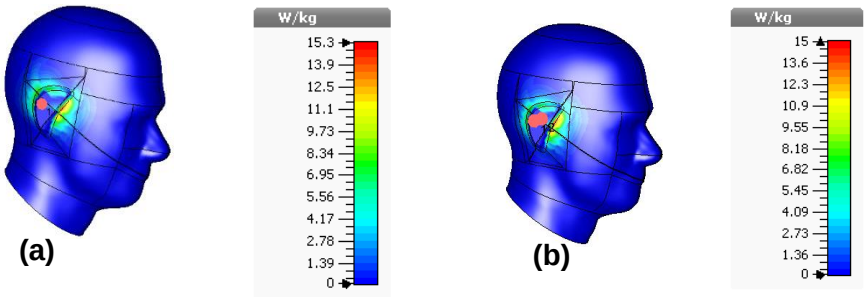

Figure 35 SAR distribution along the human head at 1800 MHz: (a) patch antenna, (b) circular patch antenna.

From the above results, it is clearly indicated that both antennas: linear and circular patch where the radiating patch is placed back to human head cannot be utilized in mobile application as

their gain is poor, and their SAR value is above the standard limit. For that, the effect of ground plane of antenna on SAR, as we place it at a distance 5mm back to human head was examined.

II.3.5. Design of patch antenna in the vicinity of SAM human head model where the ground plane is placed back to human head

The patch antenna is positioned at a distance 5mm from the SAM human head model where the ground planed is placed back to human head as shown in (Figure 36).

Figure 36 Patch antenna in the vicinity of human head: (a) Perspective view, (b) Top view.

II.3.5.1. Simulation results

The following simulation results of patch antenna in the vicinity of human head where the ground plane is placed back to human head are:

Return Loss parameter (S11)

The simulated reflection characteristic of patch antenna in the vicinity of human head is presented in (Figure 37).

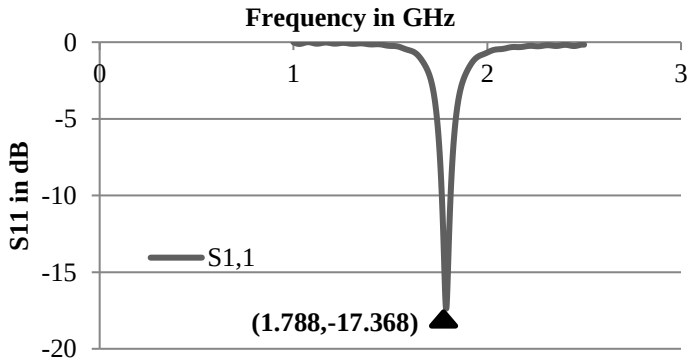

Figure 37 Graphical representation of S_{11} parameter.

3-D Radiation pattern

The three dimensional pattern of the gain of the antenna is shown in (Figure 38). Its gain is enhanced and increases to 5.12dB.

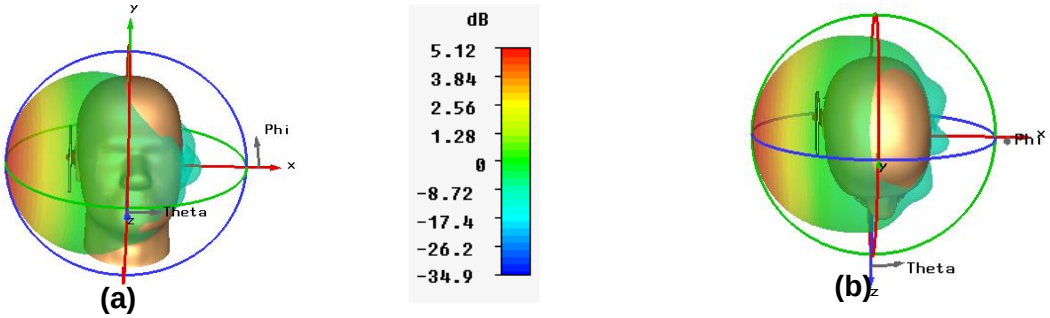

Figure 38 3D-representation of the gain of studied antennas in the vicinity of human head at 1800 MHz: Perspective view (a), Top view (b).

SAR distribution along the human head

The peak SAR distribution along human head for patch antenna is presented in (Figure 39). It is clearly observed that the peak SAR is reduced from 15.3W/Kg to 0.523W/Kg (reduction is about 96.58%) averaged over 10 g mass tissues.

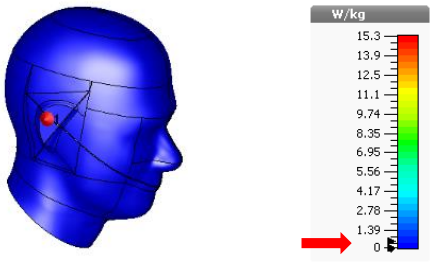

Figure 39 SAR distribution along the human head at 1800 MHz.

From the above results, it is clearly indicated that the ground plane has a great influence on the SAR distribution. This can be explained by the great correlation between the surface current density along the ground plane and the SAR. In this case, the ground plane acts as a reflector, where the electromagnetic wave reflected back from the human head, thus less penetration of fields exist toward human head leading to less SAR. For this reason, we make a parametric study on the dimension of ground plane of the above antenna for proving its impact on SAR as indicated in (Table II-4).

Table II-4 Parametric study on the dimensions of linear polarization patch antenna.

Dimensions (mm)	***Surface Current density(A/m)***	***SAR(W/Kg)***
Length=lambda, Width=Lambda	0.4	0.523
Length=lambda/2, Width=Lambda/2	1.3	4.74

From the above parametric studied result, we notice that as the dimension of ground plane increases, the surface current density decreases as well as the SAR, this is due to the role of ground plane that acts as a reflector in which it reflects the electromagnetic fields away from penetrating toward the human head.

Although we get a good result in terms of SAR for the above antenna, it cannot be applied in mobile application due to its size. For this reason, we look forward to make a study on PIFA antenna, as it is well known from the several studies that it has a lower SAR.

In the following sections, a short brief about planar inverted-F-antenna was discussed, and then the investigation on its SAR was done.

II.4. Planar inverted-F-antenna

PIFA is well considered as the most popular antenna used in mobile phone applications due to its many advantageous such as its small size, low SAR, omnidirectional radiation pattern, simple configuration, easy to manufacture, low cost, low-profile that supports multiband and wideband applications, it supports high gain in both vertical and horizontal direction [66]. It has only one disadvantage such as narrow bandwidth that limit the PIFA for its trade in mobile application [67].

Generally, PIFA antenna is a modified monopole antenna in which the top part has been bent down so that it will be parallel to the ground plane for reducing the height of antenna so that it can be applied in mobile application [67]. In addition to that, PIFA is a type of IFA antenna having a wire radiator element that is substituted by a plate to broaden the bandwidth [68]. PIFA is resonant at quarter wavelength (λ/4) consisting of a ground plane, a top radiating patch element, a feeding element that is connected between the ground plane and the top radiating patch element, and a shorting strip that is linked also between the ground plane and the top radiating patch element [69], as shown in (Figure 40) [70].

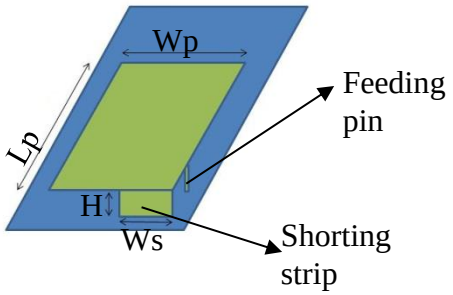

Figure 40 Geometrical structure of PIFA antenna.

The distance between the shorting strip and the feeding element controls the input impedance, so that the impedance can be diminished by moving the feeding element closer to shorting strip, while it can be increased by moving the feeding element far away from the shorting strip.

The resonant frequency is greatly dependent on the width of the shorting strip, and it is given by the following equation [70]: $f_r = \frac{C}{4(L_p+W_p-W_s)}$ equation II-1

Where C, Lp , Wp, Ws, denotes the speed of light, length of the radiating patch, width of the radiating patch, width of the shorting strip.

If the substrate applied was different from an air then: $C = \frac{C_0}{\sqrt{\varepsilon_r}}$ equation II-2

Where C_0 denotes the speed of light that it is equal to $3x10^8$, and ε_r is the permittivity of the substrate.

It can be demonstrated from the (equation II-1) that when Ws = Wp, then PIFA will be resonant at: $L_p = \frac{C}{4f_r}$ equation II-3

And when Ws = zero, then the PIFA resonant at: $L_p + W_p = \frac{C}{4f_r}$ equation II-4

There are many different types of PIFA antenna depending on its wireless applications. These types can be as presented in (Figure 41) [68].

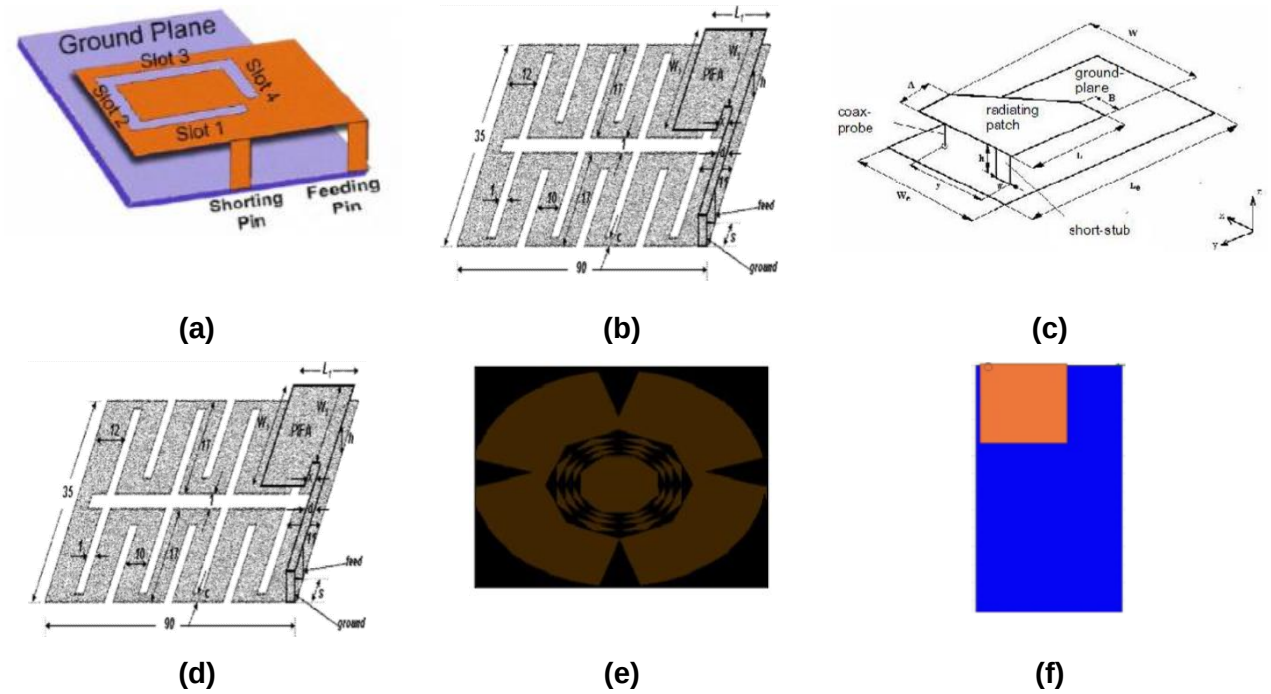

Figure 41 PIFA antenna designs: Slotted Patch PIFA (a), Reconfigurable PIFA (b), Tapered T-PIFA (c), Defected Ground Plane PIFA (d), Fractal Circular PIFA (e), Square Patch PIFA (f).

II.4.1. Design of conventional single band PIFA antenna in free space

The conventional single band PIFA antenna operating at 1800MHz consists of a ground plane, top radiating patch element, and shorting strip. All the elements of antenna are made of

perfect electric conductor, with feeding 50Ω coaxial cable as shown in (Figure 42). The feeding element consists of three parts: the pin is made of perfect electric conductor, the dielectric coat is made of teflon (loss free) with permittivity 2.1, and the cover is made of perfect electric conductor. The dimensions of the single band PIFA antenna is presented in the following (Table II-6).

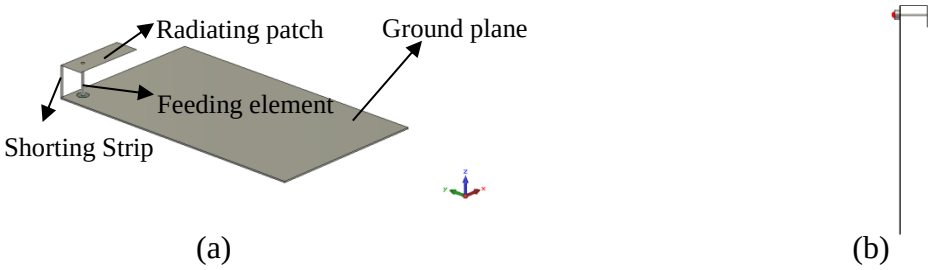

Figure 42 Single band PIFA antenna operating at 1800MHz: Perspective view(a), (b) Side view.

Table II-5 Dimensions of single band PIFA antenna in (mm).

Name	Value (mm)	Description
H_s	12	Length of shorting strip
L_c	2	Length of the cover of feeding element
L_d	2	Length of the dielectric coat of feeding element
L_g	100	Length of ground plane
L_p	9	Length of patch
L_{pin}	12	Length of the pin of the feeding element
r_c	2.2	Radius of the cover of feeding element
r_d	2.1	Radius of the dielectric coat of feeding element
r_i	0.625	Radius of the pin of the feeding element
t	0.5	Thickness of ground plane
W_g	60	Width of ground plane
W_p	27	Width of patch
W_s	1	Width of shorting pin

II.4.1.1. Simulation results

The simulation results of single band PIFA antenna shows that this antenna can be applied in mobile handset operated at GSM1800MHz band due to the following results:

Return Loss parameter (S_{11})

The simulated reflection characteristic of the single band PIFA antenna with the above design parameters is shown in (Figure 43).

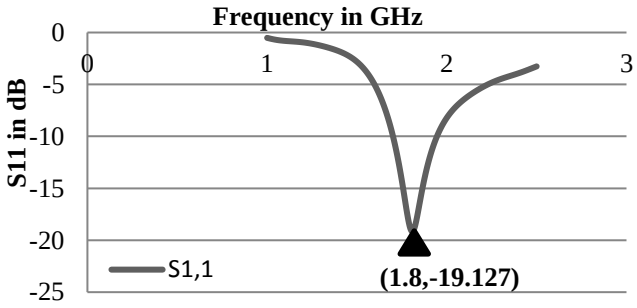

Figure 43 Graphical representation of S11 parameter.

3-D Radiation pattern

The three dimensional pattern of the gain of the single band PIFA antenna is presented in (Figure 44). Its gain is equal to 4.34dB.

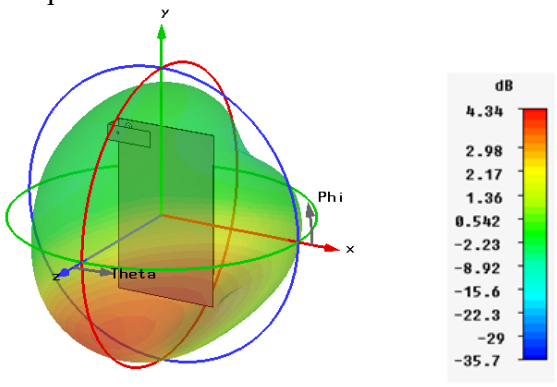

Figure 44 3D-representation of the gain of PIFA antenna.

II.4.2. Design of conventional single band PIFA Antenna in the vicinity of SAM human head model

The single band PIFA antenna in the vicinity of SAM human head model is designed and simulated using CST-MWS, and operated at GSM 1800MHz band for mobile application to evaluate the surface current density along the ground plane, the current density along the human head as well as the SAR. The conventional single band PIFA antenna is positioned at a distance 5mm from the SAM human head model as shown in (Figure 45).

(a) (b)

Figure 45 PIFA antenna in the vicinity of human head: (a) Perspective view, (b) Top view.

II.4.2.1. Simulation results

The simulation results of single band PIFA antenna are presented as follows:

Return Loss parameter (S11)

The simulated reflection characteristic of the single-band PIFA antenna in the vicinity of human head is presented as in (Figure 46).

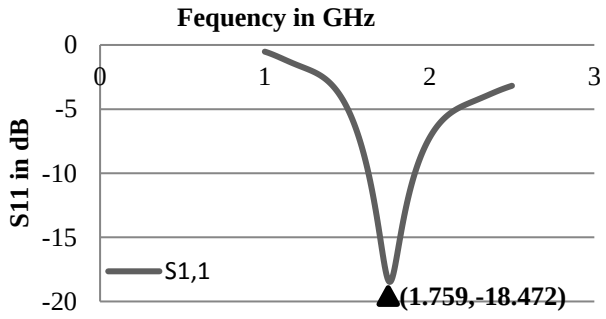

Figure 46 Graphical representation of S11 parameter.

3-D Radiation pattern

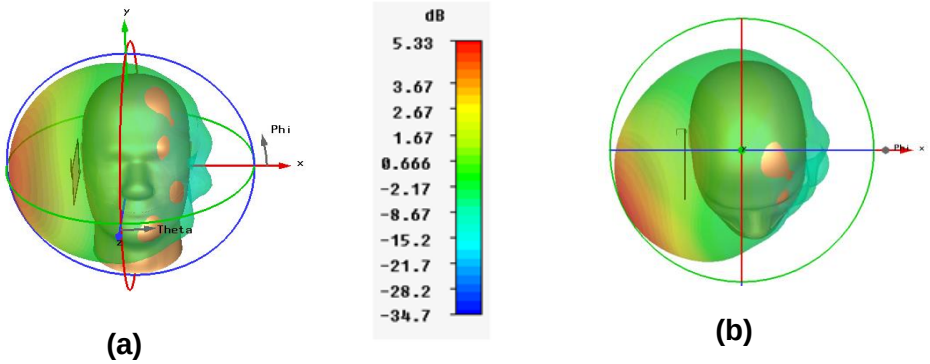

(a) (b)

Figure 47 3D-representation of the gain of studied antennas in the vicinity of human head at 1800 MHz: Perspective view (a), Top view (b).

The three dimensional pattern of the gain of single band PIFA antenna is presented in (Figure 47). Its gain is equal to 5.33dB.

Surface Current distribution along the ground plane

The maximum peak surface current distribution along the ground plane of antenna when placed in the vicinity of human head is presented in (Figure 48). It is shown that the maximum surface current is equal to 7.8 A/m.

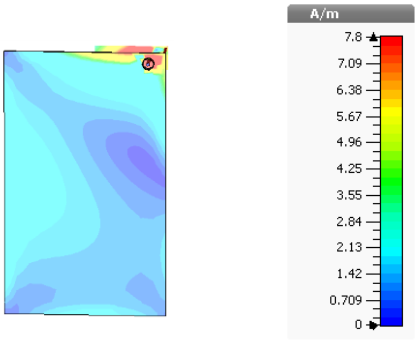

Figure 48 Surface Current distribution along the backside of ground plane.

Current Density distribution along the human head

The peak current distribution along human head is presented in (Figure 49). It is shown that the maximum current occurs at ear position where it is equal to 104A/m^2.

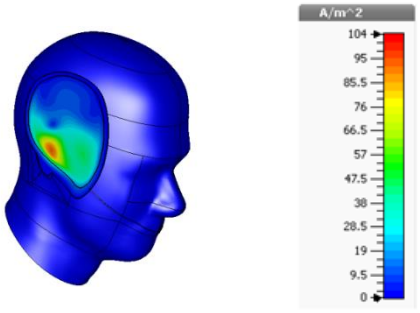

Figure 49 Current Density distribution along the human head at 1800 MHz.

SAR distribution along the human head

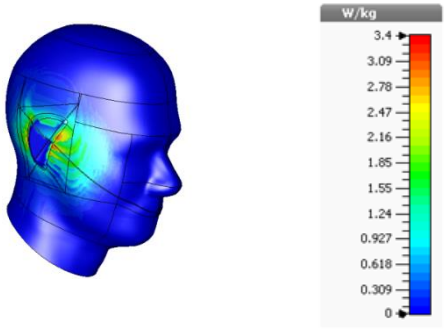

Figure 50 SAR distribution along the human head at 1800 MHz.

The peak SAR distribution along human head is presented in (Figure 50). It is indicated that the peak SAR is higher than the standard limit value; it is equal to 3.4W/Kg averaged over 10 g mass tissues.

Although it was noticed from the above results that PIFA antenna has the lowest SAR, it is still above the average standard value. Therefore, certain study on how to reduce the value of SAR was tested by making certain modification in the ground plane of antenna. This modification is based on several geometrical structures that are made of liquid, mainly salty water to investigate the reduction of SAR.

The following section explains an overview of liquid antenna, basically salty water, and then the simulation of antenna configurations will be presented.

II.5. Water antenna

Water-based liquid antennas are a kind of antenna using fluid such as water to transmit and receive radio signals. They have protruded as promising replacements to conventional antennas for several applications. They have enticed growing concern in recent years, due to several advantages such as conformability-it is easy to return to its desired shape, easy to transport, transparency, low cost, compact size since water material can be considered as a material with high permittivity, reconfigurability-the dimensions and the chemical structure of the liquid stream are used to control the bandwidth and the operated frequency.

Water antenna is based on three types namely: pure water, salty water, water with propylene glycol (PG). Water with (PG) is treated as a type of antifreeze, that is recommended as a solution to decrease the freezing point of water in cold environments, since pure water will be frozen when temperature is lower than 0^{o}C, thus, water antennas will be treated as solid antennas and the dielectric properties of ice will be completely distinct from pure water in liquid state. Water can acts as either dielectric resonator antenna when pure water is treated as the main radiator, or conducting antenna when adding salt into pure water [9].

The aim of this section is to work on designing a PIFA antenna made of salty water that is considered as a mixture between dielectric resonators and conducting antenna for investigating if it can be applied in mobile application having low SAR. In this scenario, we design and simulate several geometrical structures of such antenna using CST simulation tool.

II.5.1. Design of conventional single band PIFA antenna in the vicinity of SAM human head model with several structures made of salty water in its ground Plane

In this section, single-band water-PIFA antenna in the vicinity of human head was designed and simulated at 1.8GHz in a similar manner as previous sections, but here we investigate several structures made of salty water along the ground plane as shown in the below figures, to examine which structure can achieve an antenna with low SAR without affecting its performance, as it is well known that water is considered as an absorbing material. The permittivity of salty water is chosen to be 74, and the conductivity to be 11S/m for the antenna to be operated at 1.8GHz, the salinity about 15ppt, and the temperature about 25^{o}C.

The single-band water-PIFA antenna with several structures made of salty water along the ground plane is positioned at a distance 5mm from the SAM human head model as shown in (Figure 51).

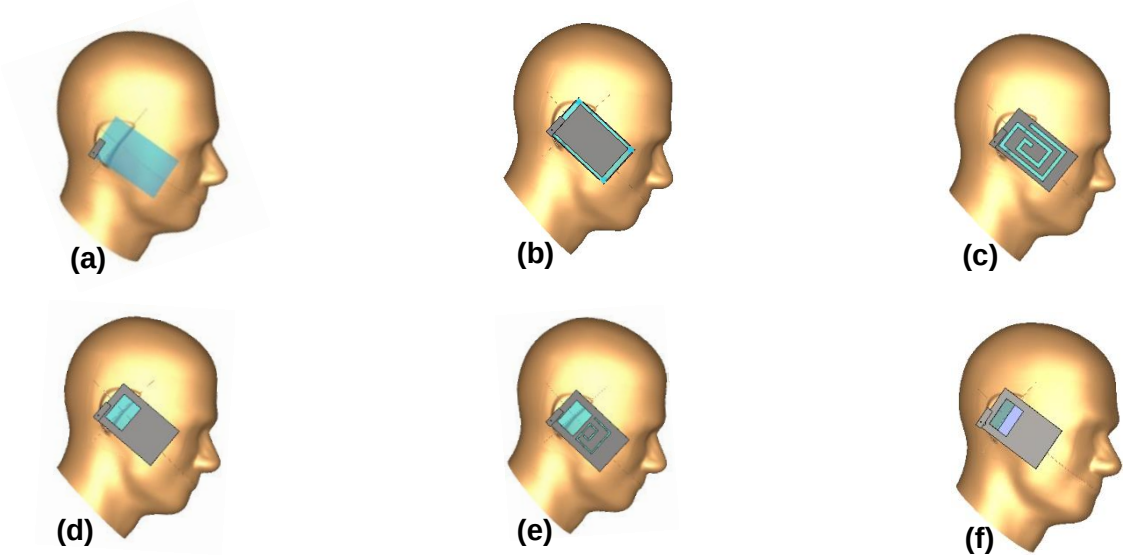

Figure 51 PIFA antenna with several modifications in ground plane: ground plane filled with salty water (a), mesh structure containing salty water (b), spiral shape made of salty water (c), cavity shape made of salty water (d), spiral and cavity filled with salty water (e), and cavity (half of it filled with salty water and the other half filled with air) (f).

II.5.1.1. Simulation results

The simulation results of single band water-PIFA antenna are presented as follows:

Return Loss parameter (S11)

The simulated reflection characteristic of the single-band water-PIFA antennas in the vicinity of human head is shown in (Figure 52).

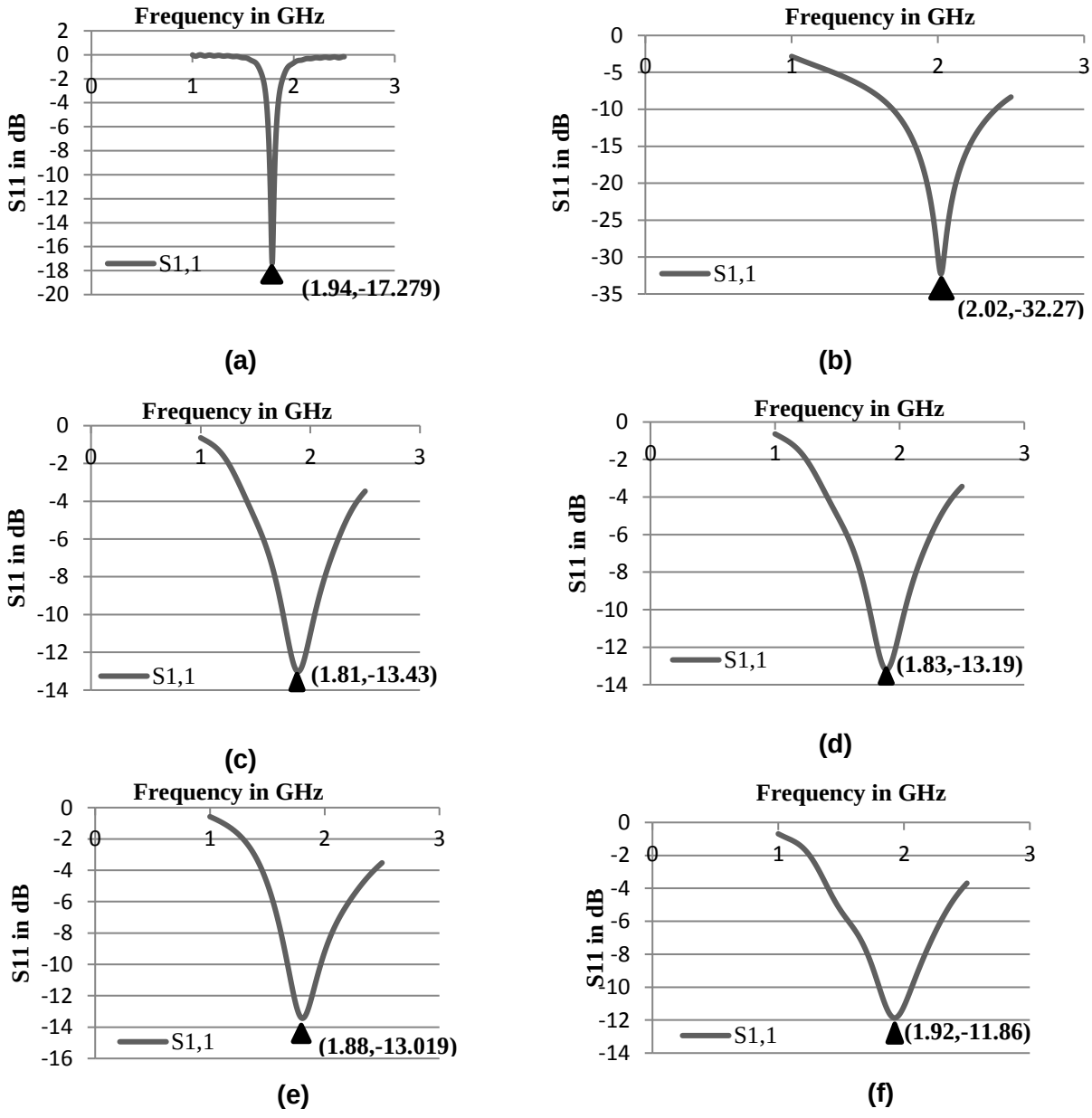

Figure 52 Graphical representation of S_{11} parameter for: figure 51 (a), figure 51 (b), figure 51(c), figure 51 (d), figure 51 (e), and figure 51 (f).

3-D Radiation pattern

The three dimensional pattern of the gain of above antennas are presented in (Figure 53)**.** The gain decreases from 5.33dB when the ground plane is made from PEC as presented in previous

section to -6.96dB, 0.498dB, 3.88dB, 4.39dB, 4.24dB, 4.71dB, in each above studied case, respectively.

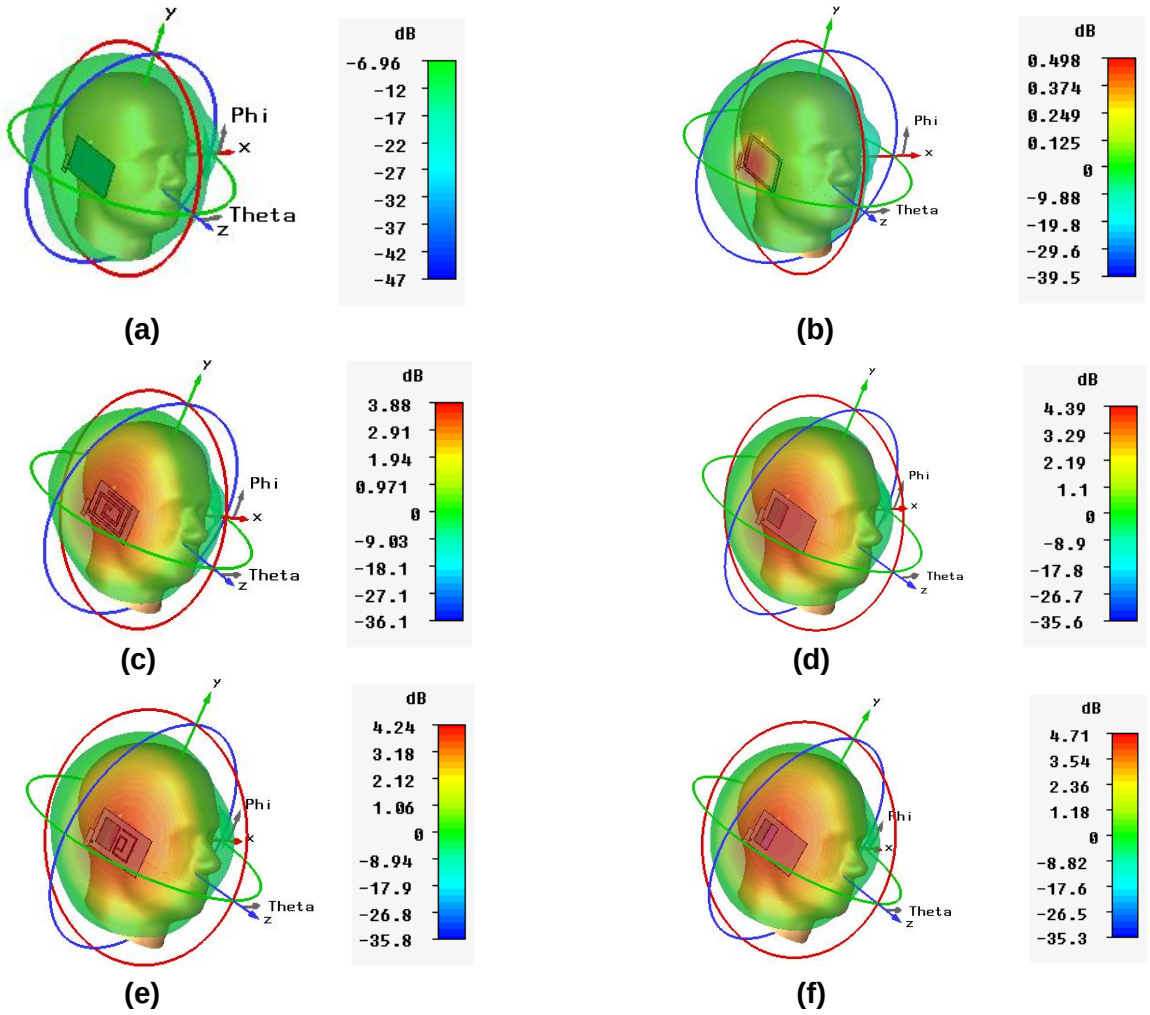

Figure 53 3D-representation of the gain of studied antennas in the vicinity of human head at 1800 MHz for: figure 51 (a), figure 51 (b), figure 51 (c), figure 51 (d) , figure 51 (e), and figure 51 (f).

SAR distribution along the human head

The peak SAR distribution along human head is presented in (Figure 54). It is indicated that although the peak SAR in (Figure 54a) is about 0.36W/Kg which is much below the average standard limit value, and the other studied antennas show that the peak SAR is about 1.7W/kg, 2.9W/Kg, 2.3W/Kg, 2.3W/Kg, and 2.5W/Kg, which is above standard limit, respectively, we notice that the amount of the gain lost by the studied antennas, make the SAR decreases.

From the below results, we can conclude that such studied antennas cannot be applied in mobile application, since we notice that as the amount of gain decreases, the value of SAR decreases.

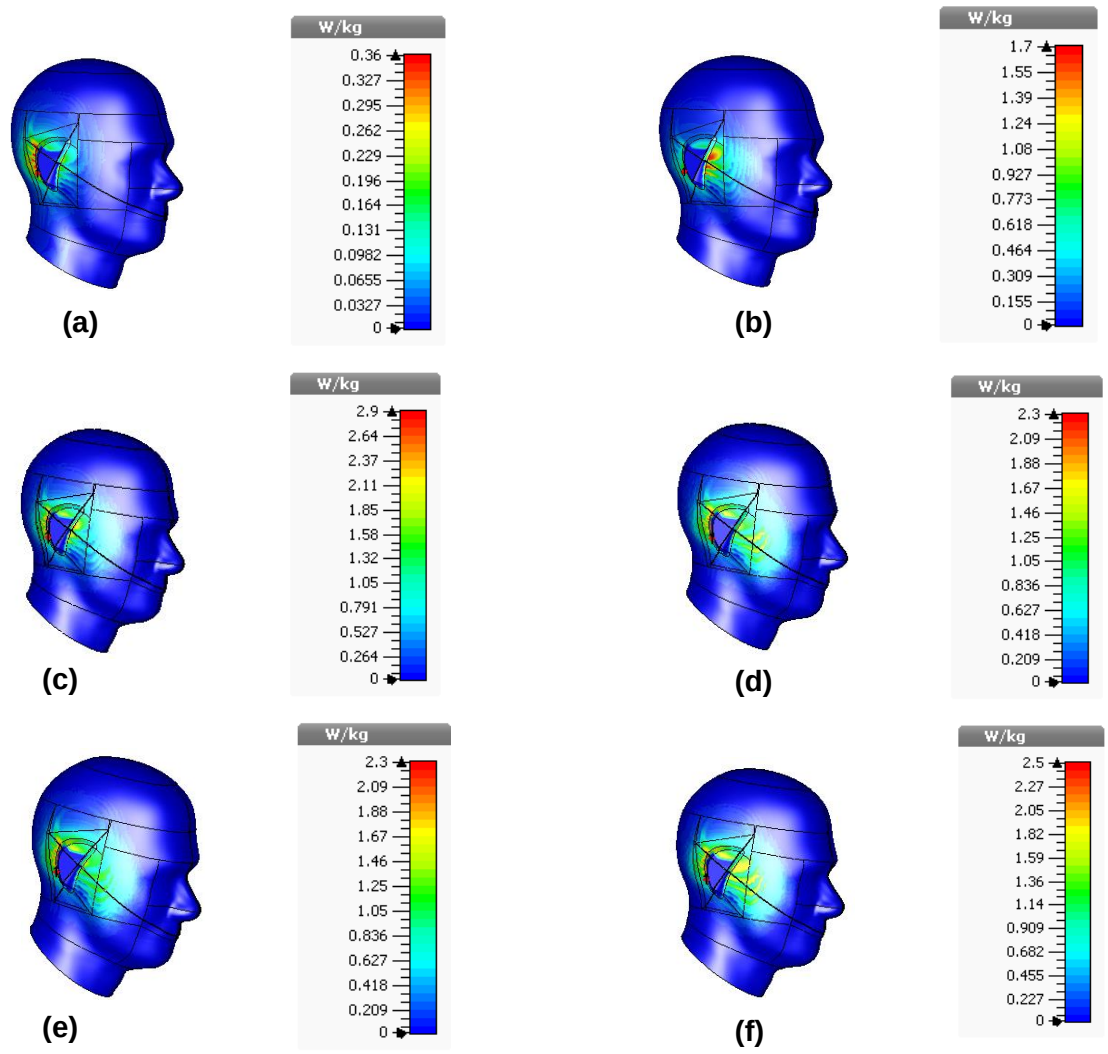

Figure 54 SAR distribution along the human head at 1800 MHz for: figure 51 (a), figure 51 (b), figure 51 (c), figure 51 (d), figure 51 (e), and figure 51 (f).

II.6. Conclusion

All the above simulation results indicate that neither the half-wavelength dipole antenna (single element and an array), nor the patch antenna, and the PIFA antenna with certain structures made of water in the ground plane can be utilized as a mobile antenna with low SAR. Only one idea from the above simulation results can take to work on it in the next chapter, which is how we can decrease the surface current density along the ground plane thus the SAR in a way that doesn't influence the performance of antenna. This idea is estimated one of the essential requirement when the antennas are placed in the vicinity of human body, as it reduces the antenna back radiation. In addition to that, the back radiation situation is not only caused by the surface waves, otherwise it would be enough with using a cavity backed PIFA antenna to suppress them. The problem is more complex as it strongly depends on the surface surrounding the antenna. In this sense, several edges

with certain shapes at each corner of the ground plane of PIFA antenna have demonstrated in the next chapter to be a good choice as they are able to terminate propagation of the electromagnetic fields toward human head, and, at the same time, they suppress the surface wave propagation, both impacts occurring at the same frequency. In this work we will show how to use a simple edge groove at each corner of ground plane to reduce the SAR. From the point of view of the designer, the employment of simple geometries with a frontier number of parameters which control the performance of antenna is always an advantage, even if more advanced designs can also find employment in specific problems with special requests. In this sense, an edge groove at each corner of the ground plane can be as well suitable as its design is simple.

Chapter III:
SAR reduction for PIFA antennas used in mobile handsets

III.1. Introduction

As the effect of mobile phones on human health is becoming a serious concern in the last decade, we propose novel safety mobile antennas for reducing the electromagnetic wave radiation toward human head without affecting the performance of antenna. Three antennas are considered: a single band PIFA operating at 1800 MHz, a dual band PIFA operating at 900 MHz and 1800 MHz, and a triband PIFA operating at 900 MHz, 1800 MHz, and 2400 MHz. Those novel antennas are based on certain modification along their ground plane by inserting different shapes edge-groove (U, L, and V) at each corner of the ground plane for reducing the surface current density distribution along it, and the distribution of current density along human head, which in turn leads to a reduction in SAR. The simulation results are clearly shown and an extensive parametric analysis is executed.

III.2. Theoretical explanation of our proposed idea in reducing the SAR

The effect of inserting U, L, and V-shape edge-groove at each corner of the ground plane of antenna plays an important role in reducing the edge reflection, and its ability in attenuating the traveling wave passing through it. Moreover, the outward traveling wave of the current conflicts with the reflected wave due to the ground plane edge, thus the distribution of surface current density along the ground plane is reduced. Also, the edge groove has an effect in reducing diffractions that produce a large back lobes radiation [71], thus less electromagnetic wave will penetrate through human head which diminishes the current density as well as the SAR.

SAR can be diminished by the ability of the surface reactance of the edges to suppress the surface waves along the ground plane, also its ability to avoid illumination of the electric field plane edges, and its ability to reduce diffractions. In addition, the surface reactance of these edges must be capacitive to null the tangential magnetic field that is parallel to the edges [72]. This can be achieved by assuming the surface reactance to be equal to [73]:

$$X = \frac{w}{w+t}\sqrt{\frac{\mu_0}{\varepsilon_0}}\tan(k_0 d) \text{ When } \begin{cases} (2n+1)\frac{\lambda_0}{4} < d < (n+1)\frac{\lambda_0}{2} \\ \frac{w}{w+t} \cong 1 \\ w < \frac{\lambda}{10} \end{cases} \quad \text{equation III-1}$$

Where μ_0, ε_0, w, t, and d denotes the permeability, permittivity in free space, width, thickness and height of the edge-groove.

So, the height of the edge must be optimized properly to achieve great performance in suppressing the surface current, and in reducing the traveling wave along human head as well as the diffracted wave. Moreover, the width must be also optimized properly since the wider or narrow width will macerate the suppression impact [74]. It has been noticed by the next shown results that during edge treatment, the surface current density along the ground plane, the current density along the human head as well as the SAR can be reduced. It has been observed that the SAR is below the limit standard value in contrast to the conventional case (without edge-treatment) where the SAR is above the limit standard value.

In the following sections, certain modification in the ground plane of conventional single band PIFA antenna presented in (chapter II, section-II.4.1.) was made by inserting several shapes edge-groove: U, L, and V at each corner of its ground plane. The procedures for simulating the proposed safety antenna in the vicinity of human head are similar to the previous conventional antenna simulation (chapter II, section-II.4.2.). The same modification in the ground plane was examined on dual band and Tri-band PIFA antennas. In this work, we make two studies for inserting edges: first one is when the edges are below the ground plane, where in this case the SAR is reduced significantly, however the total height (height of antenna plus height of edges) of antenna is increased. In this situation, two scenarios were investigated for SAR reduction: first one when the edge is made of PEC, and second one, when it is made of water. Second study is the more realistic one with SAR reduction where we insert the edges above each corner of the ground plane while preserving the height of antenna.

III.3. Proposed single band PIFA antenna when the shape-edge groove is below the ground plane

In this paragraph, the insertion of edge treatment below each corner of the ground plane of single band PIFA antenna was studied. In addition to that, a comparison between different shapes

(U, L, and V) of edges was done for predicting which shape is the best choice for mobile application in terms of SAR.

III.3.1. Design of proposed single band PIFA antenna in the vicinity of SAM human head model

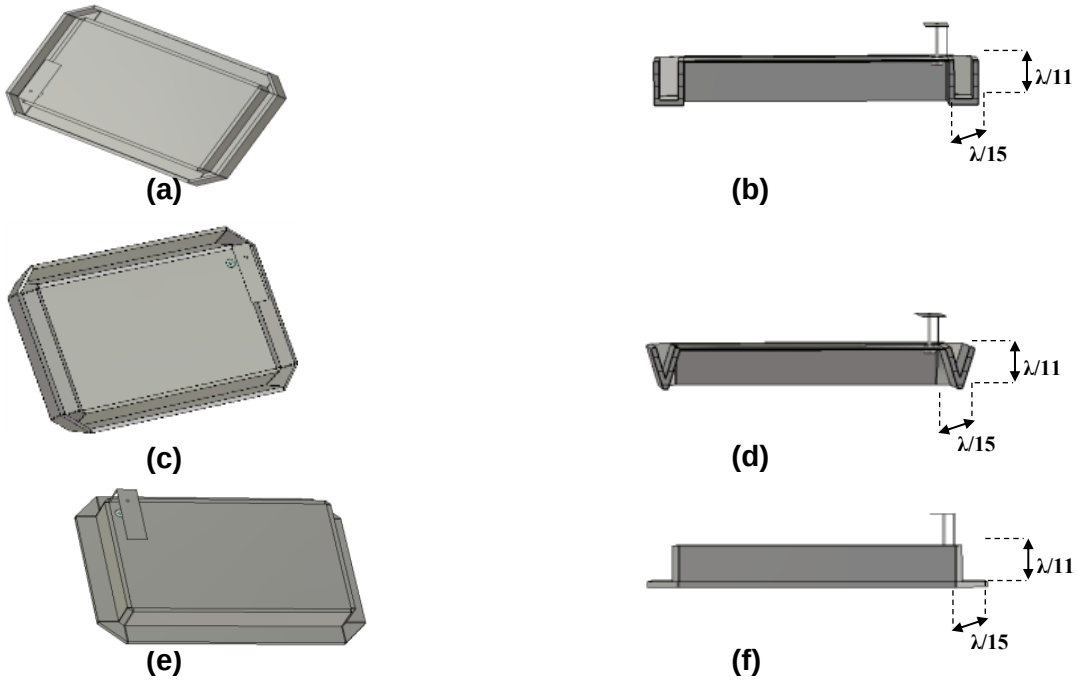

Figure 55 Geometrical structure of single band PIFA antenna with U, V, and L-shapes: Perspective view (a), (c), (e), and Top view (b), (d), and (f).

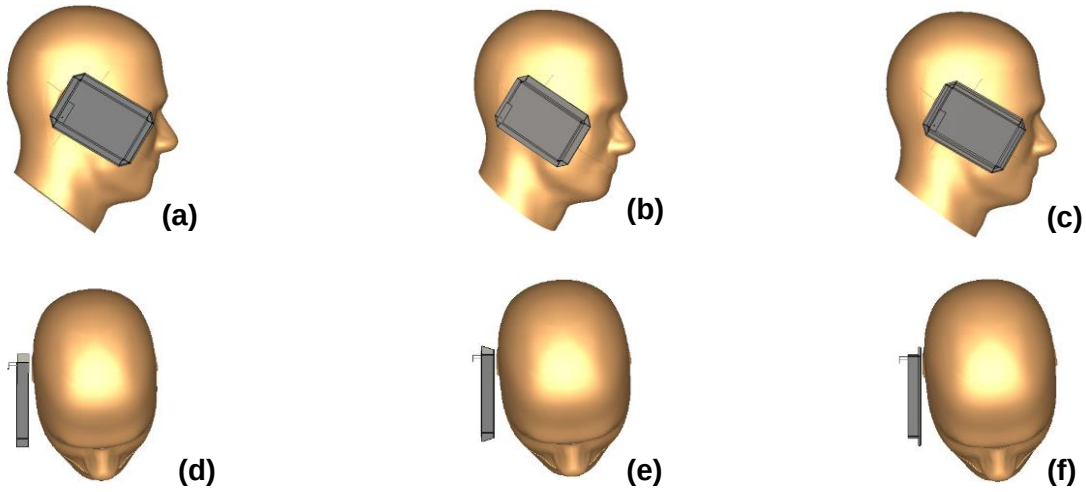

Figure 56 Geometrical structure of single band PIFA antenna with U, V, and L in the vicinity of human head: Perspective view (a), (b), (c), and Top view (d), (e), and (f).

The proposed single band PIFA antenna with U, V, and L edges at each corner of the ground plane as shown in (Figure 55) is positioned at a distance 5mm from the SAM human head model as

presented in (Figure 56). The dielctric properties of the fluid SAM phantom head at GSM1800MHz band are indicated (chapter II,Table II-1)

III.3.1.1. Simulation results

The following simulation results of single band PIFA antenna shows that U, L, and V-edges treatment will not affect the performance of antenna, and a significant reduction of SAR was obtained as indicated below:

Parametric Study

Parametric study on the dimensions of U-edge was performed in order to optimize the best performance of antenna structure that will give the lowest SAR possible values, when placed in the vicinity of human head. The height H and width W of the U-edge as illustrated in (Figure 57) are swept. Results are summarized in (Table III-1); they show that as the height decreases, the current density increases, which in turn lead to SAR, increase. On the other hand, as the width decreases, the current density increases, this in turn leads to SAR increase. At first, we start following the above preferable dimensions of the height and the width of proposed edges. We notice that with d=λ/4 and w= λ/15, SAR can be reduced to 95%. However, this dimension corresponds to 41.6 mm at 1800 MHz cannot be appropriate for mobile applications due to its size. On the other hand, the best performance of antenna was achieved is when the parameter d (height) is equal to λ/11, and w (width) is equal to λ/15.

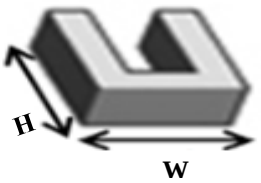

Figure 57 Sweeping height and width of U-edge.

Table III-1 Results while sweeping the height H and width W of U-edges.

	***H* (mm)**			***W* (mm)**		
	λ/4	**λ/11**	**λ/16**	**λ/15**	**λ/16**	**λ/17**
peak SAR (W/Kg)	0.3	0.77	0.89	0.722	0.752	0.781
peak current density (A/m^2)	35.1	44.5	50.7	44.5	45.9	47.1

Return Loss parameter (S_{11})

The simulated reflection characteristic of the single-band PIFA antenna with U, L, and V-edges treatment placed in the vicinity of human head is shown in (Figure 58). From the Graph, it is clear that the resonant frequency in case of U, L, and V-edges is still well matched at GSM 1800MHz band since S_{11} is less than -10dB.

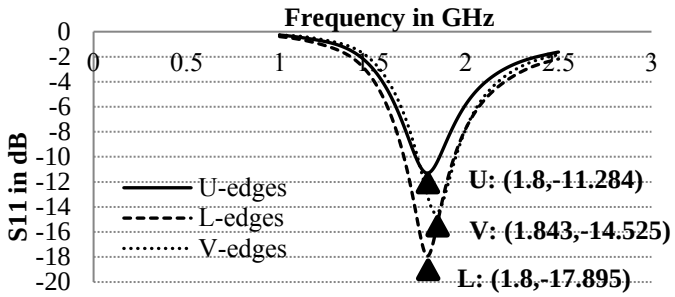

Figure 58 Graphical representation of S_{11} parameter of single band PIFA antenna with U, V, and L in the vicinity of human head.

3-D Radiation pattern

The three dimensional patterns of the gain of the above studied antennas are presented in (Figure 59). Its gain is equal to 4.56dB with U-edges, 5.08dB with V-edges, and 5.12dB with L-edges.

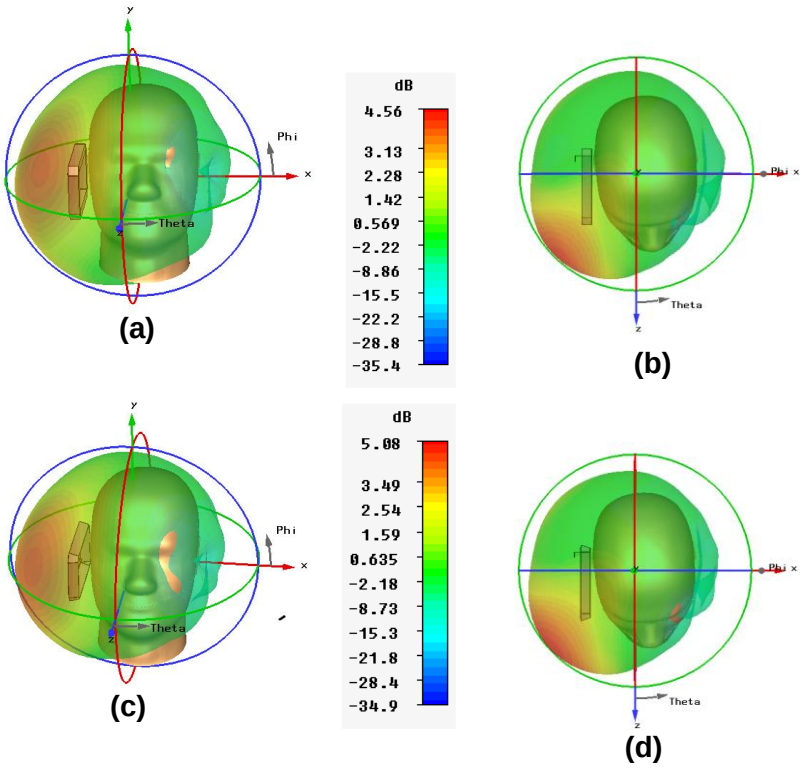

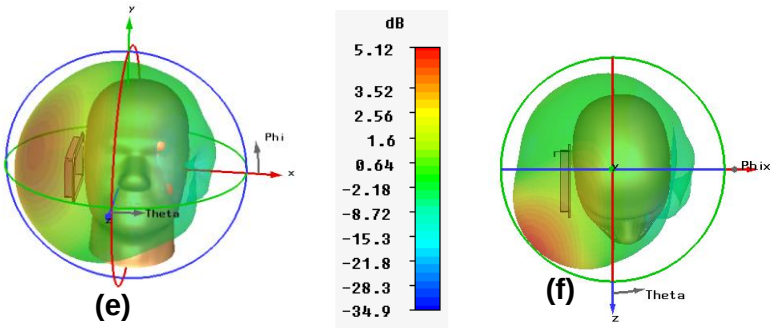

Figure 59 3D-representation of the gain of antenna with U, V, and L-shapes in the vicinity of human head: Perspective view (a), (c), (e), and Top view (b), (d), and (f).

Surface Current distribution along the ground plane

The maximum peak surface current distribution along the ground plane of antenna with U, L, and V-edges when placed in the vicinity of human head is presented in (Figure 60). It is shown that the maximum surface current is reduced from 7.8A/m (without edges treatment) to be approximately zero along the ground plane when the edges treatment are inserted.

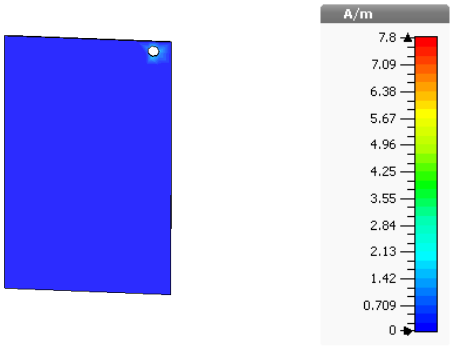

Figure 60 Surface Current distribution along the back side of ground plane of antennas with U, L, and V edges treatment.

Current Density distribution along the human head

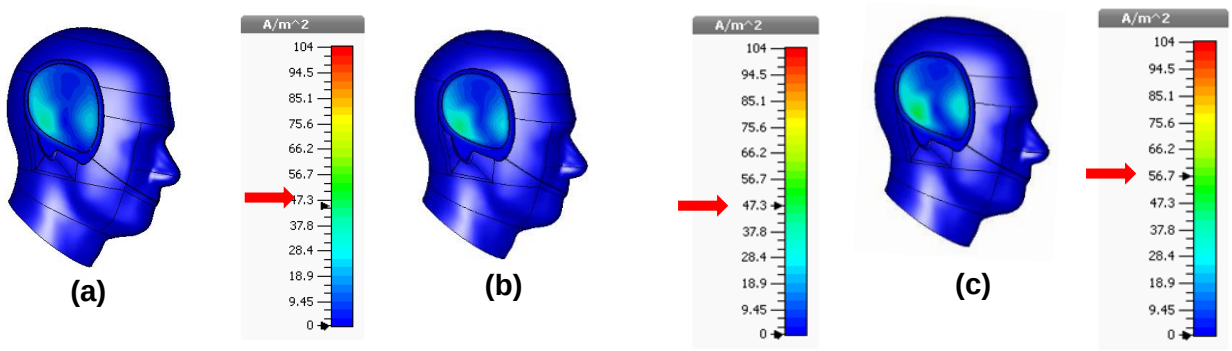

Figure 61 Current distribution along the human head with: U-edges (a), L-edges (b), and V-edges (c).

The peak current distribution along human head is presented in (Figure 61). It is shown that the maximum current distribution along human head is reduced from 104A/m^2 to 45A/ m^2, 47.3A/m^2, and 56.7A/ m^2 with U, V, and L-edges, respectively.

SAR distribution along the human head

The peak SAR distribution along human head is presented in (Figure 62). It is indicated that the peak SAR is reduced from 3.4W/Kg to 0.727 W/Kg (corresponding to 78.6% reduction of SAR), 0.755 W/Kg (corresponding to 77.79% reduction of SAR), 1.04 W/Kg(corresponding to 69.41% reduction of SAR) averaged over 10g mass tissue with U, V, and L-edge treatment, these values are much lower than the standard limit value.

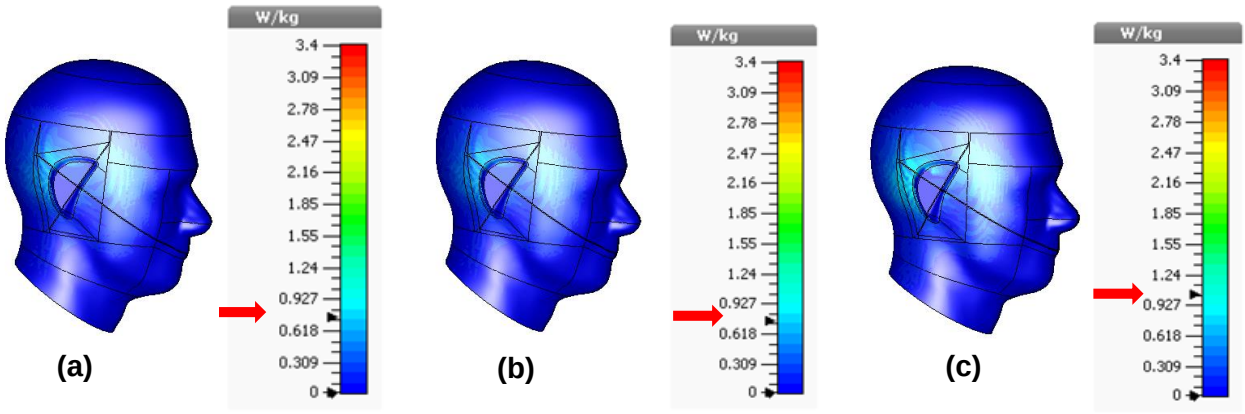

Figure 62 SAR distribution along the human head with: U-edges (a), L-edges (b), and V-edges (c).

From the results above, we can conclude that a U-edge is the best model for reducing the current density as well as the SAR; this is due to more suppressing of the surface wave along the ground plane, and more reduction of diffraction waves at these edges, which leads to less penetration of electric field toward human head. As a single band PIFA antenna with U-edges gives SAR value below the standard limit, the following sections examine the effect of this edge in case of dual band, and tri-band PIFA antenna.

III.4. Dual band PIFA Antenna

The dual band PIFA antenna is designed and simulated using CST-MWS and is operated at both bands GSM 900MHz and GSM 1800MHz for mobile application.

III.4.1. Design of conventional dual band PIFA antenna in free space

The dual band PIFA antenna consists of a ground plane, top radiating patch element, and shorting strip that are made of perfect electric conductor, in addition to a feeding 50Ω discrete port

as shown in (Figure 63). This antenna is designed with certain slots in the top radiating patch and a parasitic radiator to create dual band operation at 900MHz and 1800MHz. All the slots and spacers are made from vaccum with epsilon 1.

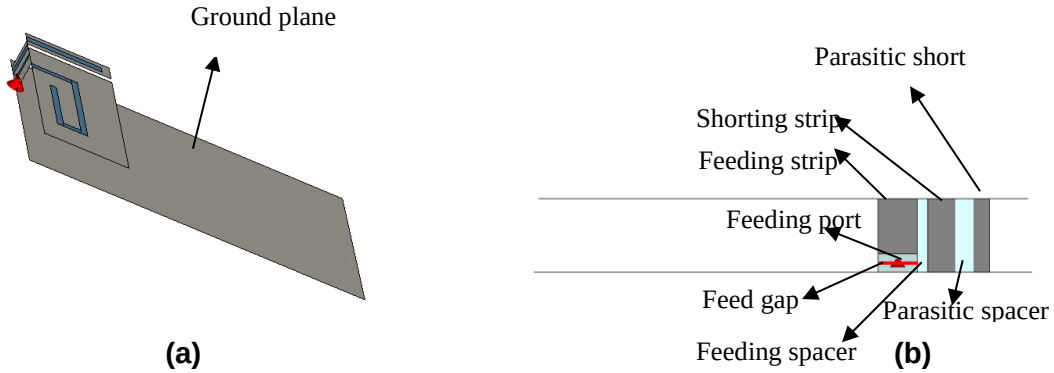

Figure 63 Geometrical structure of dual band PIFA antenna: Perspective view (a), and side view (b).

III.4.1.1. Simulation results

The simulation results of dual band PIFA antenna shows that this antenna can be applied in mobile handset operated at both bands GSM 900MHz and GSM 1800MHz due to the following results:

Return Loss parameter (S_{11})

The simulated reflection characteristic of the dual band PIFA antenna is shown in (Figure 64). The dual band PIFA antenna provides a resonance at 0.9GHz, and 1.8 GHz, thus it is well matched at those frequencies.

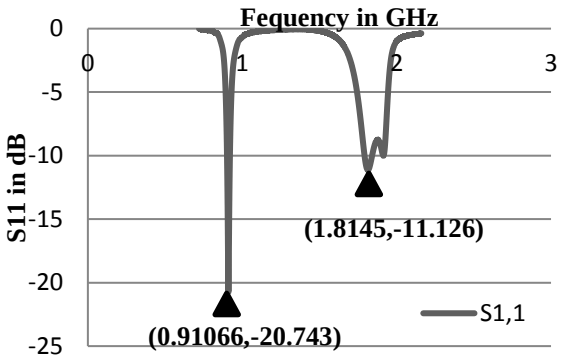

Figure 64 Graphical representation of S_{11} parameter.

3-D Radiation pattern

The three dimensional patterns are presented in (Figure 65). Its gain is equal to 2.06dB at GSM900 MHz, and 4.39dB at GSM1800 MHz.

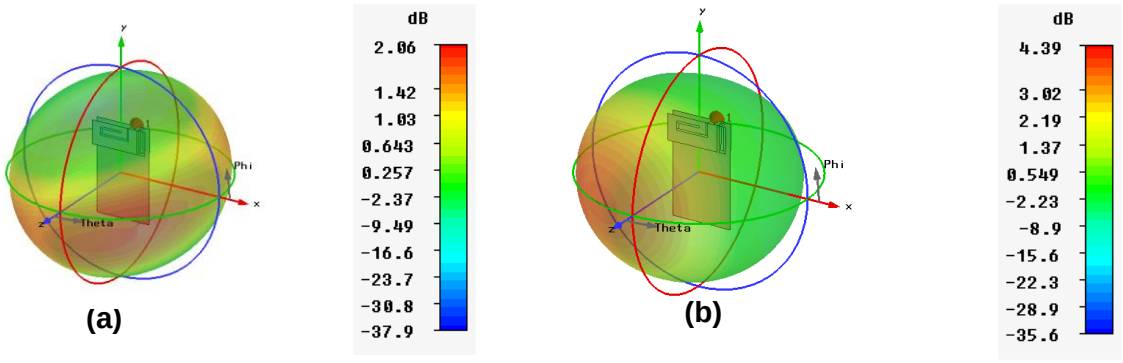

Figure 65 3D-representation of the gain of antenna at: 900MHz (a), and 1800MHz (b).

III.4.2. Design of conventional dual band PIFA Antenna in the vicinity of SAM human head model

The conventional dual band PIFA antenna is positioned at a distance 5mm from the SAM human head model as shown in (Figure 66). The dielectric properties of the fluid SAM phantom head at both bands GSM 900MHz and GSM 1800MHz is presented in (Table III-2) [75].

Table III-2 Dielectric properties of the fluid of SAM phantom both bands GSM 900MHz and GSM 1800MHz.

	Tissue Types & Frequencies	ε'_r	σ_{eff}
SAM phantom head	**Fluid @ 900 MHz**	41.5	0.97
	Fluid @ 1800 MHz	40	1.4

Figure 66 Geometrical structure of the dual band PIFA antenna in the vicinity of human head: Perspective view (a), and Top view (b).

III.4.2.1. Simulation results

The simulation results of dual band PIFA antenna are presented as follows:

Return Loss parameter (S_{11})

The simulated reflection characteristic of the dual-band PIFA antenna in the vicinity of human head is shown in (Figure 67).

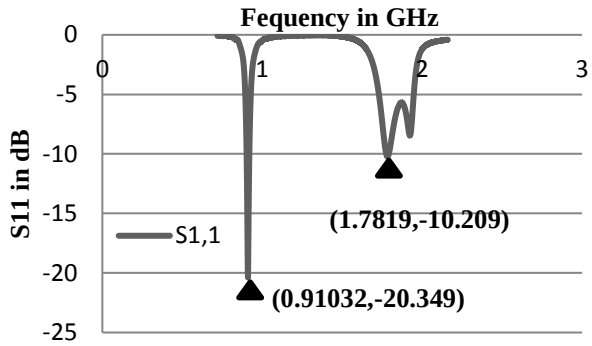

Figure 67 Graphical representation of S_{11} parameter.

3-D Radiation pattern

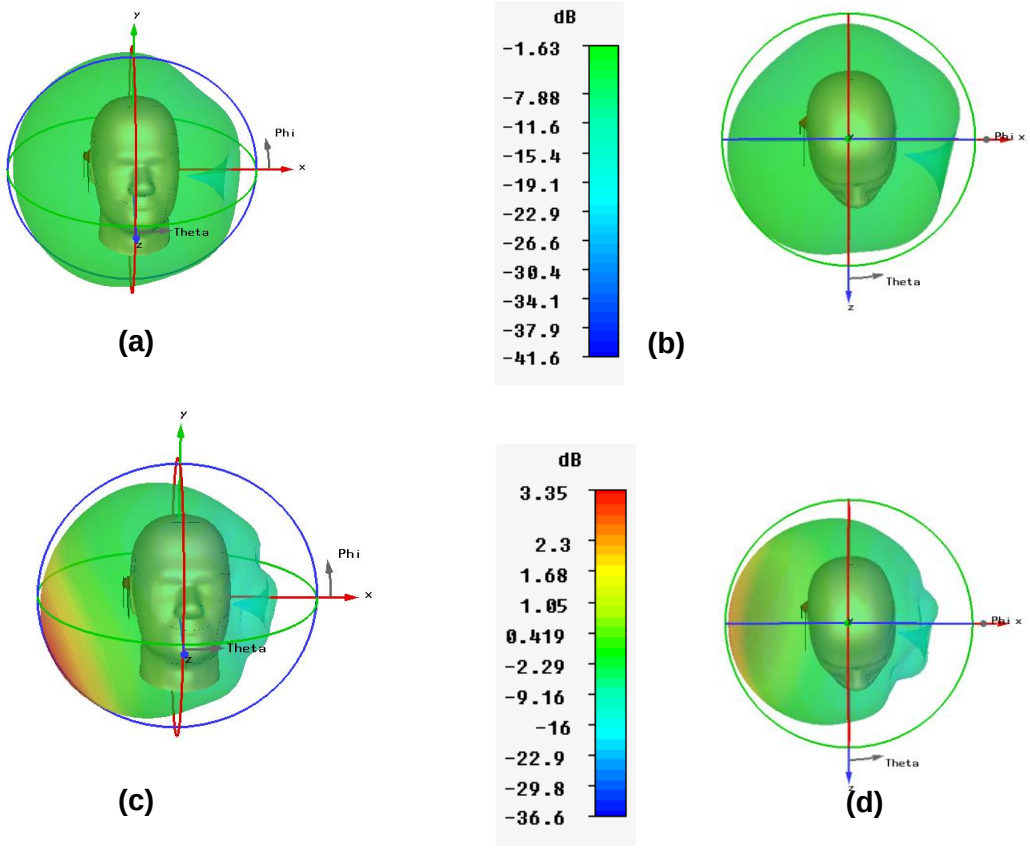

Figure 68 3D-representation of the gain of antenna: perspective view at 900MHz and 1800MHz (a) and (c), Top view at 900MHz and 1800MHz (b) and (d).

The three dimensional patterns are presented in (Figure 68). Its gain is equal to -1.63dB at GSM900MHz, and 3.35dB at GSM1800MHz.

Surface Current distribution along the ground plane

The maximum peak surface current distribution along the ground plane of antenna when placed in the vicinity of human head is presented in (Figure 69). It is shown that the maximum surface current is equal to 4 A/m at GSM900MHz, and 6 A/m at GSM1800MHz.

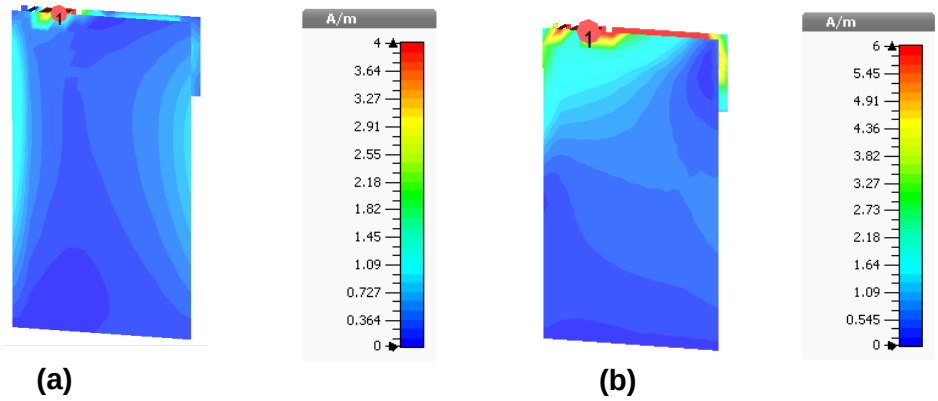

Figure 69 Surface Current distribution along the backside of ground plane at: 900MHz (a), and 1800MHz (b).

Current Density distribution along the human head

The peak current distribution along human head is presented in (Figure 70). It is shown that the maximum current occurs at ear position where it is equal to 121 A/m^2 at GSM900MHz, and 111 A/m^2 at GSM1800MHz.

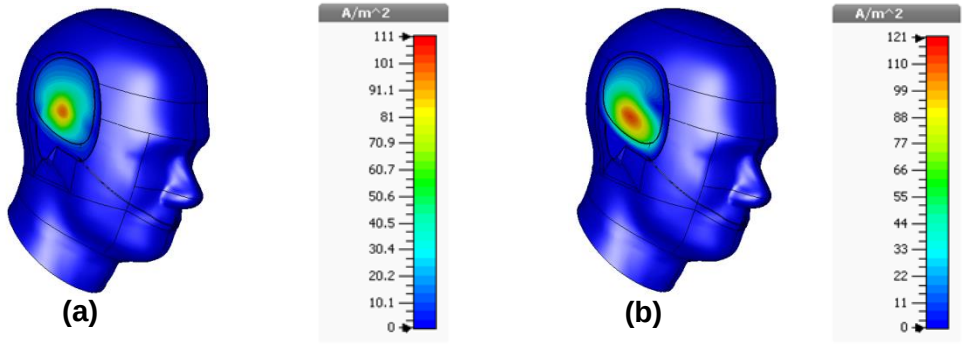

Figure 70 Current density distribution along the human head at: 900MHz (a), and 1800MHz (b).

SAR distribution along the human head

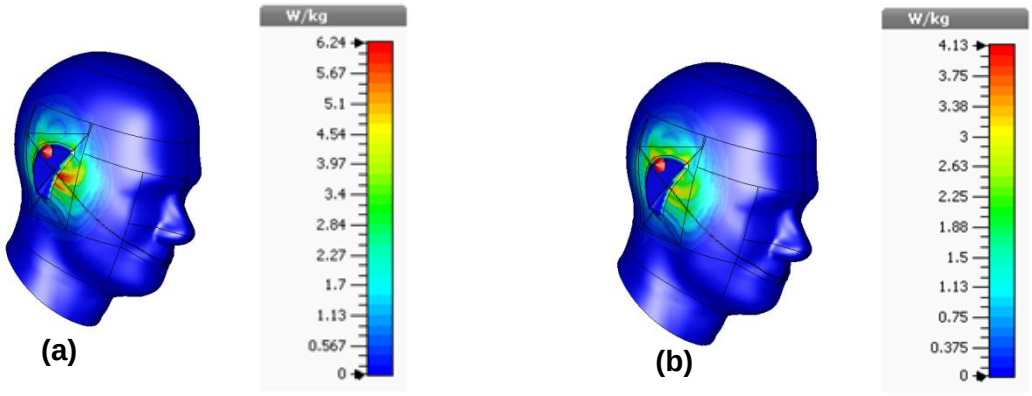

Figure 71 SAR distribution along the human head at 900 MHz: 900MHz (a), and 1800MHz (b).

The peak SAR distribution along human head is presented in (Figure 71). It is indicated that the peak SAR is higher than the standard limit value; it is equal to 6.24W/Kg at GSM900MHz, and equal to 4.1324W/Kg at GSM1800MHz averaged over 10 g mass tissues.

III.4.3. Design of proposed dual band PIFA antenna in the vicinity of human head when the U-edge groove is below the ground plane

The proposed dual band PIFA antenna with U-edge treatment at each corner of the ground plane as shown in (Figure 72) is positioned at a distance 5mm from the SAM human head model as presented in (Figure 73). The dielctric properties of the fluid SAM phantom head at both bands GSM 900MHz and GSM 1800MHz are indicated in previous section (section III.4.2., Table III-2).

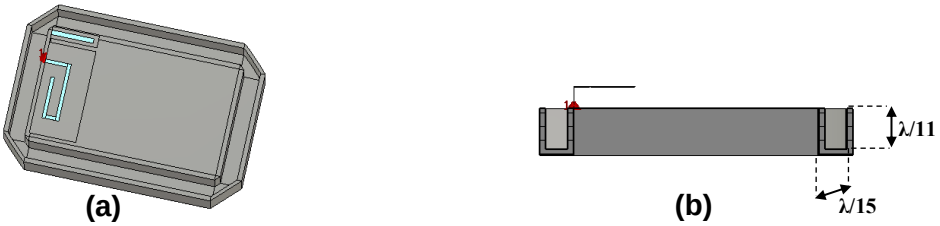

Figure 72 Geometrical structure of dual band PIFA antenna with U-edges: Perspective view (a), and Top view (b).

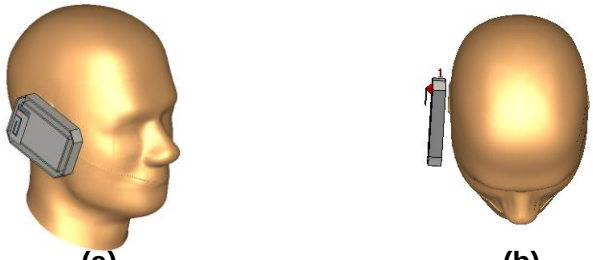

Figure 73 Geometrical structure of dual band PIFA antenna in the vicinity of human head with U-edges Perspective view (a), and Top view (b).

III.4.3.1. Simulation results

The following simulation results of the proposed dual band PIFA antenna indicates that the U-edges treatment at each corner of ground plane will not affect the performance of antenna as presented below, and grear reduction of SAR occurs.

Return Loss parameter (S_{11})

The simulated reflection characteristic of the dual-band PIFA antenna with U-edges treatment placed in the vicinity of human head is shown in (Figure 74).

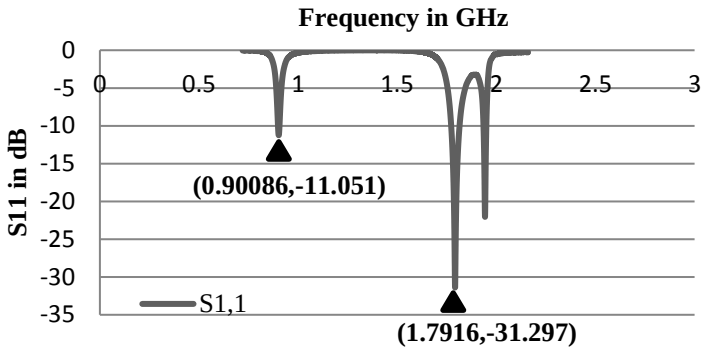

Figure 74 Graph representation of S_{11} parameter.

3-D Radiation pattern

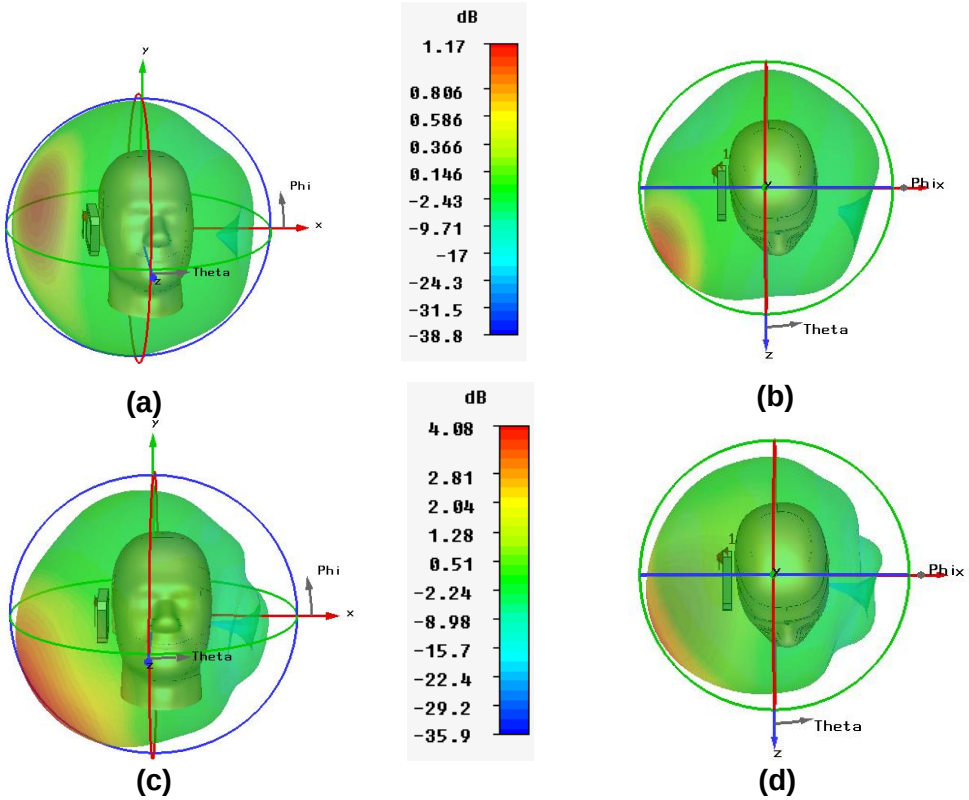

Figure 75 3D-representation of the gain of antenna: perspective view at 900MHz and 1800MHz (a) and (c), Top view at 900MHz and 1800MHz (b) and (d).

The three dimensional patterns are presented in (Figure 75). Its gain is equal to 1.17dB at GSM900MHz, and equal to 4.08dB at GSM1800MHz.

Surface Current distribution along the ground plane

The maximum peak surface current distribution along the ground plane of dual-band antenna with U-edges when placed in the vicinity of human head is presented in (Figure 76). It is shown that the maximum surface current is reduced from 4 A/m, and 6 A/m (without edges treatment) at GSM900MHz and GSM1800MHz, respectively to be approximately zero along the ground plane when the U-edges are inserted.

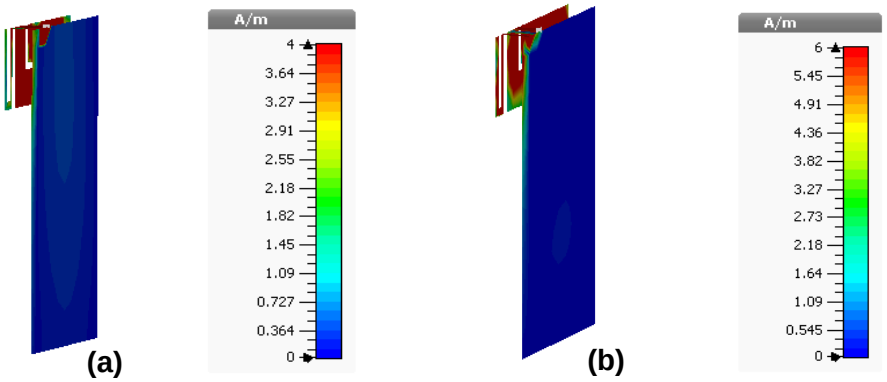

Figure 76 Surface Current distribution along the backside of ground plane at: 900MHz (a), and 1800MHz (b).

Current Density distribution along the human head

The peak current distribution along human head is presented in (Figure 77). It is shown that the maximum current density is reduced from 121 A/m^2 to 63.6 A/m^2 at GSM900MHz, and is reduced from 111 A/m^2 to 43.2 A/m^2 at GSM1800MHz for the proposed antenna.

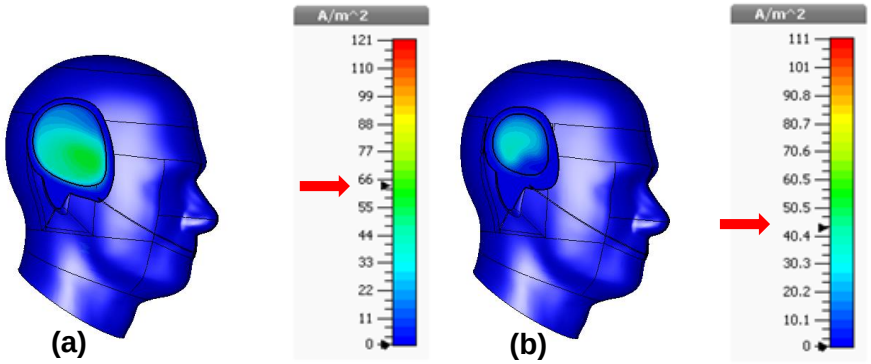

Figure 77 Current density distribution along the human head at: 900MHz (a), and 1800MHz (b).

SAR distribution along the human head

The peak SAR distribution along human head is presented in (Figure 78). It is indicated that the peak SAR is reduced from 6.24W/Kg to 1.8W/Kg(corresponding to 71.15% reduction of SAR) at GSM900MHz and from 4.13W/Kg to 0.798W/Kg (corresponding to 80.67% reduction of SAR) at GSM1800MHz averaged over 10 g mass tissues.

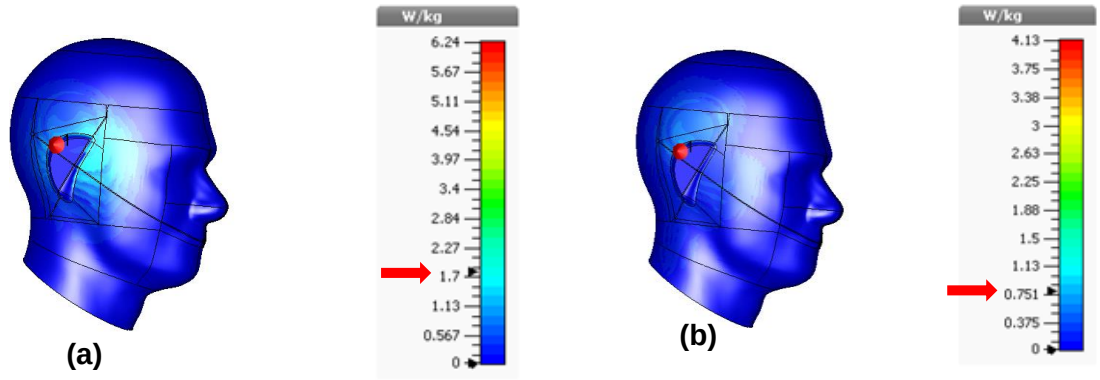

Figure 78 SAR distribution along the human head at: 900MHz (a), and 1800MHz (b).

III.5. Tri-band PIFA Antenna

The Tri-band PIFA antenna is designed and simulated using CST-MWS, and is operated at the following bands GSM 900MHz, GSM 1800MHz, and 2400MHz for mobile application.

III.5.1. Design of conventional Tri-band PIFA antenna in free space

The Tri-band PIFA antenna consists of a ground plane, top and bottom radiating patch element are made from copper (annealed), and are separated by a substrate that is made from material with epsilon equal to 3.4 and tanδ equal to 0.014, a shorting strip that is made from copper (annealed), and a feeding 50Ω coaxial cable as shown in (Figure 79). This antenna is designed with certain slots in the top and bottom of the radiating patch to create Tri-band operation at GSM 900MHz, GSM 1800MHz, and 2400MHz. Four vias that are made from copper are inserted in the radiating patch.

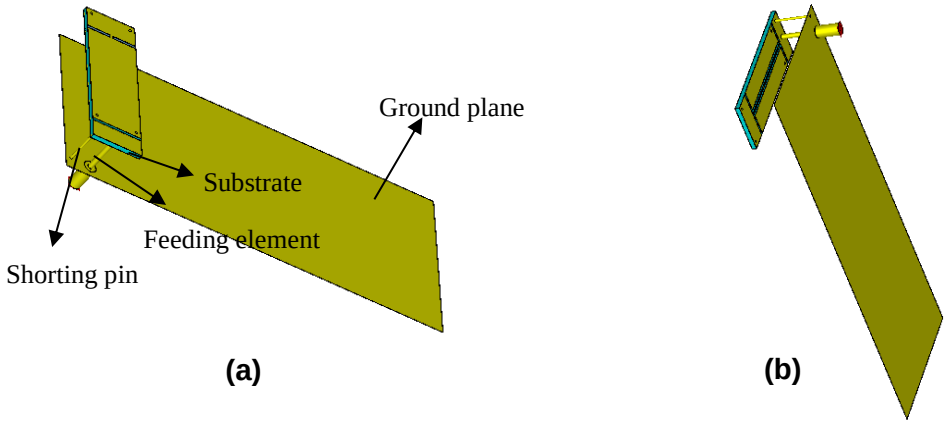

Figure 79 Geometrical structure of Tri band PIFA antenna: Perspective view (a), and Bottom view (b).

III.5.1.1. Simulation results

The simulation results of Tri-band PIFA antenna is presented in the following sections:

Return Loss parameter (S11)

The simulated reflection characteristic of Tri-band PIFA antenna is shown in (Figure 80).

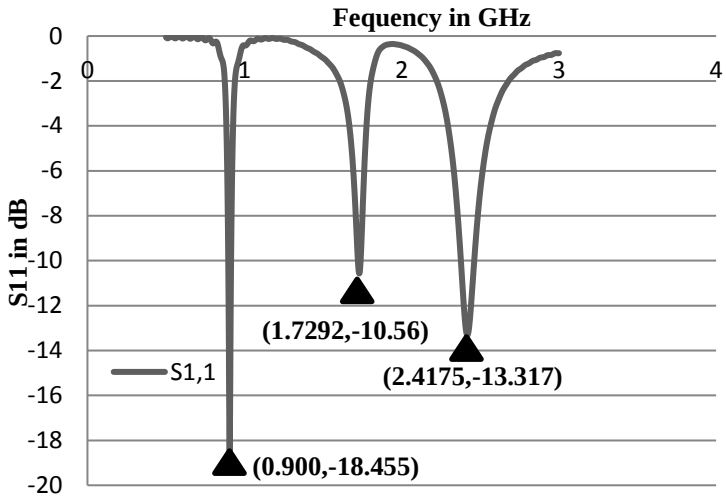

Figure 80 Geometrical structure of Tri band PIFA antenna: Perspective view (a), and Bottom view (b).

3-D Radiation pattern

The three dimensional patterns of the gain of antenna are presented in (Figure 81). Its gain is equal to 0.398dB at GSM900 MHz, 1.41dB at GSM1800MHz, and 3.38dB at 2400MHz .

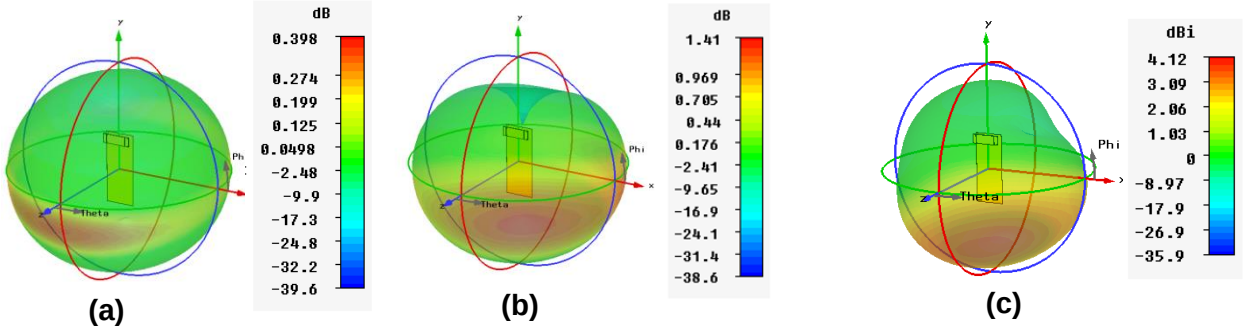

Figure 81 3D-representation of the gain of antenna: perspective view at: 900MHz (a), 1800MHz (b) and 2400MHz (c).

III.5.2. Design of conventional Tri-band PIFA Antenna in the vicinity of SAM human head model

The conventional Tri-band PIFA antenna is positioned at a distance 5mm from the SAM human head model as shown in (Figure 82). The dielectric properties of the fluid SAM phantom

head at the following bands GSM 900MHz, GSM 1800MHz, and 2400MHz is presented in (Table III-3) [76].

Table III-3 Dielectric properties of the fluid of SAM phantom both bands GSM 900MHz, GSM 1800MHz, and 2400MHz.

	Tissue Types & Frequencies	ε'_r	σ_{eff}
SAM phantom head	**Fluid @ 900 MHz**	41.5	0.97
	Fluid @ 1800 MHz	40	1.4
	Fluid @ 2400MHz	39.2	1.8

Figure 82 Geometrical structure of Tri band PIFA antenna in the vicinity of human head with U-edges: Perspective view (a), and Bottom view (b).

III.5.2.1. Simulation results

The simulation results of Tri-band PIFA antenna in the vicinity of human head is presented below:

Return Loss parameter (S11)

The simulated reflection characteristic of the Tri-band PIFA antenna in the vicinity of human head is shown in (Figure 83).

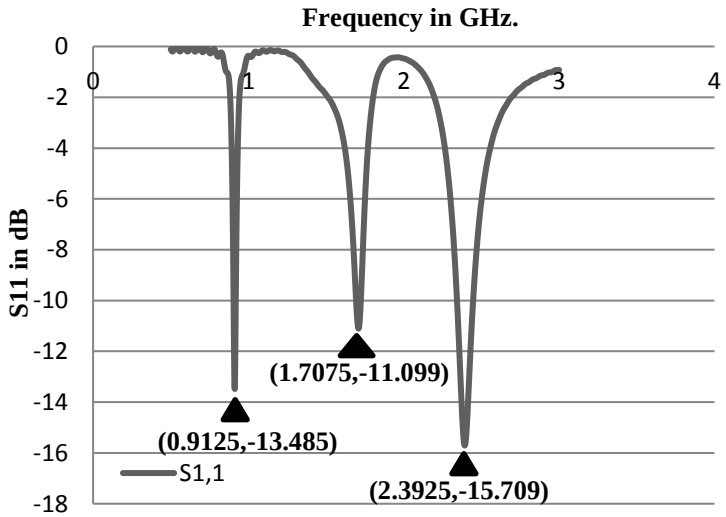

Figure 83 Graphical representation of S_{11} parameter.

3-D Radiation pattern

The three dimensional patterns are presented in (Figure 84). Its gain is equal to -3.28dB at GSM 900MHz, 2.93dB at GSM 1800MHz, and 4.3dB at GSM 2400MHz.

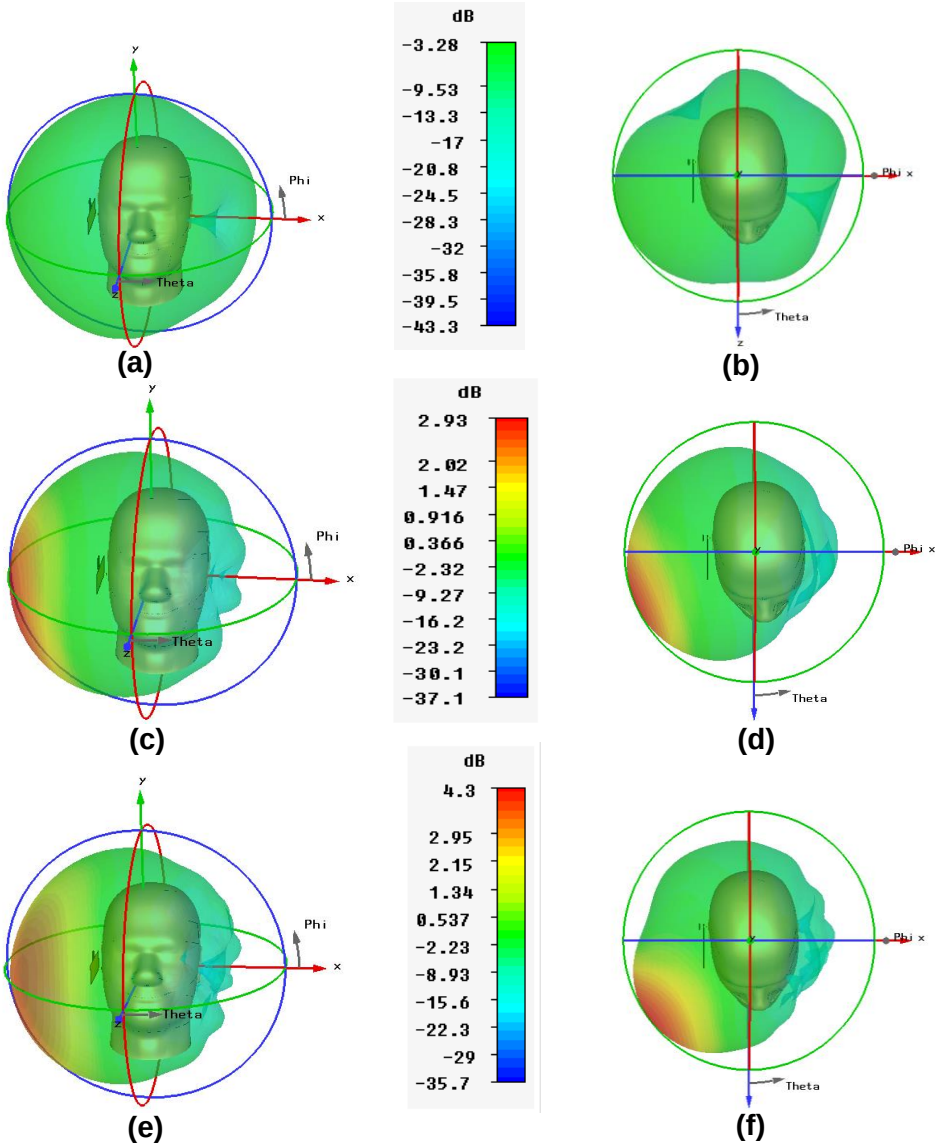

Figure 84 3D-representation of the gain of antenna: perspective view at 900MHz, 1800MHz and 2400MHz (a), (c) and (e), Top view at 900MHz, 1800MHz and 2400MHz (b),(d) and (f).

Surface Current distribution along the ground plane

The maximum peak surface current distribution along the ground plane of antenna when placed in the vicinity of human head is presented in (Figure 85). It is shown that the maximum surface current is equal to 6 A/m at GSM900MHz, 5 A/m at GSM1800MHz, and it is 6 A/m at GSM2400 MHz.

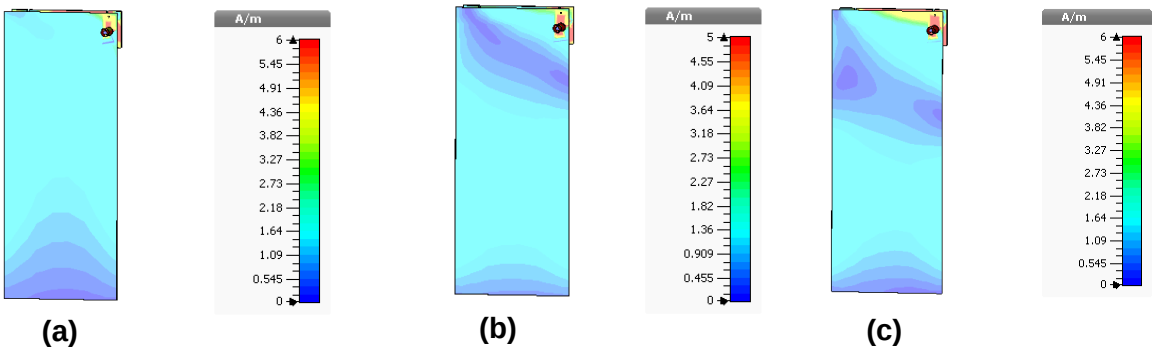

Figure 85 Surface Current distribution along the backside of ground plane at: 900MHz (a), 1800MHz (b) and 2400MHz (c).

Current Density distribution along the human head

The peak current distribution along human head is presented in (Figure 86). It is shown that the maximum current occurs at ear position where it is equal to 59 A/m^2 at GSM900MHz, 92 A/m^2 at GSM1800MHz, and 89 A/m^2 at GSM2400MHz.

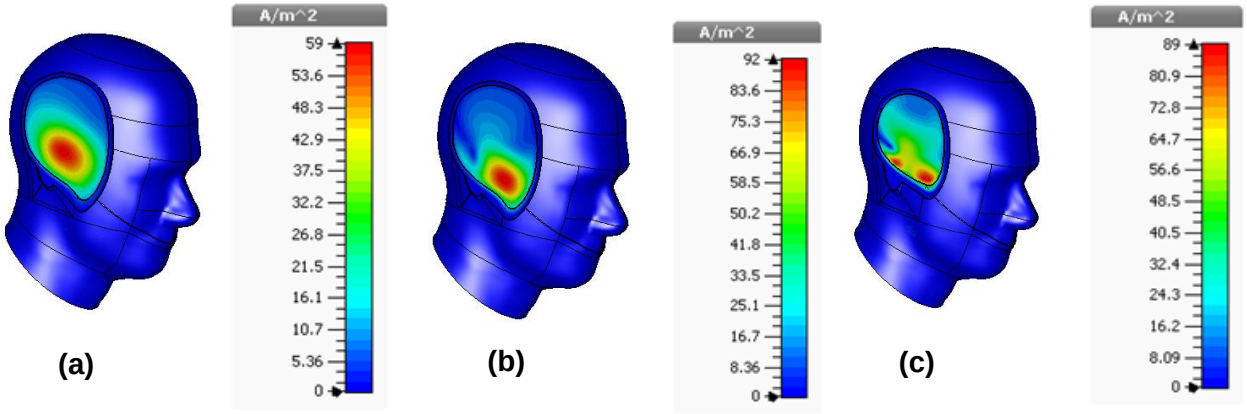

Figure 86 Current density distribution along the human head at: 900MHz (a), 1800MHz (b) and 2400MHz (c).

SAR distribution along the human head

The peak SAR distribution along human head is presented in (Figure 87). It is indicated that the peak SAR is higher than the standard limit value; it is equal to 4.07W/Kg at GSM900MHz, 3.82W/Kg at GSM1800MHz , and 2.65W/Kg at 2400 MHz averaged over 10 g mass tissues.

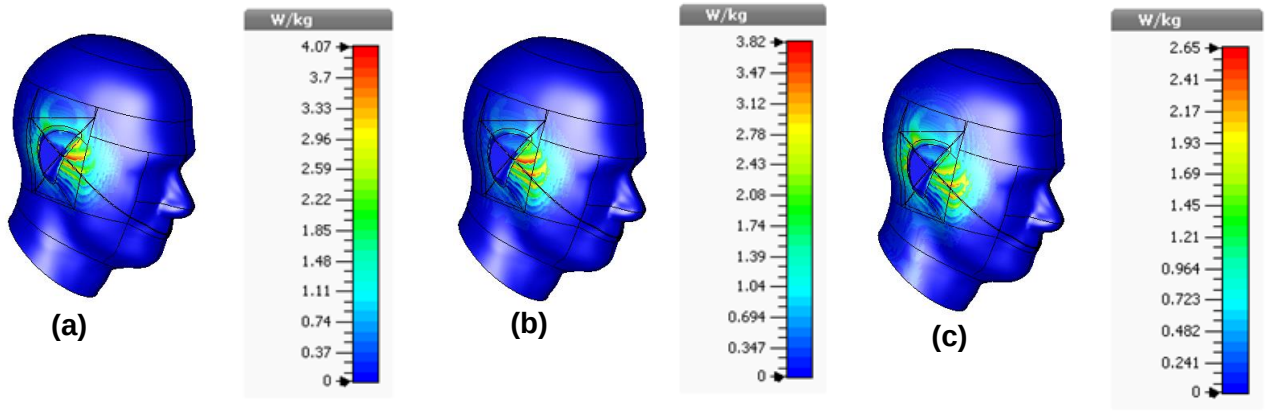

Figure 87 SAR distribution along the human head at: 900MHz (a), 1800MHz (b) and 2400MHz (c).

III.5.3. Design of proposed Tri- band PIFA antenna in the vicinity of human head when the U-edge groove is below the ground plane

The proposed Tri-band PIFA antenna with U-edge treatment at each corner of the ground plane as shown in (Figure 88) is positioned at a distance 5mm from the SAM human head model as presented in (Figure 89). The dielectric properties of the fluid SAM phantom head at three bands GSM 900MHz, GSM 1800MHz, and 2400MHz are indicated in the previous (section III.5.2., Table III-3).

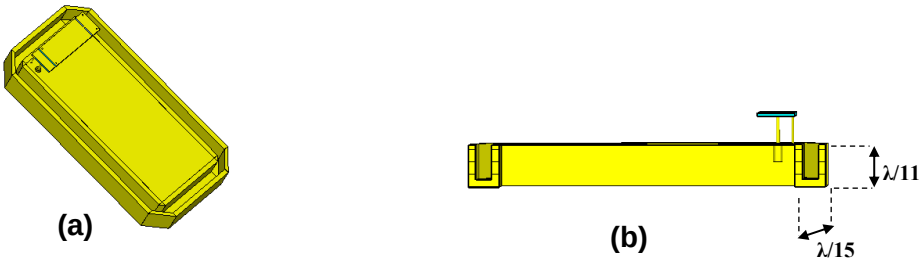

Figure 88 Geometrical structure of Tri band PIFA antenna with U-edges: Perspective view (a), and Side view (b).

Figure 89 Geometrical structure of Tri band PIFA antenna with U-edges in the vicinity of human head: Perspective view (a), and Top view (b).

III.5.3.1. Simulation results

The following simulation results of the proposed Tri-band PIFA antenna indicates that the U-edges treatment at each corner of ground plane will not have any influence on the performance of antenna, in addition to perfect reduction of SAR.

Return Loss parameter (S_{11})

The simulated reflection characteristic of the Tri-band PIFA antenna with U-edges treatment placed in the vicinity of human head is shown in (Figure 90).

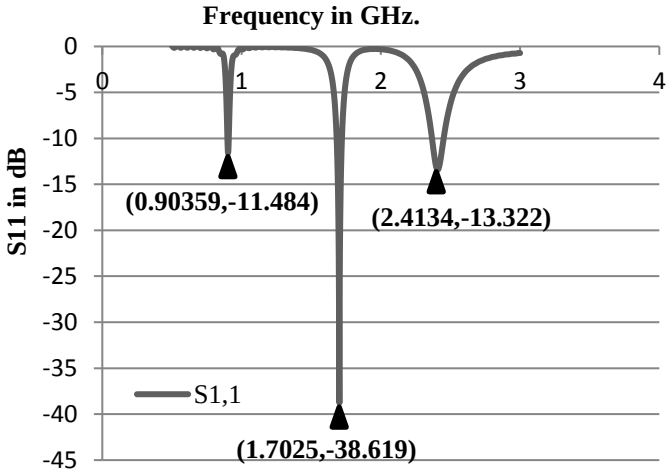

Figure 90 Graph representation of S_{11} parameter.

3-D Radiation pattern

The three dimensional patterns are presented in (Figure 91). Its gain is equal to 3.1dB at GSM 900MHz, 4.03dB at GSM 1800MHz, and 5.22dB at GSM 2400MHz.

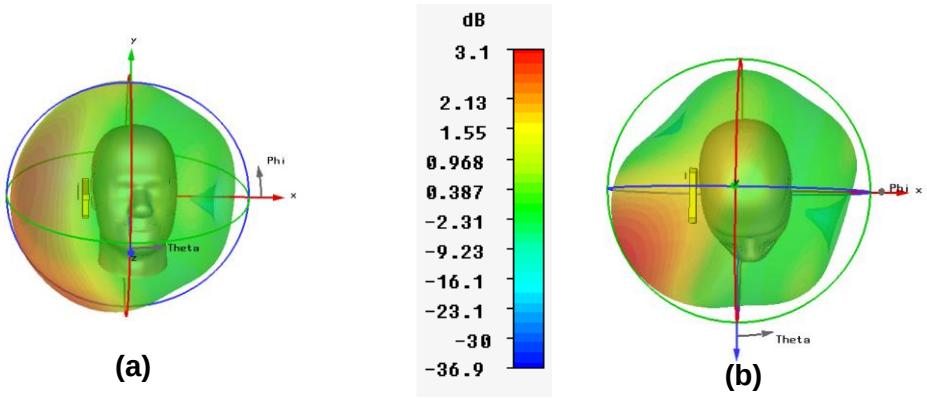

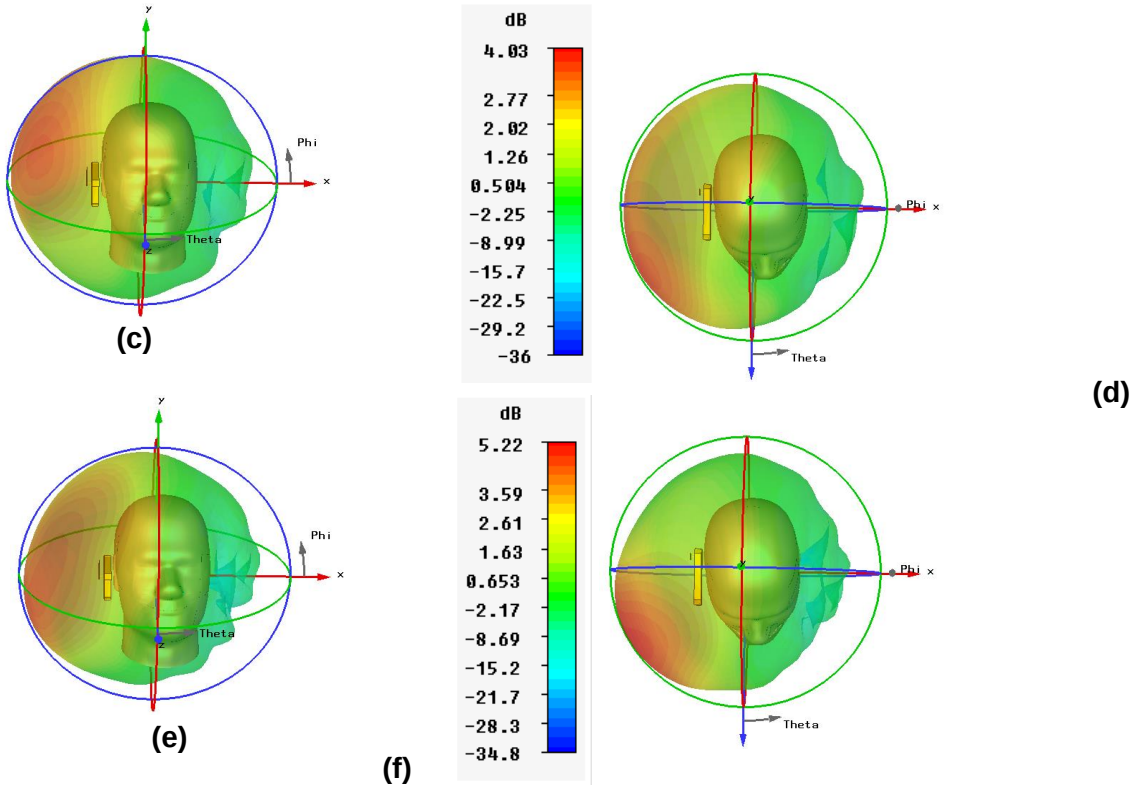

Figure 91 3D-representation of the gain of antenna: perspective view at 900MHz, 1800MHz and 2400MHz (a), (c) and (e), Top view at 900MHz, 1800MHz and 2400MHz (b),(d) and (f).

Surface Current distribution along the ground plane

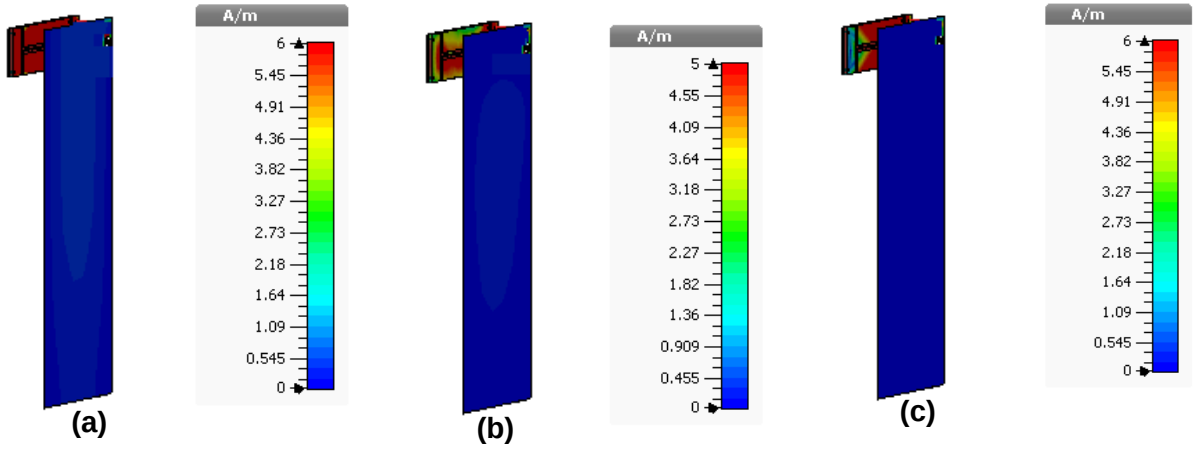

Figure 92 Surface Current distribution along the backside of ground plane at: 900MHz (a), 1800MHz (b) and 2400MHz (c).

The maximum peak surface current distribution along the ground plane of Tri-band antenna with U-edges when placed in the vicinity of human head is presented in (Figure 92). It is shown that the maximum surface current is reduced from 6 A/m, 5 A/m, and 6 A/m (without edges treatment) at GSM900MHz, GSM1800MHz, and GSM2400MHz respectively to be approximately zero along the ground plane when the U-edges are inserted.

Current Density distribution along the human head

The peak current distribution along human head is presented in (Figure 93). It is shown that the maximum current is reduced from 59 A/m^2, 92 A/m^2, and 89 A/m^2 to 44 A/ m^2, 29 A/m^2, and 53 A/m^2 at GSM 900 MHz, GSM 1800 MHz, and GSM 2400 MHz, respectively.

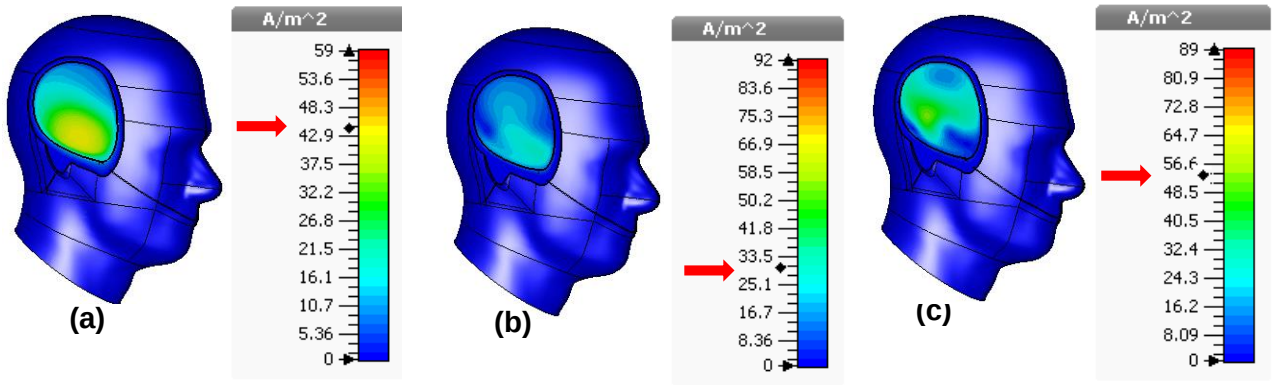

Figure 93 Current density distribution along the human head at: 900MHz (a), 1800MHz (b) and 2400MHz (c).

SAR distribution along the human head

The peak SAR distribution along human head is presented in (Figure 94). It is indicated that the peak SAR is reduced from 4.07W/Kg, 3.82W/Kg, and 2.65W/Kg to 1.46W/Kg (corresponding to 71.15% reduction of SAR), 0.433W/Kg (corresponding to 88.66% reduction of SAR), and 0.917W/Kg (corresponding to 65.66% reduction of SAR) at GSM900MHz, GSM1800MHz, and 2400 MHz, respectively averaged over 10g mass tissue.

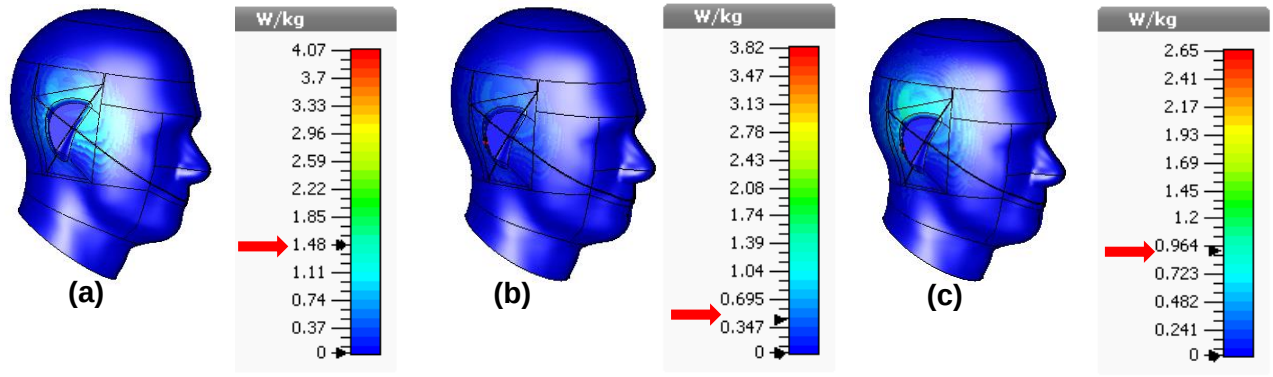

Figure 94 SAR distribution along the human head at: 900MHz (a), 1800MHz (b) and 2400MHz (c).

All the above results verify the ability of U-shape edge-groove to null the distribution of the surface current density along the ground plane of antenna, thus less propagation of electromagnetic

waves toward human head occurs, leading to a great reduction in current density along the human head that has a great correlation with SAR.

After the above scenario, a method based on liquid material was investigated to predict if lower SAR with better performance than the above investigation method can be achieved. This method is based on U-shape edge groove that is inserted below each corner of the ground plane, being made of an absorbing material such as: salty water instead of PEC. Although the liquid antenna is considered the most advanced technology, till now there isn't shown any study done on liquid antenna to be applied in mobile application.

III.5.4. Design of Single-band PIFA Antenna with U-edges made of salty water in the vicinity of SAM human head model

In this section, we propose to make the U-edges of previous discussed single-band PIFA antenna (section-III.3.) to be made of liquid (salty water) that acts an absorbing material having dielectric properties (ε_r=74, σ=11 S/m) as presented in (Figure 95). The proposed antenna is operated at 1800MHz, and placed at a distance 5mm from the SAM human head phantom as shown in (Figure 96) with the same dielectric properties as presented in (chapter II, Table II-1).

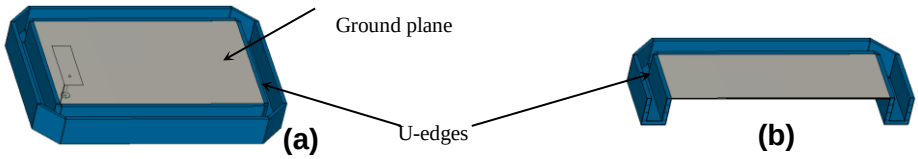

Figure 95 Perspective view of the geometrical structure of the proposed single band PIFA antenna: Perspective view (a), and Side view (b).

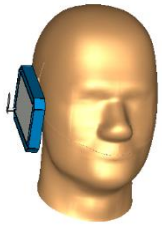

Figure 96 Perspective view of the geometrical structure of the proposed single band PIFA antenna in the vicinity of human head.

III.5.4.1. Simulation results

The simulation results of the insertion of water U-edge grooves to the ground plane of antenna is presented below:

Parametric Study

In this paragraph, we perform a parametric study in the purpose of optimizing the dimensions of the U-shaped wall by sweeping its height in order to obtain the lowest SAR values. (Table III-4) summarize the results obtained for the single band low SAR PIFA antenna, in terms of peak SAR and peak current density.

Table III-4 Results while sweeping the height of single band low SAR antenna

	H (mm)	
	λ/11	***λ/20***
Peak SAR (W/Kg)	0.9	1.6
Peak Current Density (A/m^2)	35.1	40.17

Results show that as the height decreases, the peak current density increases, which in turn leads to SAR increase. This confirms the operation of the U-edges added as an extension of the ground plane, which are responsible for reducing the near electromagnetic fields and therefore the reduction of the SAR on the human head. The more the height of these edges is, the more important is the fields reduction and therefore the less is the SAR. We choose the value of H= λ/11 as an optimal height dimension of the U-edge wall that gives a sufficiently low SAR.

Return Loss parameter (S11)

The simulated reflection characteristic of the single band PIFA antenna with U-edges made of salty water at each corner of the ground plane is shown in (Figure 97). The Graph below shows the comparison between proposed antenna, and the conventional antenna that is presented in (Chapter II, section II.4.2.).

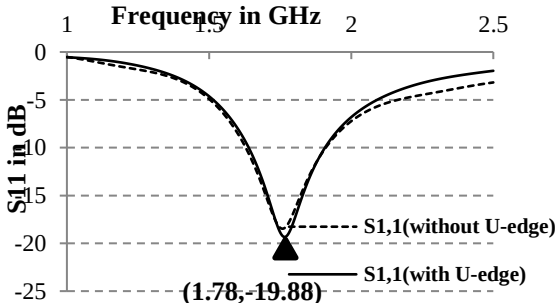

Figure 97 Graphical comparison representation of S_{11} parameter between proposed (with U-edges) and conventional (without U-edges) antennas.

Polar Plot of the Radiation pattern

The comparison between proposed (with U-edges) and conventional (without U-edges) antennas in terms of gain is presented in (Figure 98). Its gain is equal to 2.32dB in comparison to conventional antenna where the gain is equal to 5.33dB.

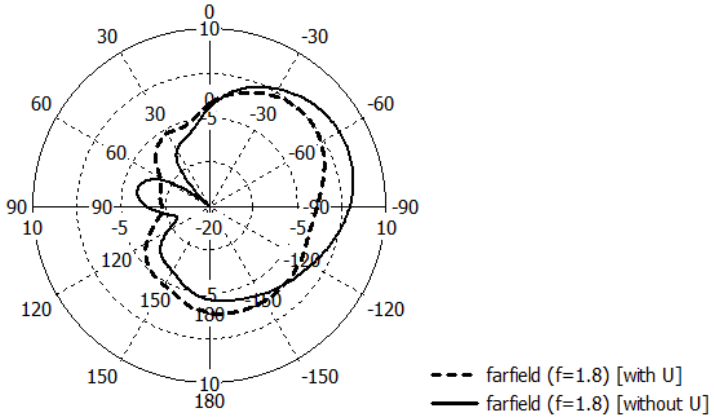

Figure 98 Polar plot of the gain of proposed (with U-edges) and conventional (without U-edges) antenna in the vicinity of human head at 1800 MHz.

Current Density distribution along the human head

The comparison between proposed and conventional antennas in terms of peak current distribution along human head is presented in (Figure 99). Simulation results indicate that the peak current density is tremendously reduced from 104 A/m^2 to 35.1 A/m^2. Moreover, the conduction current is no more concentrated near the ear and becomes distributed evenly with less concentration after insertion of the water U-edges behind the ground plane.

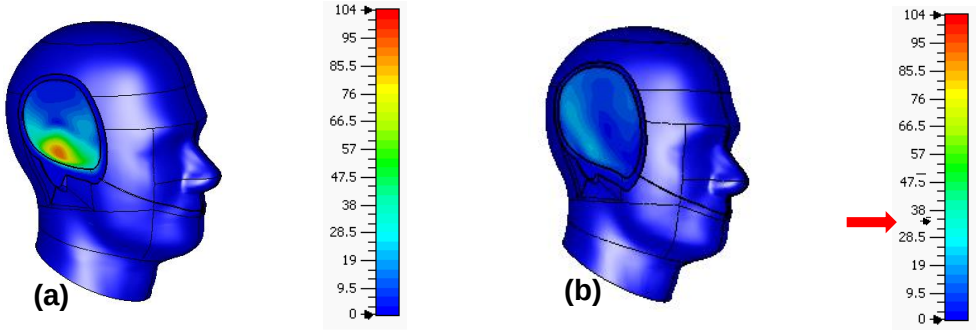

Figure 99 Current density distribution along the human head of: Conventional antenna (a), and Proposed antenna (b).

SAR distribution along the human head

The reduction in the current distribution is translated into an important reduction in the SAR, as depicted in (Figure 100). It can be observed that the peak SAR averaged over 10g mass tissue is reduced from 3.4 W/Kg to 0.9 W/Kg, which corresponds to 73.52% reduction of SAR. This can be

explained by the fact that the insertion of water U-edges is responsible for absorbing, reflecting and refracting the electromagnetic wave that is propagating toward the human head, which in turns leads to a reduction in current density as well as SAR on the human head.

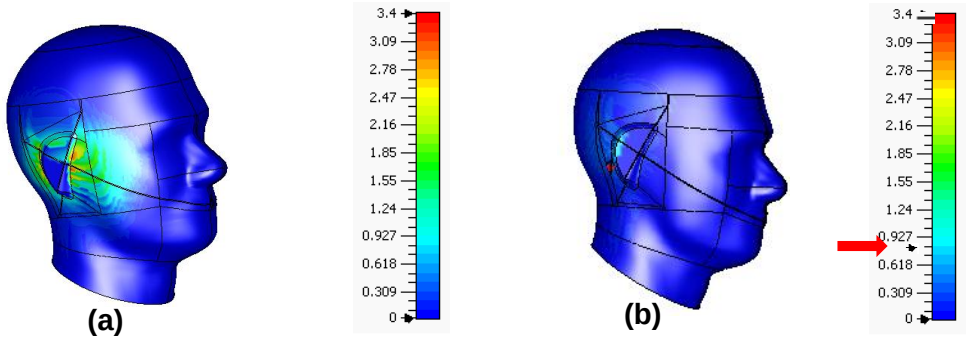

Figure 100 SAR distribution along the human head of: Conventional antenna (a), and Proposed antenna (b).

III.5.5. Design of dual band PIFA Antenna with U-edges made of salty water in the vicinity of SAM human head model

We apply the same concept as before on a dual band PIFA antenna operating at 900MHz and 1800MHz, as shown in (Figure 101), where a water U-shaped extension is added on the back side of the antenna. This proposed antenna is placed at a distance 5mm from the SAM human head phantom as shown in (Figure 102) with the same dielectric properties as presented in (Table III-2).

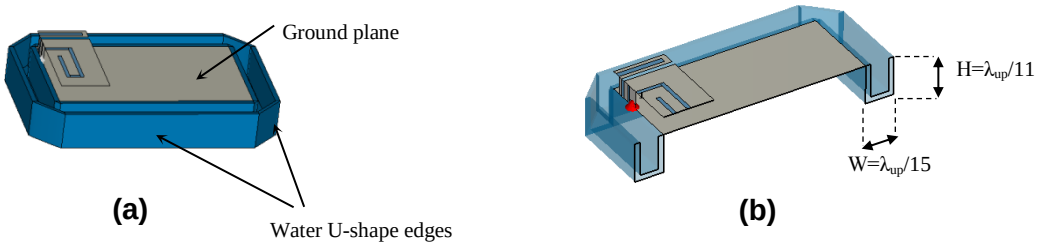

Figure 101 Perspective view of the geometrical structure of the proposed dual band PIFA antenna: Perspective view (a), and Side view (b).

Figure 102 Perspective view of the geometrical structure of the proposed dual band PIFA antenna in the vicinity of human head.

III.5.5.1. Simulation results

The performance of the antenna in terms of radiation and impedance matching is not affected by the presence of the water U-edge around the ground plane in the vicinity of human head as shown in the following results, so that the suggested antenna can be applied in mobile application.

Parametric Study

We also perform a parametric study to optimize the dimensions of the U-shaped wall by sweeping its height for obtaining lowest SAR values. (Table III-5) summarize the results obtained for the dual band low SAR PIFA antenna, in terms of peak SAR and peak current density.

Table III-5 Results while sweeping the height of dual band low SAR antenna.

		H (mm)	
		λ_{up} /11	λ_{up} /20
900 MHz	Peak Current Density	35	28.3
	Peak SAR (W/Kg)	0.7	1.18
1800 MHz	Peak Current Density	32	23
	Peak SAR (W/Kg)	0.4	0.51

Return Loss parameter (S_{11})

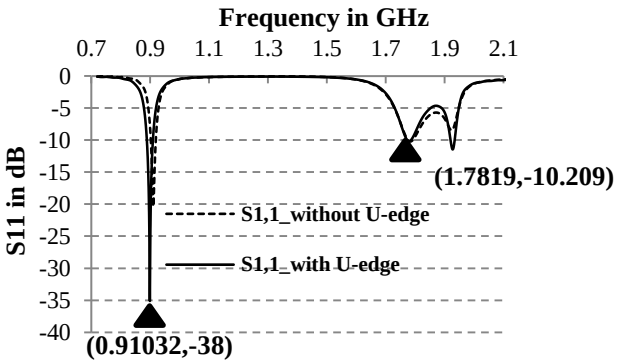

Figure 103 Graphical comparison representation of S_{11} parameter between proposed (with U-edges) and conventional (without U-edges) antennas.

The simulated reflection characteristic of the dual-band PIFA antenna with U-edges made of salty water at each corner of the ground plane is shown in (Figure 103). The Graph below shows the comparison between proposed antenna (with U-edges), and the conventional antenna (without U-edges) that is presented in (Section III.4.2.).

Polar Plot of the Gain of antennas

The comparison between proposed and conventional antennas in terms of gain is presented in (Figure 104). Its gain is equal to -1.11dB at 900MHz, and about 0.77dB at 1800MHz in comparison to conventional antenna where the gain is equal to -1.63dB at 900MHz, and about 3.35dB at 1800MHz.

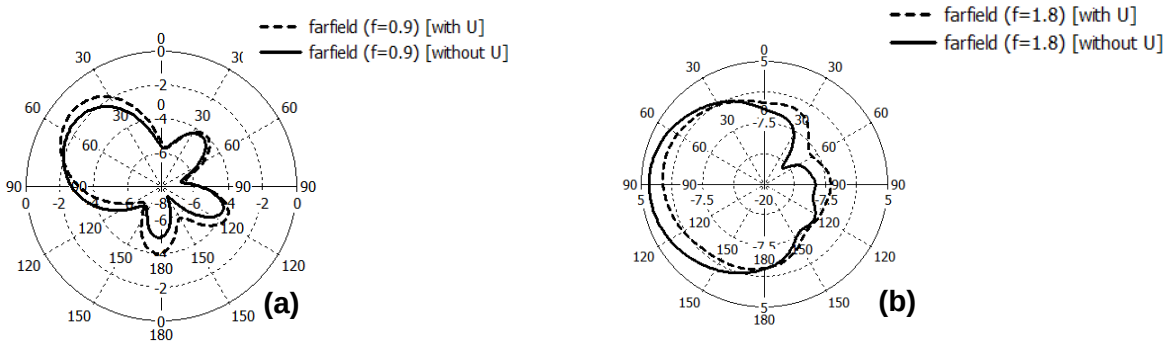

Figure 104 Polar plot of the gain of proposed (with U-edges) and conventional (without U-edges) antenna in the vicinity of human head at: 900MHz (a), and 1800 MHz (b).

Current Density distribution along the human head

The current distribution along the human head of the conventional dual band PIFA antenna and our proposed low SAR antenna respectively is presented in (Figure 105). Simulation Results indicate that the peak current density is reduced from 121 A/m^2 to 35 A/m^2 at 900 MHz, and it is reduced from 111 A/m^2 to 32 A/m^2 at 1800 MHz.

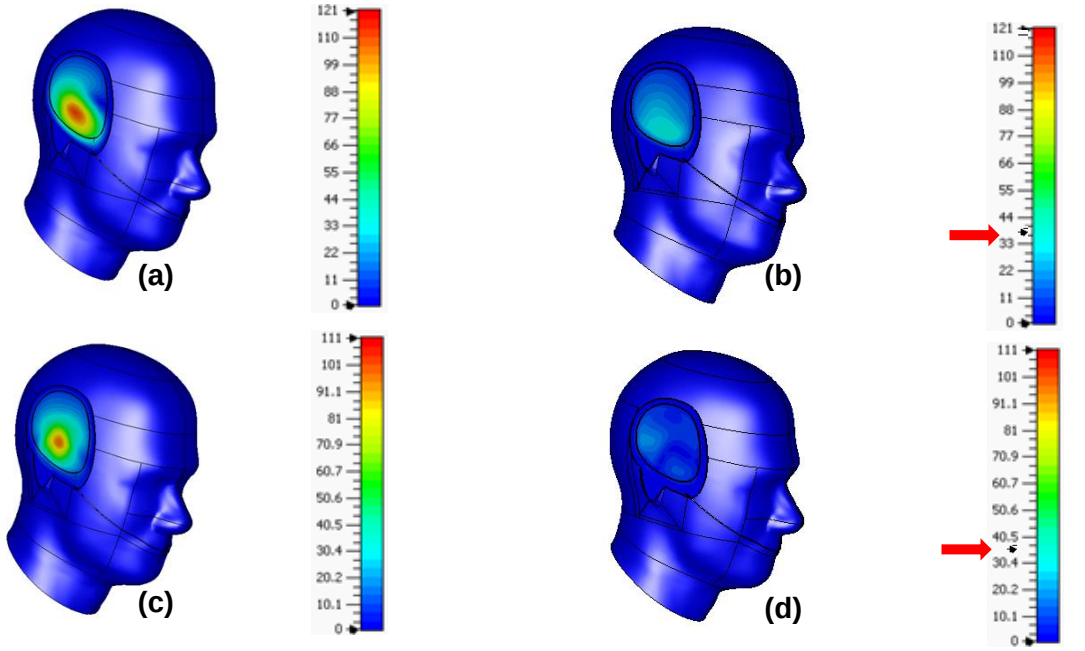

Figure 105 Current distribution along the human head of: Conventional antenna at 900MHz (a), and 1800MHz (c), and of Proposed antenna at 900MHz (b), and 1800MHz (d).

SAR distribution along the human head

The reduction in the current distribution is translated into an important reduction in the SAR, as depicted in (Figure 106). It can be observed that the peak SAR averaged over 10g mass tissue is reduced from 6.24W/Kg to 0.7W/Kg at 900 MHz, and it is reduced from 4.13W/Kg to 0.4W/Kg at 1800 MHz, which corresponds to 88.78% and 90.31% reduction of SAR at 900 MHz and 1800 MHz, respectively.

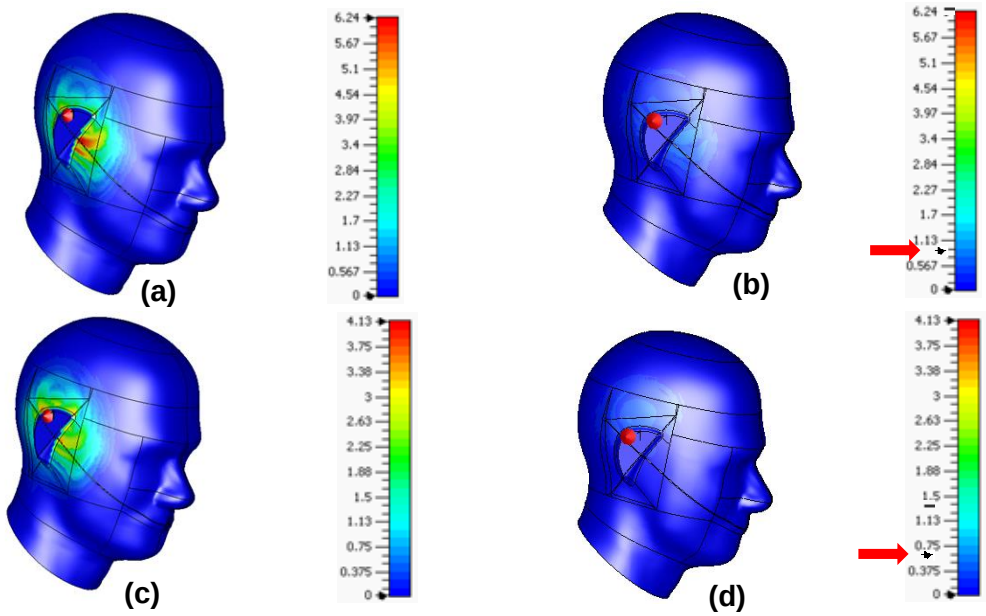

Figure 106 SAR distribution along the human head of: Conventional antenna at 900MHz (a), and 1800MHz (c), and of proposed antenna at 900MHz (b), and 1800MHz (d).

Although these results show that the insertion of water U-edges below the ground plane of a single band, dual band PIFA antenna is responsible for limiting the electromagnetic wave from propagating toward the human head which in turns leads to a reduction in current density as well as SAR on the human head, there exist a degradation in the gain of antenna. Thus, the following sections present another method for enhancing the gain of antenna, in addition to SAR reduction.

III.6. Enhanced Model of Low SAR Water Antenna Structure

The low SAR antenna structure proposed so far presents manufacturing limitations and degradation in the performance of antenna. The water edges cannot be implemented in mobile handsets without any support to hold the water material. For this reason, we propose in this paragraph an enhanced antenna model to overcome those problems, for both single band and dual band PIFA antenna.

III.6.1. Design of Single-band PIFA Antenna with U-edges filled by salty water in the vicinity of SAM human head model

This model consists of replacing the water edges by metallic ones, and filling them with water material as depicted in (Figure 107). The suggested model of antenna is placed at a distance 5mm from the human head as presented in (Figure 108).

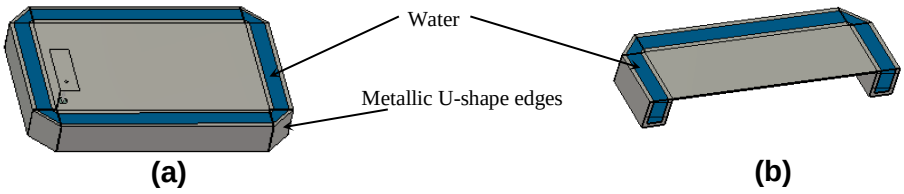

Figure 107 Geometrical structure of the proposed single band PIFA antenna: Perspective view (a), and Side view (b).

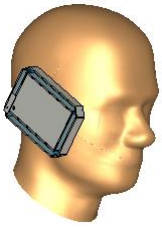

Figure 108 Geometrical structure of the proposed single band PIFA antenna in the vicinity of human head.

III.6.1.1. Simulation results

The new model provides a better performance in terms of impedance matching and Gain as depicted in the following results. This can be explained by the fact that the surrounding metallic edges prevent more loss in power and therefore provide more Gain.

Return Loss parameter (S11)

The simulated reflection characteristic of the enhanced single-band low SAR antenna is shown in (Figure 109). From the Graph below which shows the comparison between single band PIFA antenna with U-edges being made of water and enhanced single-band low SAR antenna in the vicinity of human head, it is clear that the suggested model antenna provides a resonance at 1.8 GHz, thus it is well matched at that frequency since S_{11} is less than -10dB.

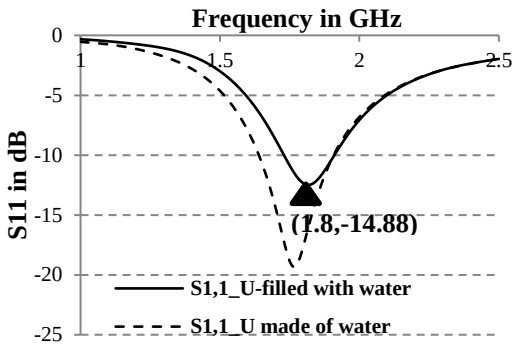

Figure 109 Graphical comparison representation of S_{11} parameter between antennas with U-filled with water and U-made of water.

Polar Plot of the Gain of antennas

The comparison between an antenna (with U-edges made of salty water) and enhanced single-band low SAR antenna in terms of gain is presented in (Figure 110)**.** Its gain is enhanced from 5.33dB of conventional antenna (without U-edges) to be 5.42dB, thus this case shows a better performance than when the U-edge is made of water.

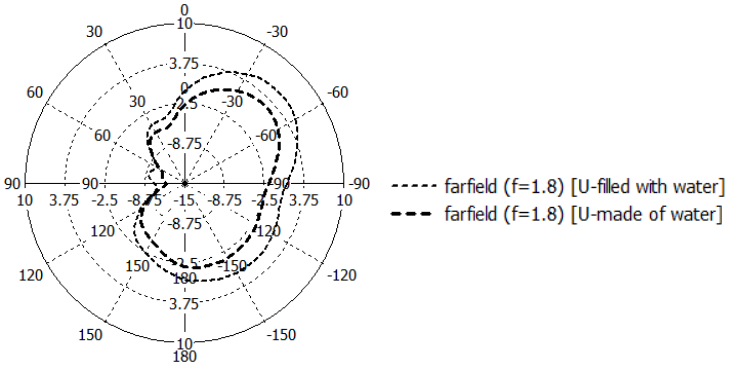

Figure 110 Polar plot of the gain of suggested antenna (with U-edges filled with water) and antenna (with U-edges made of water) in the vicinity of human head at 1800 MHz.

SAR distribution along the human head

The reduction in the current distribution is translated into an important reduction in the SAR, as depicted in (Figure 111). It can be observed that the peak SAR averaged over 10g mass tissue is reduced from 3.4 W/Kg to 0.7 W/Kg, which corresponds to 79.41% reduction of SAR.

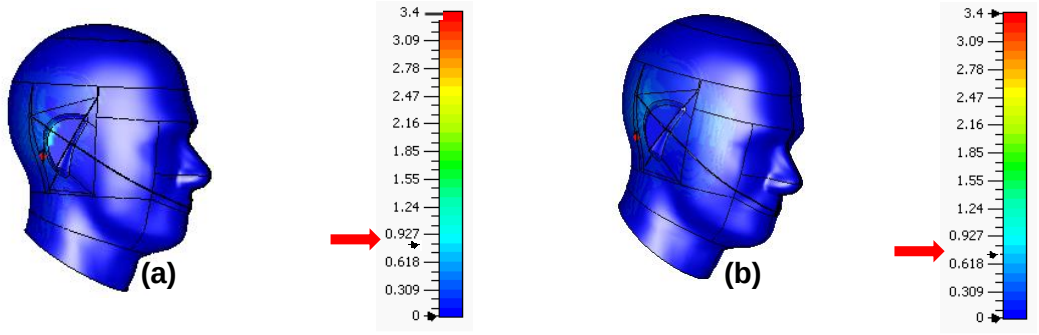

Figure 111 SAR distribution along the human head of suggested antenna (with U-edges filled with water) (a), and antenna (with U-edges made of water) (b).

From the above results, it is clearly indicated that an enhanced model for single band antenna is the better choice in terms of the performance of antenna as the gain is enhanced while achieving same result of SAR reduction as when the U-edge grooves are made of PEC (section-III.3.1.).

III.6.2. Design of dual band PIFA Antenna with U-edges filled by salty water in the vicinity of SAM human head model

The same concept is followed for designing the enhanced model of low SAR dual-band antenna, as illustrated in (Figure 112), where the U-edges are metallic and filled with water. The suggested model of antenna is placed at a distance 5mm from the human head as presented in (Figure 113).

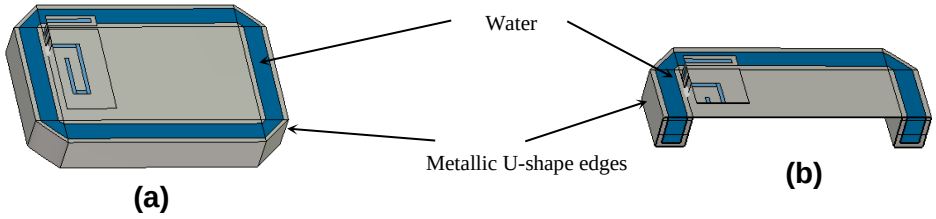

Figure 112 Geometrical structure of the proposed single band PIFA antenna: Perspective view (a), and Side view (b).

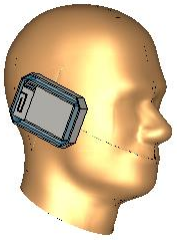

Figure 113 Geometrical structure of the proposed single band PIFA antenna in the vicinity of human head: Perspective view (c)

III.6.2.1. Simulation results

The performance of the antenna in terms of reflection coefficient and radiation pattern is improved as shown in the following results.

Return Loss parameter (S11)

The simulated reflection characteristic of the enhanced dual-band low SAR antenna. is shown in (Figure 114). The Graph below shows the comparison between dual band PIFA antenna with U-edges being made of water and an enhanced dual-band low SAR antenna in the vicinity of human head.

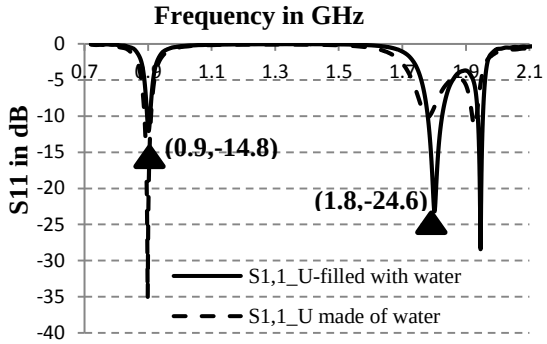

Figure 114 Graphical comparison representation of S11 parameter between antennas with U-filled with water and U-made of water.

Polar Plot of the Gain of antennas

The comparison between an antenna (with U-edges made of salty water) and enhanced dual-band low SAR antenna in terms of gain is presented in (Figure 115). Its gain is enhanced from -1.63dB of conventional antenna (without U-edges) to be 0.737dB at 900MHz, and from 3.53dB to 3.84dB at 1800MHz, thus this case shows a better performance than when the U-edge is made of water, where it is about-1.11dB at 900MHz, and about 0.77dB at 1800MHz.

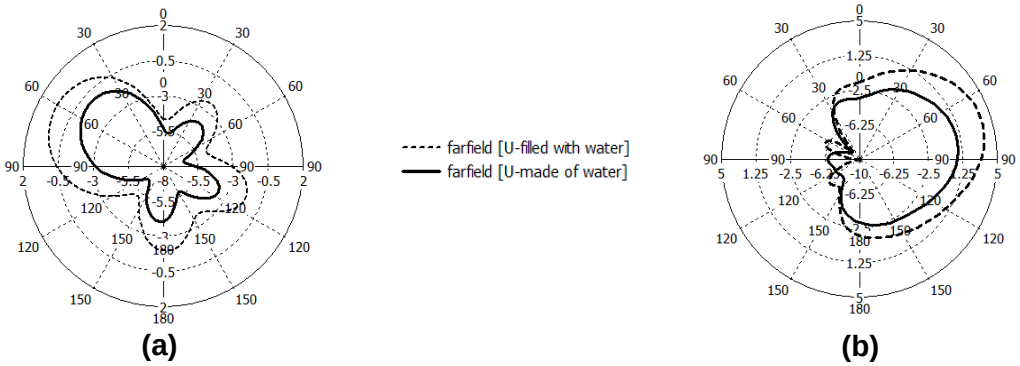

Figure 115 Polar plot of the gain of suggested antenna (with U-edges filled with water) and antenna (with U-edges made of water) in the vicinity of human head at: 900MHz (a), and at 1800 MHz (b).

SAR distribution along the human head

The enhancement in terms of Gain is responsible for a slight increase of the SAR as illustrated in (Figure 116), where the peak value is 1.6 W/Kg at 900 MHz and 0.6 W/Kg at 1800 MHz. Nevertheless, these values remain much lower than what exists in the literature.

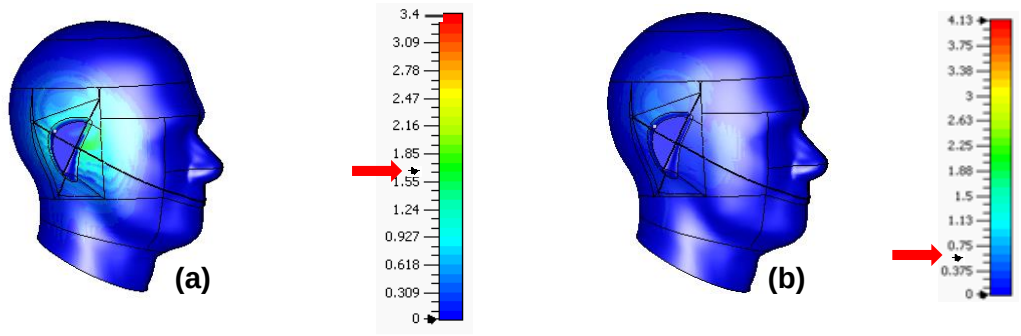

Figure 116 SAR distribution along the human head of suggested antenna at 900MHz (a), and 1800MHz (b).

III.7. Proposed PIFA antennas when the shape-edge groove is above the ground plane

In this section, we make a study on the U edge-treatment when inserted above each corner of the ground plane of: single band, and Tri-band PIFA antennas for maintaining their height, since the above study where the U-edge is inserted below each corner of ground plane, the height of antenna increases, and will not be applicable to be utilized in mobile application, nevertheless we get a good result in terms of SAR.

III.7.1. Design of proposed single band PIFA Antenna in the vicinity of SAM human head model

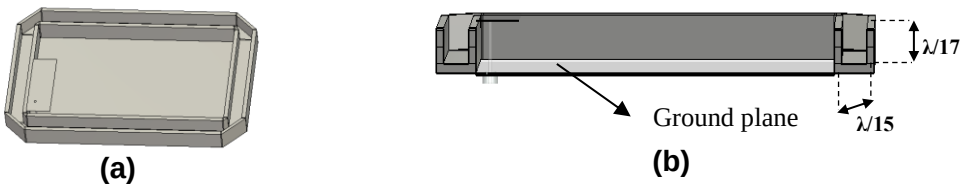

Figure 117 Geometrical structure of single band PIFA antenna with U-edge above ground plane: Perspective view (a), and Side view (b).

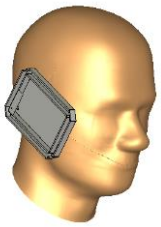

Figure 118 Geometrical structure of single band PIFA antenna with U-edges above ground plane in the vicinity of human head.

The proposed single band PIFA antenna with U-edges above each corner of the ground plane is shown in (Figure 117). The height of U-edge is optimized to achieve best performance of antenna at 1800MHz, and it is examined that height equal to λ/17 is the best choice. This antenna is positioned at a distance 5mm from the SAM human head model as presented in (Figure 118).

III.7.1.1. Simulation results

The following simulation results of the proposed single-band PIFA antenna with U-edges above each corner of the ground plane is presented:

Return Loss parameter (S11)

The simulated reflection characteristic of the single-band PIFA antenna with U-edges treatment above each corner of ground plane of the antenna placed in the vicinity of human head is shown in (Figure 119).

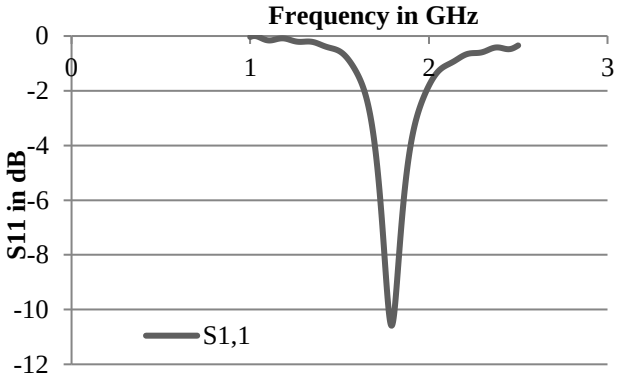

Figure 119 Graphical representation of S_{11} parameter.

3-D Radiation pattern

The three dimensional pattern of the gain of proposed antenna is presented in (Figure 120). Its gain is equal to 6.36dB at GSM 1800MHz.

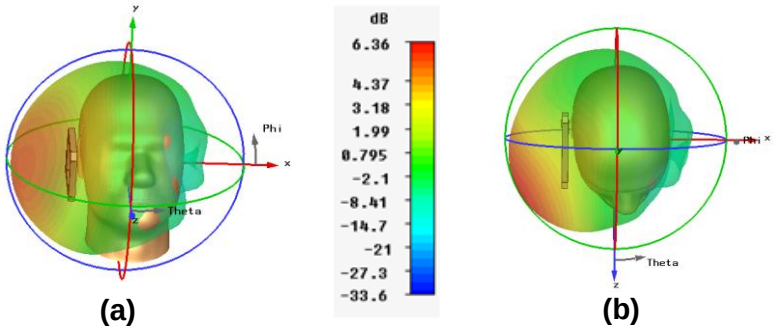

Figure 120 3D-representation of the gain of proposed antenna in the vicinity of human head at 1800 MHz: Perspective view (a), and Top view (b).

Surface Current distribution along the ground plane

The maximum peak surface current distribution along the ground plane of single-band antenna with U-edges above each corner of ground plane when placed in the vicinity of human head is presented in (Figure 121). It is shown that the maximum surface current is reduced from 7.3 A/m (without edges treatment) at GSM1800MHz to be approximately zero along the ground plane when the U-edges are inserted.

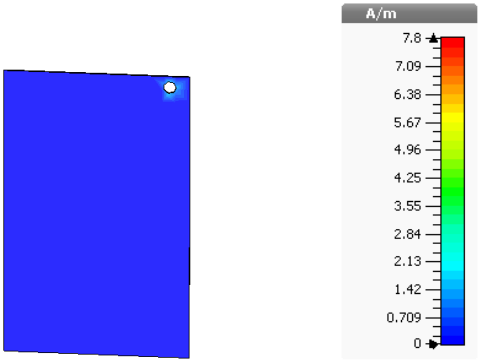

Figure 121 Surface Current distribution along the back side of ground plane with U- edges treatment above each corner of ground plane.

Current Density distribution along the human head

The peak current distribution along human head is presented in (Figure 122). It is shown that the maximum current distribution along human head is reduced from 104A/m^2 to 45A/ m^2, with U-edges above each corner of ground plane.

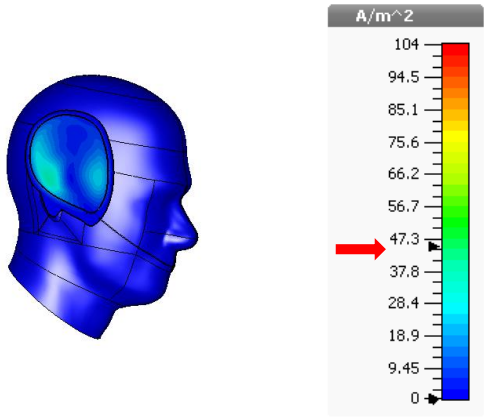

Figure 122 Current distribution along the human head at 1800 MHz, with U-edges treatment above each corner of ground plane.

SAR distribution along the human head

The peak SAR distribution along human head is presented in (Figure 123). It is indicated that the peak SAR is reduced from 3.4W/Kg to 0.867 W/Kg (corresponding to 74.5%), averaged over 10g mass tissue with U-edges treatment at each corner of ground plane, these values are much lower than the standard limit value.

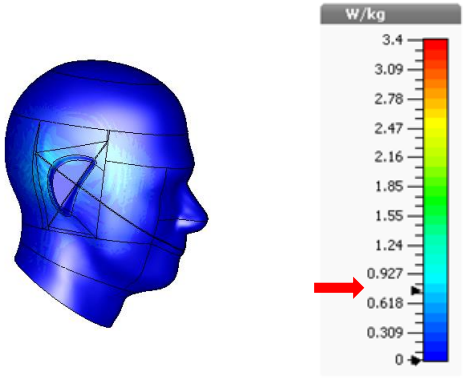

Figure 123 SAR distribution along the human head at 1800 MHz, with U-edges treatment above each corner of ground plane.

III.7.2. Design of proposed Tri-band PIFA Antenna in the vicinity of SAM human head model

The proposed Tri-band PIFA antenna with U-edges above each corner of the ground plane is shown in (Figure 124). The height of U-edge is optimized to get the best performance of antenna at three bands GSM 900MHz, GSM 1800MHz, and 2400MHz, and it is examined that height equal to λ/60 is the best choice. This antenna is positioned at a distance 5mm from the SAM human head model as presented in (Figure 125).

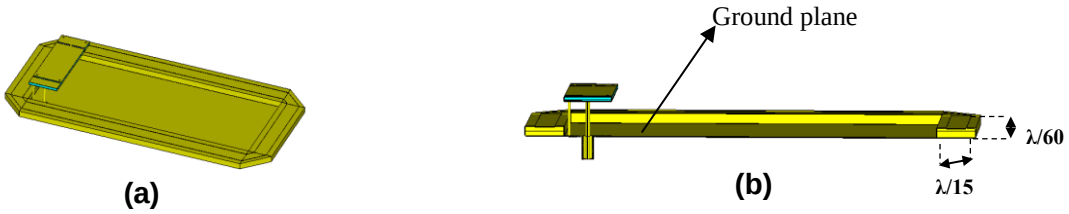

Figure 124 Geometrical structure of Tri-band PIFA antenna with U-edge above ground plane: Perspective view (a), and Side view (b).

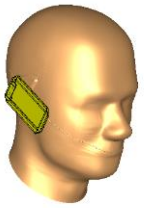

Figure 125 Geometrical structure of Tri-band PIFA antenna with U-edges above ground plane in the vicinity of human head.

III.7.2.1. Simulation results

The following simulation results of the proposed Tri-band PIFA antenna with U-edges above each corner of the ground plane is indicated below:

Return Loss parameter (S11)

The simulated reflection characteristic of the Tri-band PIFA antenna with U-edges treatment above each corner of ground plane of the antenna placed in the vicinity of human head is shown in (Figure 126).

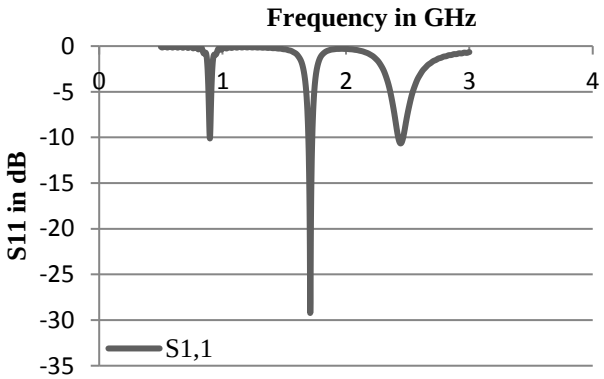

Figure 126 Graph representation of S11 parameter.

3-D Radiation pattern

The three dimensional pattern of the gain of antenna are presented in (Figure 127). Its gain is equal to 3.31dB, 4.33dB, 6.65dB at GSM 900MHz, GSM 1800MHz, and GSM 2400MHz, respectively.

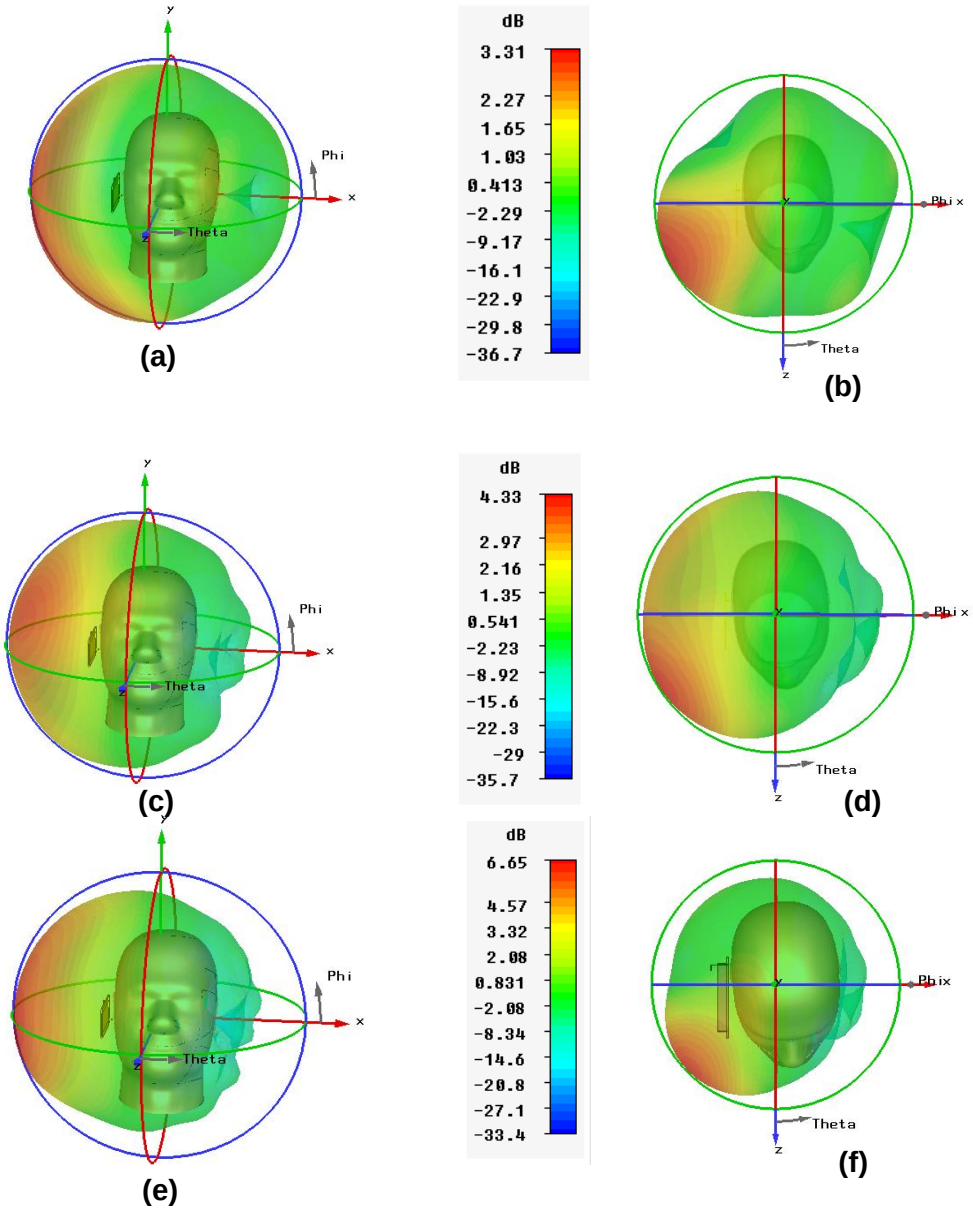

Figure 127 3D-representation of the gain of antenna: perspective view at 900MHz, 1800MHz and 2400MHz (a), (c) and (e), Top view at 900MHz, 1800MHz and 2400MHz (b),(d) and (f).

Surface Current distribution along the ground plane

The maximum peak surface current distribution along the ground plane of Tri-band antenna with U-edges above each corner of ground plane when placed in the vicinity of human head is presented in (Figure 128). It is shown that the maximum surface current is reduced from 6 A/m, 5 A/m, and 6 A/m (without edges treatment) at GSM900MHz, GSM1800MHz, and GSM2400MHz

respectively to be approximately zero along the ground plane when the U-edges are inserted above each corner of ground plane.

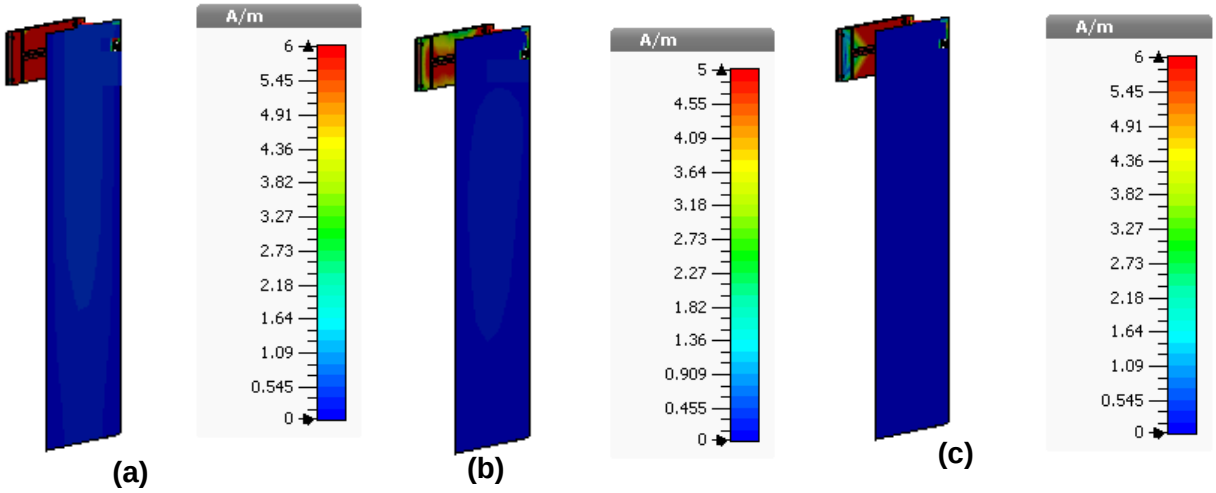

Figure 128 Surface Current distribution along the backside of ground plane at: 900MHz (a), 1800MHz (b) and 2400MHz (c).

Current Density distribution along the human head

The peak current distribution along human head is presented in (Figure 129). It is shown that the maximum current is reduced from 59 A/m^2, 92 A/m^2, and 89 A/m^2 to 45.6 A/ m^2, 43 A/m^2, and 47 A/m^{2}at GSM900MHz, GSM1800MHz, and GSM2400MHz, respectively.

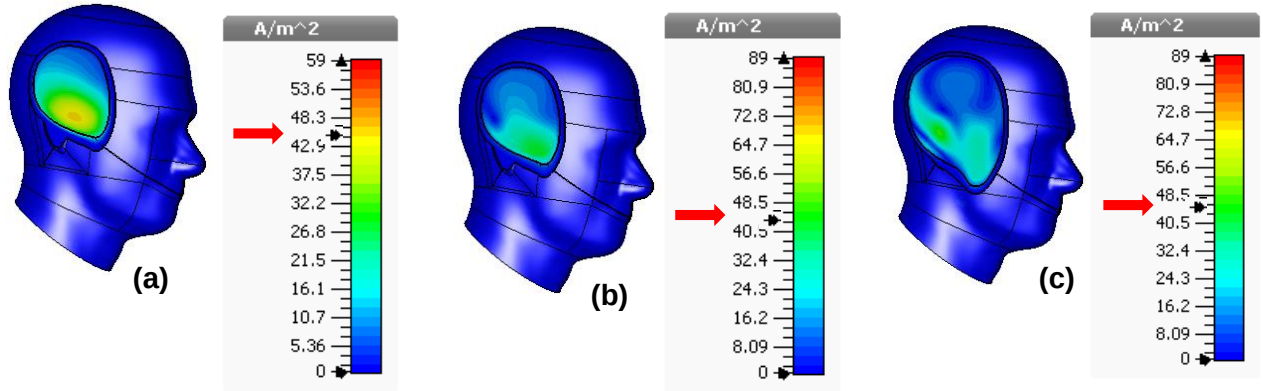

Figure 129 Current density distribution along the human head at: 900MHz (a), 1800MHz (b) and 2400MHz (c).

SAR distribution along the human head

The peak SAR distribution along human head is presented in (Figure 130). It is indicated that the peak SAR is reduced from 4.07W/Kg, 3.82W/Kg, and 2.65W/Kg to 1.45W/Kg(corresponding to 64.37%), 0.767W/Kg(corresponding to 79.92%), and

1.2W/Kg(corresponding to 54.71%) at GSM900MHz, GSM1800MHz, and 2400 MHz averaged over 10g mass tissue.

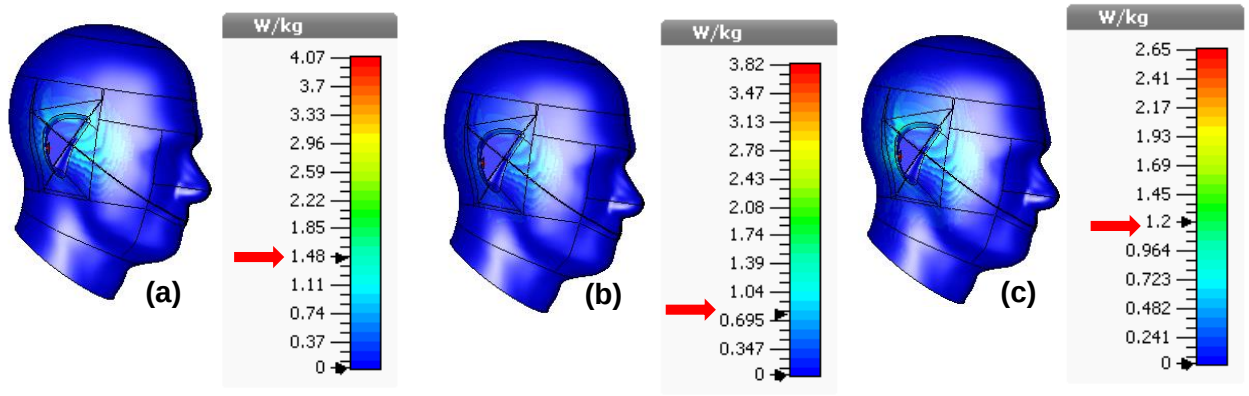

Figure 130 SAR distribution along the human head at: 900MHz (a), 1800MHz (b) and 2400MHz (c).

III.8. Conclusion

This chapter presented the design and simulation results of single band, dual band and Tri-band PIFA antenna used in mobile application, in terms of S_{11}, radiation pattern, surface current density, current density, and SAR. The study was done on method how to reduce the electromagnetic wave radiation toward human head, in deed the SAR. This method predict that inserting edge-grooves of certain shape at each corner of ground plane of the above antennas can make the surface current density null along the ground plane, thus reducing the current density along the human head, as well as the SAR.

Several works were investigated: first one, when the edge-groove is inserted below each corner of ground plane. In this case, several shapes (U, L, and V) were examined, and the results show that U-shape achieves the lowest value of SAR. In this scenario, we studied two types: first one, when U-edges are made of PEC, we get SAR reduction about 78.6% in case of single band PIFA antenna. In case of dual band, we get SAR reduction about 71.15%, 80.67% at 900 MHz, and 1800 MHz, respectively. In case of tri-band, we get SAR reduction about 71.15%, 88.66%, and 65.66% at 900 MHz, 1800 MHz and 2400 MHz respectively. Second one is a liquid type that considered as more advanced type. For this type, two antennas are considered: a single band PIFA operating at 1.8 GHz, and a dual band PIFA operating at 0.9 MHz and 1.8 GHz. In this method, two cases were studied: first one when the U-edge is made of water, we noticed that the peak SAR value averaged over 10 g mass tissue was reduced to 73.52% in the case of single band PIFA, whereas the peak SAR was reduced to 88.78% and 90.31% in case of dual band. Second case, when U-edge filled with water, this enhanced structure was presented to overcome the manufacturing limitations of the first case design. Simulation results showed a better performance in terms of reflection

coefficient and radiation pattern for both single-band and dual-band antennas. The results of SAR were also similar to the first case structure design for the single-band antenna. However, the SAR was slightly higher for the dual-band antenna, but it still remains very low (1.6 W/Kg at 900 MHz and 0.6 W/Kg at 1800 MHz). After that, for preserving the height of antenna, and making it more realistic to be applied in mobile application, another study was done by inserting U-edges above each corner of the ground plane. In this case, we get SAR reduction as follows: 74.5% at GSM1800MHz in case of single band, and about 64.37%, 79.92%, and 54.71% at GSM900MHz, GSM1800MHz, and 2400 MHz in case of Tri-band averaged over 10g mass tissue. This result provides valuable information in designing communication equipment that strictly respects safety compliance.

Chapter IV:
New antenna design with cosecant beam for safety radiation health risk in mobile

IV.1. Introduction

With the growing in the number of cell phone technology, the number of cell towers or base transceiver stations has also been increased, where many of these towers are installed on roof tops of apartments and in a heavily populated area, leading to adverse effects on human health. However, many people do not know how radio technology works and some wonder if it is safe. Their main concerns regard the possible effects on health from radio waves that mobile phones and base stations transmit in order to communicate with each other. On the other hand, rapid development in modern wireless communications raises the demand for antennas operating at wide frequency bands to facilitate the application for various needs.

There are several types of cell tower antenna such as: Omni-directional antenna [77], Sector antenna, and Circular (Parabolic) antenna [78]. Most studies on such types of antenna are based on performing best coverage of signal strength across certain area; nevertheless they don't mention any safe concern in the designing of such types.

In this chapter, the main objective is to investigate a safety BTS-antenna that provides a constant power density with uniform coverage over a certain BTS-cell, and this is greatly depend on the environmental structure for protecting human health from the harmful biological effects that comes from the radio frequency radiation of the BTS antenna. For that purpose, our aim is to propose an antenna that has radiation pattern characterized by uniform coverage with constant power density. Design considerations of the proposed antenna are described using SARA (Synthesis of Antenna Array), CST, and Atoll simulation software.

IV.2. Uniform Coverage over Mobile Reception Level

The design of modern safety antenna is achievable in a way to create a radiation pattern that can compensate losses presented by the environment with respecting the specifications of human health. This can be achieved by maintaining constant power density level with uniform coverage all over the ground reception level.

IV.2.1. Constant Power Density-Uniform Coverage

The design of maintaining a uniform coverage depends on type of the area whether it is densely urban, rural, open area etc...An example of pattern with uniform coverage is discussed below:

IV.2.2. Cosecant-Squared Pattern (CSP)

Using the geometry of (Figure 131), substitute (equation IV-1) in (equation I-19) from (chapter I):

$$r = \frac{h}{\sin\theta} \qquad \text{equation IV-1}$$

Where h, r, θ, φ, and R are the antenna height, distance from the antenna to the mobile unit, observation angle, sectorial angle, and the radius.

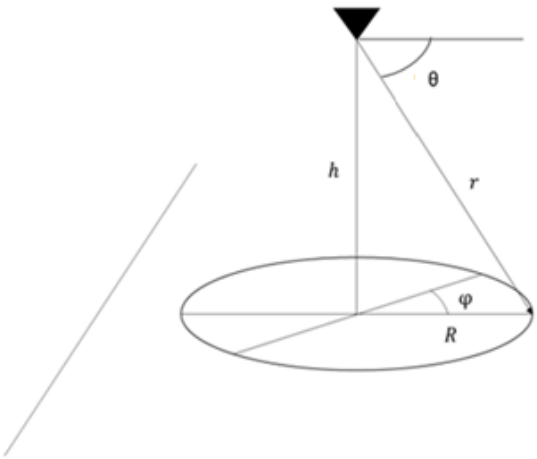

Figure 131 Geometrical Representation from Transmitter to Receiver

Therefore, the power density can be expressed as:

$$P(h,\theta,\varphi) = \frac{P_T \times G(\theta,\varphi) \times (\sin\theta)^2}{4\pi h^2} \qquad \text{equation IV-2}$$

It is required to have constant power density all over cell area, where θ varies from $\arctan\frac{R}{h}$ to $\frac{\pi}{2}$. In an omnidirectional case.

The expression of the gain function is then: $G(\theta,\varphi) = \frac{P_0 \times 4\pi \times (h_0)^2}{P_T \times (\sin\theta)^2}$ equation IV-3

Hence $G(\theta,\varphi) \propto \frac{1}{(\sin\theta)^2} \propto csc^2\theta$

This is the cosecant squared gain equation, which in turn gives the cosecant-squared pattern.

The below graph as presented in (Figure 132) shows the plot of normalized gain of the cosecant squared equation with respect to coverage angle, taking an electrical tilt of 14° from the horizon, and fixing the rest values of the gain above the cell radius edges. It is important to notice that this relation is the ideal case, for which, the propagation model is assumed to be in a free space environment, which fits perfectly with the radar application.

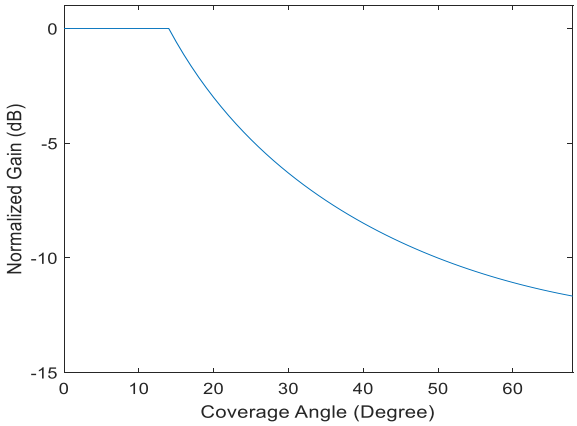

Figure 132 Cosecant Squared Pattern Normalized Gain Plot

Cosecant squared pattern is specially designed for air-surveillance radar set. This permit an adapted distribution of the radiation in the beam and causing more ideal space scanning. This antenna pattern can get the required elevation coverage where the received power is independent of the radar range for a constant height target. It is a means of achieving more uniform signal strength at the input of the receiver as a target moves with a constant height within the beam. (Figure 133) shows the cosecant squared pattern in the theoretical idealized form and the practical synthesized form. Another example is the vessel radar. The coverage diagram of (Figure 134) shows the antenna pattern of vessel radar with an inverse cosecant squared antenna pattern. The antenna is designed to preferentially radiate below 0° (the horizon line) to provide constant detection for targets approaching on sea surface [79].

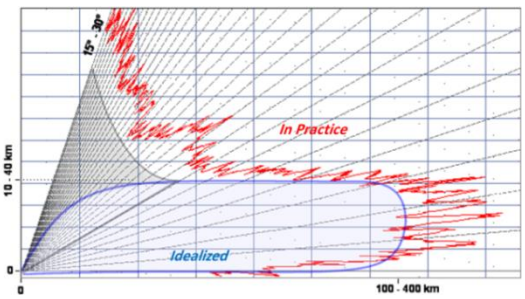

Figure 133 CSP for Air-Surveillance.

Figure 134 Inverse CSP for Vessel Radar.

IV.3. Relation between gain and path loss

In mobile communications, the link budget relation can be expressed as:

$$\text{Rx Power(dB)} = \text{Tx Power(dB)} + \text{Gains(dB)} - \text{Losses(dB)} \qquad \text{equation IV-4}$$

In the linear form:

$$\frac{P_R}{P_T} = \frac{G_T \times G_R}{P_L} \qquad \text{equation IV-5}$$

Where G_T, G_R, P_L, P_R, P_R are the gain of the transmitting antenna and it's a function of the direction of observation, the gain of the receiving antenna, the path loss, the received power, and the total transmitted power.

Hence the gain function is: $G_T = \frac{\lambda^2 \times P(r,\theta,\varphi)}{4\pi \times P_T} \times P_L$ equation IV-6

Note that the path loss P_L is not constant, it depends on the directions as well as the distance between transmitting and receiving antennas.

By selecting the desired safe power density that do not affect the health of the mobile user over a fixed ground level h_0, the gain function for this observation is achieved.

$P(r, \theta, \varphi) = P_0$ at $h = h_0$

Hence, $G(\theta, \varphi) = G_T = \frac{\lambda^2 \times P_0}{4\pi \times P_T} \times P_L(\theta, \varphi)$ equation IV-7

IV.4. Propagation Models in Mobile Communications

The use of path loss models is to predict the signal losses within the distance between transmitter and receiver. Path loss (or path attenuation) is the reduction in power density of an electromagnetic wave as it propagates through space or underground. The path loss depends on signals frequency, specifics of the terrain, building types and density, clutter, the transmitting antenna height of the base station and the distance to the mobile (user) station [80].

In GSM, the recommended path loss propagations models are Okumura-Hata [80], ITU 529-3, Standard Propagation Model, CrossWave Model, and Aster Propagation Model [81]. In this study, we work on COST 231 – Walfisch-Ikegami-Model, as it takes into consideration the complex environment.

IV.4.1. COST 231 – Walfisch-Ikegami-Model

This model is based on different contributions from members of the "COST 231 Subgroup on Propagation Models". It is called the COST-Walfisch-Ikegami-Model (COSTWI) [82]. The model allows for improved path-loss estimation by consideration of more data to describe the

character of the urban environment, namely heights of buildings h_r, widths of roads W, building separation B and road orientation with respect to the direct radio path ϕ. Parameters are defined in (Figure 135). This model is still statistical and not deterministic because only characteristic values can be inserted whereas the topographical database of the buildings isn't considered.

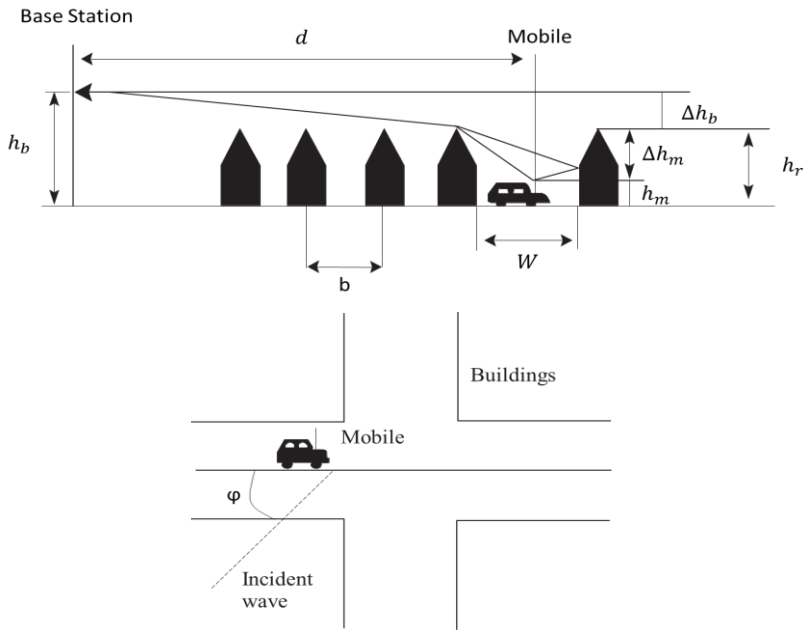

Figure 135 Propagation Situation in Urban Areas

In the LOS-case between base and mobile antennas within a street canyon- a simple propagation loss formula different from free space loss is applied.

For $\geq 20m$:

$$P_L(\text{dB}) = 42.6 + 26\log_{10}\left(\frac{\text{d}}{\text{km}}\right) + 20\log_{10}\left(\frac{\text{f}}{\text{MHz}}\right) \qquad \text{equation IV-8}$$

Where the first constant is determined in such a way that PL is equal to free space loss for $d = 20m$.

In the NLOS-case the basic transmission loss is composed of the terms free space loss L_0, multiple screen diffraction loss L_{msd}, and roof-top-to-street diffraction and scatter loss L_{rts}.

$$P_L = \begin{cases} L_0 + L_{rts} + L_{msd} & \text{for } L_{rts} + L_{msd} > 0 \\ L_0 & \text{for } L_{rts} + L_{msd} \leq 0 \end{cases} \qquad \text{equation IV-9}$$

The free-space loss is given by:

$$L_0(\text{dB}) = 32.4 + 26\log_{10}\left(\frac{\text{d}}{\text{km}}\right) + 20\log_{10}\left(\frac{\text{f}}{\text{MHz}}\right) \qquad \text{equation IV-10}$$

The determination of L_{rts} takes into account the width of the street and its orientation.

$$L_{rts} = -16.9 - 10\log_{10}\left(\frac{W}{m}\right) + 10\log_{10}\left(\frac{f}{MHz}\right) + 20\log_{10}\left(\frac{\Delta h_m}{m}\right) + L_{Ori} \quad \text{equation IV-11}$$

$$\Delta h_m = h_r - h_m \quad \text{equation IV-12}$$

$$\Delta h_b = h_b - h_r \quad \text{equation IV-13}$$

$$L_{Ori} = \begin{cases} -10 + 0.354\frac{\varphi}{deg} & \text{for } 0^\circ < \varphi \leq 35^\circ \\ 2.5 + 0.075\left(\frac{\varphi}{deg} - 35\right) & \text{for } 35^\circ < \varphi \leq 55^\circ \\ 4.0 - 0.114\left(\frac{\varphi}{deg} - 55\right) & \text{for } 55 < \varphi \leq 90 \end{cases} \quad \text{equation IV-14}$$

The heights of buildings and their spatial separations along the direct radio path are modelled by absorbing screens for the determination of L_{msd}:

$$L_{msd} = L_{bsh} + k_a + k_d\log_{10}\left(\frac{d}{km}\right) + k_f\log_{10}\left(\frac{f}{MHz}\right) - 9\log_{10}\left(\frac{b}{m}\right) \quad \text{equation IV-15}$$

Where,

$$L_{bsh} = \begin{cases} -18\log_{10}\left(1 + \frac{\Delta h_b}{m}\right) & \text{for } h_b > h_r \\ 0 & \text{for } h_b \leq h_r \end{cases} \quad \text{equation IV-16}$$

$$k_a = \begin{cases} 54 & \text{for } h_b > h_r \\ 54 - \frac{0.8\Delta h_b}{m} & \text{for } d \geq 0.5 \text{ km and } h_b \leq h_r \\ 54 - \frac{0.8\Delta h_b}{m}\,\frac{\frac{d}{km}}{0.5} & \text{for } d < 0.5 \text{ km and } h_b \leq h_r \end{cases} \quad \text{equation IV-17}$$

$$k_d = \begin{cases} 18 & \text{for } h_b > h_r \\ 18 - \frac{15\Delta h_b}{h_r} & \text{for } h_b \leq h_r \end{cases} \quad \text{equation IV-18}$$

For medium sized city and suburban centers with medium tree density:

$$k_f = -4 + 0.7\left(\frac{f(MHz)}{925} - 1\right) \quad \text{equation IV-19}$$

For metropolitan centers:

$$k_f = -4 + 1.5\left(\frac{f(MHz)}{925} - 1\right) \quad \text{equation IV-20}$$

The COST-WI model is restricted to:

f : $800 \ldots 2000\ MHz$

h_b : $4 \ldots 50\ m$

h_m : $1 \ldots 3\ m$

d ∶ 0.02 … 5 km

The estimation of path loss agrees rather well with measurements for base-station antenna heights above rooftop level. However the prediction error becomes large for $h_b \approx h_r$ compared to situations where $h_b \gg h_r$. Furthermore the performance of the model is poor for $h_b \ll h_r$.

The figure below (Figure 136) shows a comparison between gains of CSP high orders and COST 231 – WI path loss model in medium sized city and suburban centers with medium tree density, taking an electrical tilt of 14° from the horizon, and fixing the rest values of the gain above the cell radius edges.

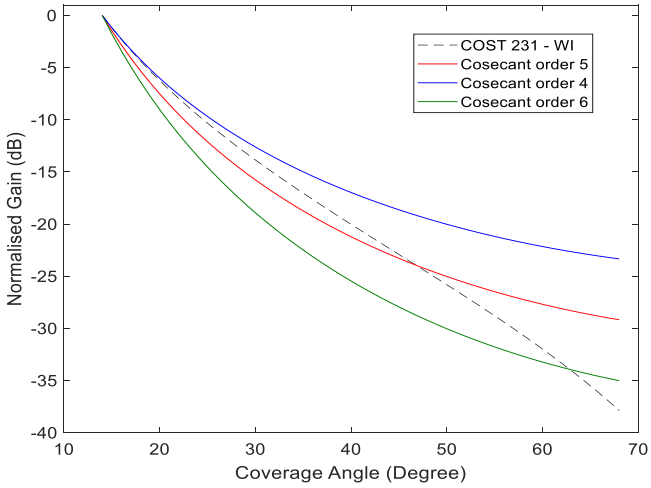

Figure 136 COST 231 - WI vs Higher Order Cosecant Pattern

IV.5. Synthesis of Array of Antenna

Pattern synthesis [83], [84], is necessary to design an antenna system that will yield to a desired radiation characteristics. The task, in general, is to find the number of elements and their excitation distribution. The designed system should yield, either exactly or approximately, an acceptable radiation pattern, and it should satisfy other system constraints.

IV.5.1. Theoretical Method

Theoretically, the angular behaviour of the far field E of a linear uniformly spaced array of $2N$ isotropic radiators can be written as:

$$E(\theta_j) = \sum_{n=1}^{2N} I_n e^{jK_0 x_n \sin(\theta_j)} \qquad \text{equation IV-21}$$

Where I_n: the weighting coefficient or the excitation (magnitude and phase) of the nth element, x_n: the position of the nth element.

Desired patterns are usually not realizable, and an optimal realizable pattern can only be defined with respect to some error criterion. In SARA, we consider the mini-max norm, defined as the minimization of the function:

$$\mathrm{Err}(\theta_j) = \underset{j}{\mathrm{Max}}\left\|E_c(\theta_j) - E_d(\theta_j)\right\| \quad j = 1, \ldots, M \qquad \text{equation IV-22}$$

M: Number of sampled angular direction

E_d: Desired pattern field

E_c: Computed pattern field

Two categories of error criterion are usually employed: the first one supposes a real radiation pattern, the second one consists of a 'power synthesis', where the radiation pattern becomes complex. The minimization condition is only applied on the magnitude of these patterns [10].

The hypothesis of the real formalism is that the excitation law is symmetric and conjugate with the array center. With the complex formalism, no hypothesis is made about the phase of the required pattern. So many complex solutions can be determined, and the best one is compared with the real solution.

In the real-field synthesis case, the calculated field is real, and the excitation distribution is symmetrical and conjugated with the array center. The computed field becomes:

$$E_c(\theta_j) = \sum_{n=1}^{N} I_n \cos(K_0 x'_n \sin(\theta_j)) \qquad \text{equation IV-23}$$

With x'_n, the relative position if the nth element with respect to the array center.

In the case of power synthesis, the error to minimize is equal to the difference between the modulus of the computed function, and the required one.

IV.5.2. Using the SARA Software:

While synthesizing a cosecant pattern there are three main parameters to consider, side lobe level, cover and cutoff rate. The SARA software takes the values of the field required.

Normalized gain is plotted versus coverage angle, having -90° to be vertically upwards, 0° to be the horizon, and an electrical tilt of about 14° in order to cover 200-meter radius with height of base station antenna mounted at 50 meter. The desired beam is that of COST231-WI model presented previously. From -90° to 0° is to be minimized because this is the region of lost power.

The figures below show respectively the type and the number of element with best position selection. Position is selected with multiple trials to give the best result for a certain synthesis type.

The first one shows the gain pattern of eight elements power synthesis with linear phased array type, and second one shows the gain pattern of eight elements real synthesis type (Figure 137).

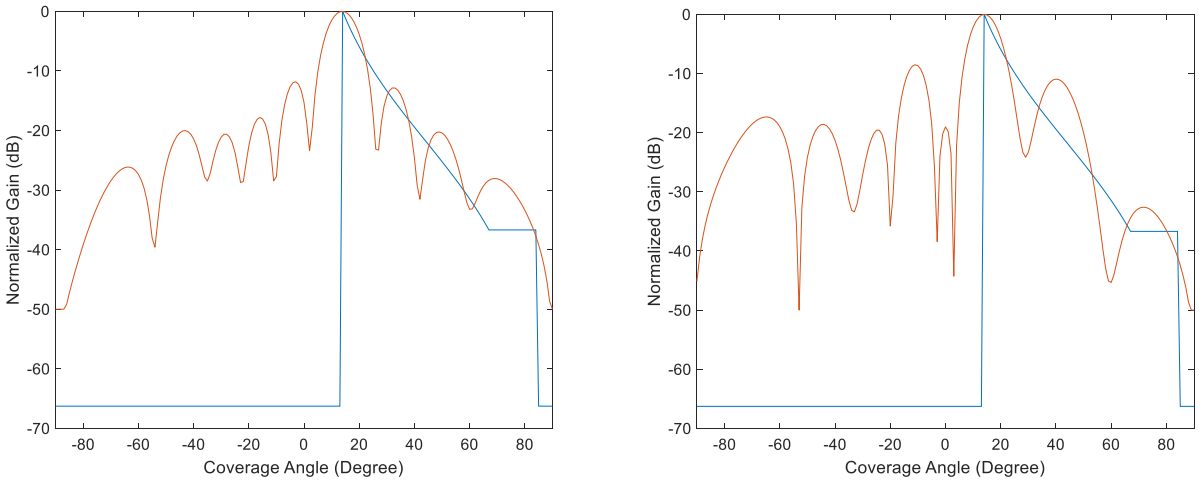

Figure 137 Eight Element Power Synthesis (a), Real Synthesis (b)

The figure below (Figure 138) shows the gain pattern of four elements power synthesis type. This type clearly results with better beam forming. As the number of elements increases, the beam formed will fit better our desired beam, but this will depend on many factors, because as the number of elements increases, the cost, the size of the array and the complexity of the design (power divider) are also increased.

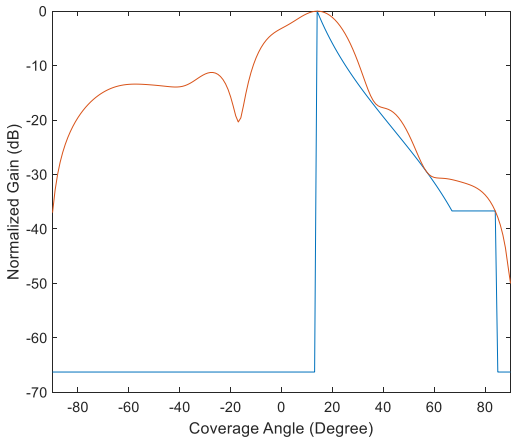

Figure 138 Four-Element Power Synthesis

IV.5.3. *Synthesis & Analysis*

The synthesized beam in (figure 138) requires the configuration in (Table IV-1):

Table IV-1 Antenna Array Configuration

Element Number	Position X, Y	Excitation	
		Magnitude	Phase
1	0.0, 0.0	0.59	39.7˚
2	0.7, 0.0	1.00	0˚
3	1.6, 0.0	0.59	289.4˚
4	2.9, 0.0	0.19	113.1˚

IV.6. CST Design & Realization

In this section, we propose a design of printed dipole antenna array with same number, positions, and excitation that we achieve during the above synthesis. With this omnidirectional radiation and the wideband characteristics, it is an excellent candidate as the unit of the omnidirectional array for mobile communication with an equivalent cosecant radiation beam. Design considerations of the proposed antenna are described.

IV.6.1. Proposed Omni-Directional Antenna Structure

The proposed micro-strip antenna is designed as shown in (Figure 139) to generate an omnidirectional radiation pattern. It is simulated through CST-Microwave-Studio simulation software**.** TLX-0-0310-C1/C1 is a substrate material with relative permittivity $\varepsilon_r = 2.45$, dielectric thickness of 0.78mm and copper thickness of 0.035mm. A 50Ω micro-strip feed line excites this antenna. The dimensions are in (mm) (L1=lambda guided/4, L2=49.7241, L3=40, W1=88, W2=85, W3=1.9).

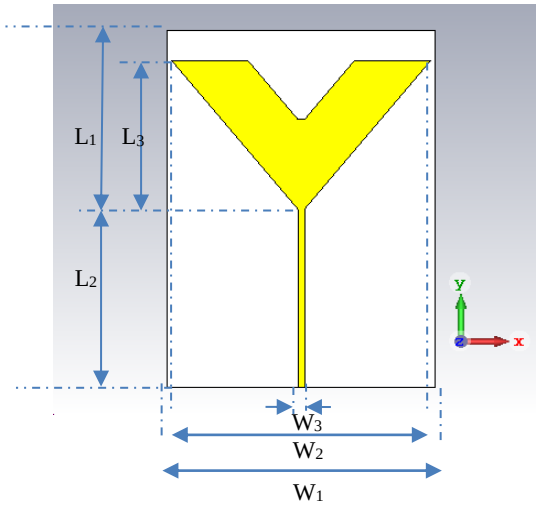

Figure 139 Proposed antenna

IV.6.2. Simulation Results

(Figure 140) shows the antenna array with the modification of triangular gap, with the same numbers, positions and excitations as presented in the above configuration result (Table IV.1). (Figure 141) shows the vertical pattern of this array. (Figure 142) shows the 3D pattern of the

antenna array. It is clearly shown that this proposed antenna performs a perfect omnidirectional pattern.

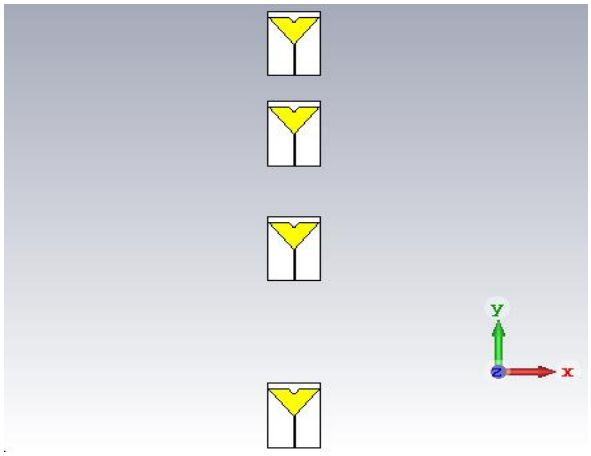

Figure 140 Antenna Array in CST

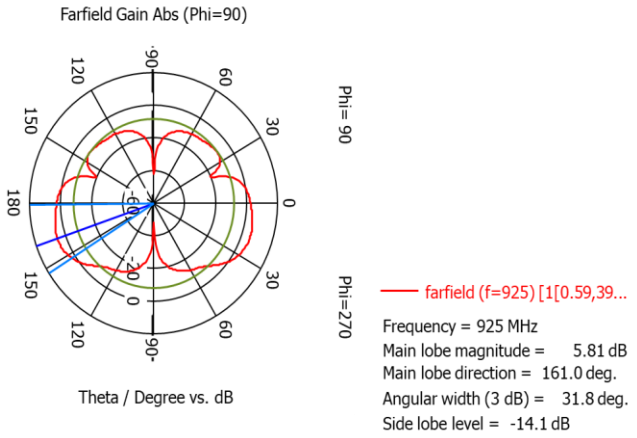

Figure 141 Vertical Pattern

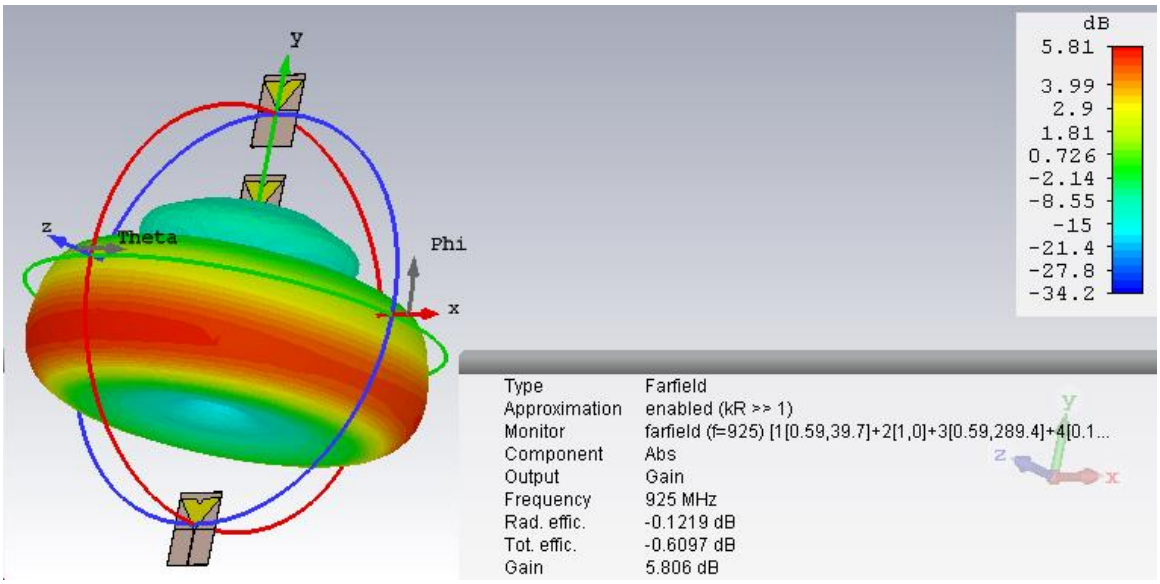

Figure 142 3D Far-Field Pattern

IV.7. ATOLL – The Radio-Planning Software

Atoll [81] is a multi-technology wireless network design and optimization platform that supports wireless operators throughout the network lifecycle, from initial design to densification and optimization. Concerning its State-of-the-Art Features, Atoll supports multi-format geographical data. High-resolution urban and country-wide datasets are supported and displayed interactively as multiple layers including engineering and prediction plots. The most advanced information technology techniques and propagation algorithms are also integrated.

IV.7.1. ATOLL-Simulations

For the GSM network, the aim is to have a signal strength level $-75dBm$ with a $\pm 15dBm$. This range gives us low level for EM-exposure, and good signal strength for the GSM network within the area of coverage or at the edges while going to handover. Testing will be on a DTM (Digital Terrain Map). An area of 2 km^2 in dense urban city shown in (Figure 143).

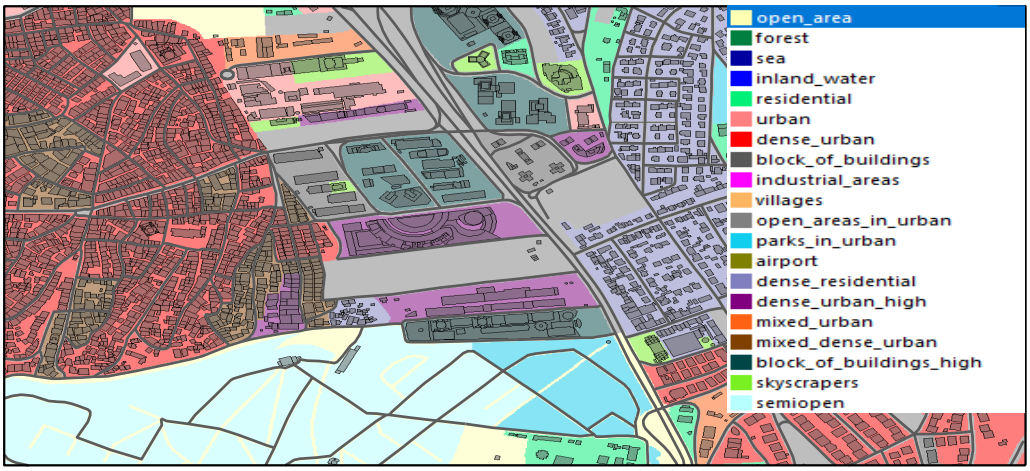

Figure 143 Dense Urban City DTM

Statistical information of clutter classes in this map are shown in (Table IV.2) below:

Table IV-2 Clutter Classes Statistical Information.

Name	Surface (km²)	Percentage
Open area	0.086088	4.4
Residential	0.051432	2.6
Urban	0.067964	3.4
Dense urban	0.416176	21.1
Block of buildings	0.053552	2.7
Industrial areas	0.010832	0.5
Open areas in urban	0.330604	16.7
Parks in urban	0.0561	2.8
Dense residential	0.395264	20
Dense urban high	0.073648	3.7
Mixed urban	0.036692	1.9
Mixed dense urban	0.069416	3.5
Block of buildings high	0.095656	4.8
Skyscrapers	0.031728	1.6
Semi-open	0.201472	10.2
Forest	0	0
Sea	0	0
Inland water	0	0
Villages	0	0
Airport	0	0

A dense urban part of 200 $meter$ radius (14° electrical tilt) from this area will be chosen for our simulation.

We build our site (Microwave Tower) on a building of 30 $meter$ height. Assigning a transmitter to this site, the transmitting antenna will be fixed over 20 $meters$ over the microwave tower. Testing our synthesized antenna, the transmitting antenna is of 50 $meters$ height. The transmitter has the antenna pattern as shown in (Figure 144).

(Figure 145) shows the site covering a certain radius of the city, with predictions of coverage by signal level. (Figure 146) shows the percentage histogram of statistics based on prediction conditions.

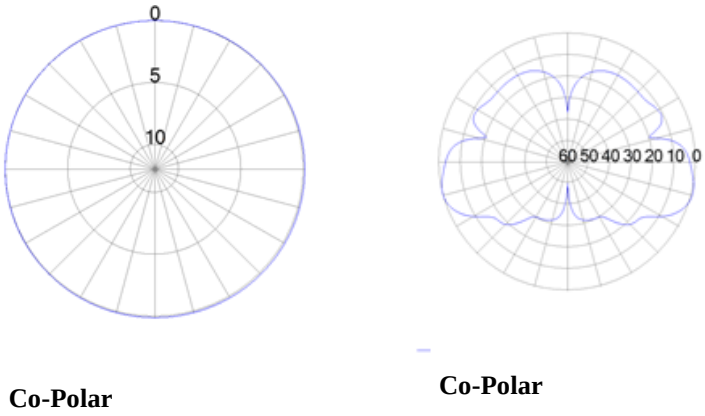

Figure 144 Horizontal Radiation Pattern (a), Vertical Radiation Pattern (b)

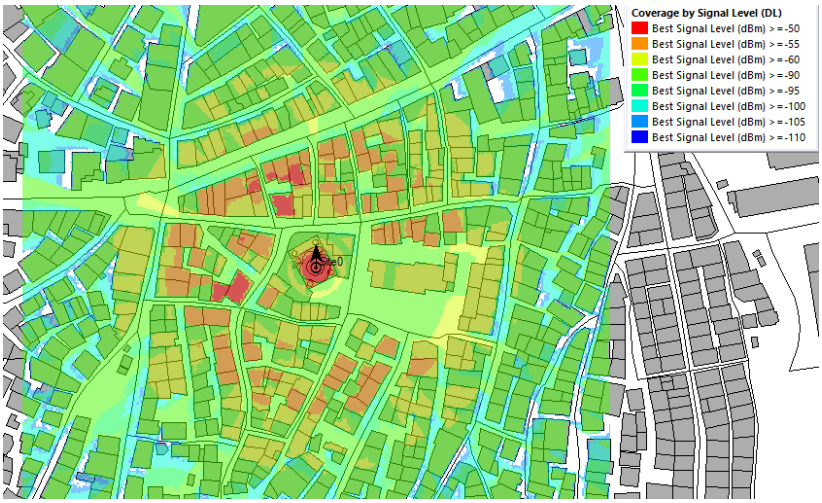

Figure 145 Prediction by Signal Level

Following the uniform coverage idea, beamforming is done to match the desired beam of losses presented by COST231-WI model. The beam is synthesized with power synthesis which is better for cosecant beam [10].

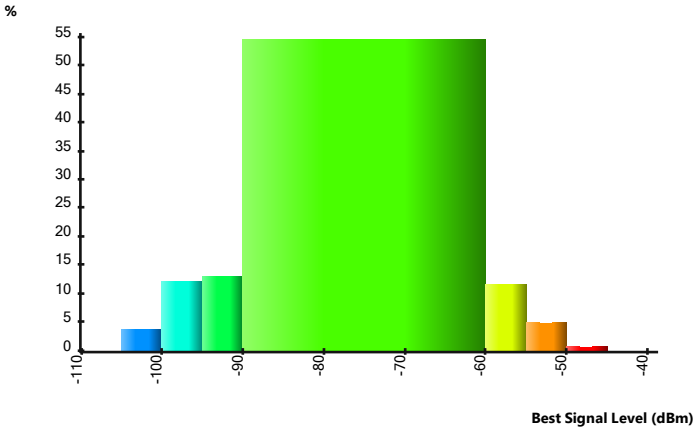

Figure 146 Percentage of Area Covered with Signal Level Interval.

IV.8. Conclusion

By taking the advantage of the general idea and the concept about cosecant-squared radiation pattern, which is designed for air-surveillance radar and vessel radar sets, the safety antenna is a mean of achieving uniform signal strength all over any constant height level within the beam, below the BTS.

Thus, uniform coverage with a desired power density can control the electromagnetic wave exposure and health concerns, and help not to have a poor communication quality. Another bad thing other than communication that is related to poor quality is the automatic power control of the phones as it increases their output power for sustaining the connection, thus decreasing the battery life, duration of talking, in addition to the harmful side effects on human head. Regarding this, the safety antenna is designed to serve our concerns and solving the poor communication effects from the user side between base station and mobile station.

Therefore, our illustrated and designed network will optimize coverage and therefore operate at only the lowest power level that is necessary to provide good communications.

General Conclusion and perspective

General Conclusion and perspective

The motivation for this thesis work came into being from the prerequisite to be able answer to the defiance of an antenna design task of a modern mobile handset as well as cell tower antenna. The objective of this thesis was to reduce the peak SAR distribution along the human head when placed in the proximity of human head without affecting the performance of antenna. Also, to predict radiation pattern of a safety cell tower antenna that achieves a uniform coverage with constant field strength over a certain area. The aim of this work is to minimize the possible hazardous biological effects coming from mobile antenna and cell tower antenna that affect human health.

The beginning of this work consisted of study dealing with the basics types of the electromagnetic wave radiation and its impact on human body. The SAR, power density, and their standards regulations were presented. Also, available literatures discussing several methods to enable reductions in SAR along human head were presented.

After the literary work, research on methods to produce reduction in SAR, and to achieve a uniform coverage with constant field along certain site were conducted with the target of implementing them in the realistic mobile and cell tower antennas. Improvements in the understanding of methods were needed to be able to optimize them to the requirements of the given mobile and cell tower antennas. When dealing with mobile and cell tower antennas certain parameters are emphasized. The most important parameters, including size, bandwidth, gain, and SAR were said to be strongly interrelated and improvements in one of the parameters often means sacrificing the performance measured in one or several of the other parameters. As for SAR reduction, the method is based on an edge-groove with certain shapes (U, L, and V) attached to each corner of the ground plane of mobile antenna. The aim was to be able to use the method in a several communication bands handset platform. The method was mostly investigated with simulations that present how these edges can reduce the surface current density along the ground plane, which in turn reduce the penetration of fields toward human head, thus, reducing SAR. The challenge in implementing the method within the project was the tight boundary conditions regarding the dimensions of the U-shape edge groove. As always in the design process of the handset, the antenna designer has to struggle to find the necessary means for an adequate antenna performance among the competing structural demands of the different parts of the phone.

On the other hand, the method for performing uniform signal coverage from base station along certain area is achieved by designing an antenna with an equivalent cosecant radiation pattern. This proposed antenna should be a good candidate as a unit of the omnidirectional array with synthesis results. Due to these performances, the antenna has wide and potential applications in recent mobile communication.

The research with simulations gave valuable information about the methods. Very promising SAR reductions were found at single band (1800MHz), dual band (900MHz, 1800MHz), and Tri-band (900MHz, 1800MHz, and 2450MHz) PIFA antennas. Also, very promising constant field strength with uniform coverage along studied site having dense urban area was achieved by keeping the power density, the power transmitting, and the height of antenna constant.

Several types of PIFA models were investigated in this thesis for reducing the SAR. One type is when U-shape edge groove is inserted below each corner of ground plane. In this type several structures were made: First one is when the U-shape is made of PEC, and then is made of Liquid. In second structure, two cases were studied. First case, when the U-shape is made of water, and second case, when U-shape is filled with water. In both types, promising SAR reductions were found. Nevertheless, it isn't applicable to be applied in mobile application as the height of antenna increases. On the other hand, another type that is more realistic to be applied in mobile application is when the U-shape is inserted above each corner of the ground plane. Sweeping the height and width of U-shape is important to optimize the best dimension in terms of antenna performance and SAR reduction. Therefore the method in total seems attractive for implementation in real handsets. By taking the advantage of the general idea and the concept about cosecant-squared radiation pattern, which is designed for air-surveillance radar and vessel radar sets, the safety antenna, is a means of achieving uniform signal strength all over any constant height level within the beam, below the BTS. Having a uniform coverage with a desired power density give us a control on EM wave exposure and health concerns, and help with having no poor communication quality. Another bad thing other than communication with poor quality is the automatic power control of phones to increase their output power to sustain the connection, thus decreasing battery life, talk time, and harmful to human head. Regarding this, the safety antenna serves our concerns also for solving poor communication effects from the user side between base station and mobile station. Therefore, our illustrated and designed network will optimize coverage and therefore operate at only the lowest power levels necessary to provide good communications.

From an industrial point of view, the investigated method offers a very potential option for keeping the SAR produced by a mobile antenna within the regulative limits. The amount of SAR reduction attained with the method is enticing, but since the successful realization and validation of the method requires precise prototype and measurement setups, the implementation probably would need a considerable amount of time.

As another conclusion of the research it can be said, that simulations with simple models are advantageous for discovering useful trends and methods to reduce. However, tenacious engineering work is required for bringing these methods into reality, because even small changes in the evaluation setup under investigation can cause misleading variation in SAR. The principles found in simulations could also be brought closer to reality by a more thorough modeling of the studied handset and its different parts.

For the future, it is necessary to examine if the above mobile phone antenna with low SAR as well as the safety GSM-BTS antenna could be designed to function as multiband antenna which can function for several applications of different frequency bands simultaneously (3G, Wifi, Wimax etc.).

List of Publications

International Journals

1. **N. Nasser**, D. Serhal, R. Barake, M. Rammal, P. Vaudon, “A novel low SAR water-based mobile handset antenna". Analog Integrated Circuits and Signal Processing (2018) 96:353–361 https://doi.org/10.1007/s10470-018-1130-8, 28 February 2018.

2. **N. Nasser**, D. Serhal, R. Barake, M. Rammal, P. Vaudon, “SAR reduction for PIFA antennas used in mobile phones”. In Advances in antenna engineering and wireless systems research (pp. 57–77). CreateSpace Independent Publishing Platform. Chapter in the book “Raad, H. (2017)”.

3. **N. Nasser**, M. Jadid, D. Serhal, M. Rammal, P. Vaudon, “New Design of GSM-BTS Antenna for Safety Radiation Health Risk in Mobile Communication”. International Journal of RF and Microwave Computer Aided Engineerining..(submitted)

International Conferences

1. **N. Nasser**, D. Serhal, R. Barake, M. Rammal, P. Vaudon, “A novel low SAR water-based mobile handset antenna". 2017 Sensors Networks Smart and Emerging Technologies (SENSET), IEEE, Beirut, Lebanon, 12-14 Sept. 2017.

2. D. Serhal, **N. Nasser**, M. Rammal, “Impact of Phone and Hand Position on SAR Distribution Using Liquid-Based PIFA Antenna. Still in progress”. The 8th International Conference Sciences of Electronics, Technologies of Information and Telecommunications (SETIT 2018),Genoa-Italy / Hammamet-Tunisia, December 18-20, 2018.

[1] Statista, the statistics portal, « Number of mobile phone users worldwide from 2013 to 2019 (in billions) », website: https://www.statista.com/statistics/274774/forecast-of-mobile-phone-users-worldwide/.

[2] G. Kumar, « Report on Cell Tower Radiation », Electrical Engineering Department, IIT Bombay, Powai, Mumai – 400 076, December 2010.

[3] H. P. Schwan, « Bio electromagnetics, Carl Durney, and dosimetry: Some historical remarks », Bioelectromagnetics, pp. 3-8, 1999.

[4] T. Kurniawan, « Analytical Methods for Near Field Radio Frequency Dosimetry for Tissue Layers and Cellular Structures », February 2009.

[5] A. Tsiaras, « SAR Evaluation in Multi-Antenna Mobile Handsets », Department of Electrical and Information Technology Faculty of Engineering, LTH, Lund University SE-221 00 Lund, Sweden. March 2014.

[6] IEEE, « IEEE standard for safety levels with respect to human exposure to radio frequency electromagnetic fields, 3 kHz to 300 GHz », IEEE Std C95.1, 1999 Edition, 1999.

[7] NRPB, « Health Effects from Radiofrequency Electromagnetic Fields », 2003.

[8] J. Wilén, « Radiofrequency fields – exposure, dose and health », 2002.

[9] L. Xing, « Investigations of Water-Based Liquid Antennas for Wireless Communications », University of Liver pool, September 2015.

[10] D. Eclercy, M. Rammal, A. Reineix, and B. Jecko, « Comparison between real and power optimisation methods for arrays synthesis of antennas », Electronics Letters, vol. 32, no. 2. pp. 84–85, 1996.

[11] H. Rammal, P. Vaudon, N. Fadlallah, M. Rammal, R. Ghayoula, and A. Gharsallah, « General synthesis method for linear phased antenna array », IET Microwaves, Antennas Propag., vol. 2, no. 4, pp. 338–342, Jun. 2008.

[12] N. A. Samsuri, « The Effect of Jewellery and the Human Hand on SAR and Antenna Performance », Loughborough University Institutional Repository, January 2009.

[13] R. L. McIntosh, V. Anderson and R. J. McKenzie, « A numercial evaluation of SAR distribution and temperature changes around a metallic plate in the head of a RF exposed worker », Bioelectromagnetics, vo!. 26, pp. 377-388, 2005.

[14] J. F. Femandbes, C. A. Faz, A. M. Gonzalez and D. S. Hemandez, « Effect of pierced metallic objects on SAR distributions at 900 MHz », Bioelectromagnetics, vol. 27, pp. 337-353,2006.

[15] S. Hawar, S. Al-Bazzaz, « Theoretical Estimation of Power Density Levels around Mobile Telephone Base Stations », Faculty of Science and Engineering, University of Science and Technology, Sana'a, Yemen. Journal of Science & Technology, Vol. (13) No.(2) 2008.

[16] « http://copradar.com/preview/chapt8/ch8d1.html ».

[17] C. Furse, D.A. Christensen, C. H. Durney, « Basic Introduction to Bioelectromagnetics », 2nd edition, Taylor & Francis Group, 2009.

[18] L. D, « Development and Investigation of Mobile Antennas for less Radiation Hazards », Department of electronics, Faculty of Technology, Cochin university of Science and Technology, India, October 2012.

[19] J.Wilén, « Radiofrequency fields – exposure, dose and health », UMEÅ university medical dissertations, New series No. 808 ISSN 0346-6612, ISBN 91-7305-293-3. Department of Radiation Sciences Radiation Physics 2002.

[20] A. P. S. Balbani , J. C. Montovani, « Mobile phones: influence on auditory and vestibular systems », Brazilian journal of otorhinolaryngology 74 (1) january/february 2008. http://www.rborl.org.br / e-mail: revista@aborlccf.org.br.

[21] A. Hirata and T Shiozawa, « Correlation of maximum temperature increase and peak SAR in the human head due to handset antennas », IEEE Transactions on Microwave theory and techniques, Vol. 51, No. 7, pp1834-1841. , July 2003.

[22] E. Joo', « Absorption of the electromagnetic energy in human head », Doctoral School of technical science, 2005.

[23] M. Bakro, « Investigation of Mobile Phone SAR Reduction »,Von der Fakultät für Ingenieurwissenschaften, Abteilung Elektrotechnik und Informationstechnik der Universität Duisburg-Essen, 26.07.2016.

[24] H. P. Schwan, « Bioelectromagnetics, Carl Durney, and dosimetry: Some historical remarks », Bioelectromagnetics, pp. 3-8, 1999.

[25] IEEE P1528, « Recommended Practice for Determining the Peak Spatial-Average Specific Absorption Rate (SAR) in the Human Head from Wireless Communications Devices », Measurement Techniques, 2003.

[26] C95.3-1991-IEEE, « Recommended Practice for the Measurement of Potentially Hazardous Electromagnetic Fields RF and Microwave 1992 ».

[27] T. A. MILLIGAN, Chapter 1 –, « Modern Antenna Design,"2nd edition, John Wiley & Sons, 2005 ».

[28] R. A. Serway and R. J. Beichner, « Physics for Scientists and Engineers », Orlando, Florida: Harcourt College Publishers, 2000.

[29] S, Y. Abdulrahman, « Electromagnetic Emission-aware Resource Allocation for the Uplink of Wireless Systems », Institute for Communication Systems. Faculty of Engineering and Physical Sciences. University of Surrey Guildford, Surrey GU2 7XH, U.K, February, 2016.

[30] « IEEE Standard for Safety Levels With Respect to Human Exposure to Radio Frequency Electromagnetic Fields, 3 kHz to 300 GHz », IEEE Std C95.1-2005 (Revision of IEEE Std C95.1-1991), pp. 01–238, 2006.

[31] P. Halla, « Specific absorption rate design of 3rd generation handsets », Helsinki University Of Technology, Faculty of Electronics, Communications and Automation Department of Radio Science and Engineering, February 2008.

[32] A. V. Räisänen and A. Lehto, « Radio engineering for wireless communication and sensor applications », Boston, USA, 2003, Artech House, 396 p.

[33] M. J. Hagmann, O. P. Gandhi and C. H. Durney, « Numerical Calculation of Electromagnetic Energy Deposition for a Realistic Model of Man », IEEE Trans. on Microwave Theory and Techniques, Vol. MTT-27, No. 9, September 1979, pp. 804–809.

[34] P. J. Dimbylow, « FDTD calculations of the whole-body averaged SAR in an anatomically realistic voxel model of the human body from 1 MHz to 1 GHz », Physics in Medicine and Biology, Vol. 42, No, 3, March 1997, pp. 479–490.

[35] H. Nyberg and K. Jokela (Editors), « Ionisoimaton säteily – Sähkömagneettiset kentät (Non-ionizing radiation – Electromagnetic fields, in Finnish) », Helsinki, Finland, 2006, Radiation and Nuclear Safety Authority of Finland, 555 p.

[36] K. Jokela, D. Leszczynski, W. Paile, S. Salomaa, L. Puranen, P. Hyysalo, « Radiation safety of handheld mobile phones and base stations », STUK-A161, Helsinki, Finland, 1999, Radiation and Nuclear Safety Authority of Finland, 76 p. January 1999.

[37] « World Health Organization, Electromagnetic fields », www-page, available at http://www.who.int/peh-emf/en/, cited 15.09.2007.

[38] « International Commission on Non-Ionizing Radiation Protection », Publications – EMF, www-page, available at http://www.icnirp.de/pubEMF.htm, cited 15.09.2007.

[39] International Commission on Non-Ionizing Radiation Protection (ICNIRP), « Guidelines for limiting exposure to time-varying electric, magnetic, and electromagnetic fields (up to 300 GHz) », Health Physics, April 1998, Vol. 74, No. 4, pp. 494-522.

[40] IEEE Std. C95.1 - 2005, « IEEE Standard for Safety Levels with Respect to Human Exposure to Radio Frequency Electromagnetic Fields, 3 kHz to 300 GHz », IEEE, New York, USA, April 2006, 248 p.

[41] A. H. Kusuma, A. F. Sheta, I. Elshafiey, M. Alkanhal, S. Aldosari, Z. Siddiqui, and S. A. Alshebeili, « A Novel Low SAR PIFA for Mobile Terminal », 2010 IEEE 21st International Symposium on Personal Indoor and Mobile Radio Communications pp 1-5.

[42] T. Anita Jones Mary, and C. S. Ravichandran, « Sar Reduction in Slotted Pifa for Mobile Handsets Using RF Shield », Department of Electronics and Communication, Karunya University, Coimbatore 641114, E-mail: anitajones@karunya.edu. I J W C N, June 2012.

[43] M. R. I. Faruque, M. T. Islam, M. A. M. Ali, « A New Design of Metamaterials for SAR Reduction », Institute of Space Science, Faculty of Engineering & Built Environment Building. Measurement Science Review, Volume 13, No. 2, 2013.

[44] H.-H. Chou, H.-T. Hsu, H.-T. Chou, K.-H. Liu, and F.-Y. Kuo, « Reduction of Peak SAR in Human Head for Handset Applications with Resistive Sheets (R-cards) », Department of Communications Engineering, Communication Research Center, Yuan Ze University, Chungli 320, Taiwan. Progress In Electromagnetics Research, PIER 94, 281–296, 2009.

[45] M. R. I. Faruque, M. I. Hossain, N. Misran, M. Singh, M .T . Islam, « Metamaterial-Embedded Low SAR PIFA for Cellular Phone », Space Science Centre (ANGKASA),UniversitiKebangsaanMalaysia,43600UKM,Bangi,Selangor,Malaysia.PLOSO NE|DOI:10.1371/journal.pone.0142663 November23, 2015.

[46] J. Wang, O. Fujiwara, T. Takagi, « Effects of Ferrite Sheet Attachment to Portable Telephone in Reducing Electromagnetic Absorption in Human Head », Department of Electrical and Computer Engineering ,Nagoya Institute of Technology, Nagoya 466-8555, Japan. Faculty of Science and Technology Tohoku Bunka Gakuen University, Sendai 981-8551, Japan. IEEE 1999.

[47] N. Sghaier, L. Latrach, and A. Gharsallah, « Effect of Complementary Split Ring Resonator Structure on PIFA Antenna », Unit of Research Circuits and Electronics Systems HF, Faculty of Science, departement Electronics. Journal of Microwaves, Optoelectronics and Electromagnetic Applications, Vol. 15, No. 3, September 2016 DOI: http://dx.doi.org/10.1590/2179-10742016v15i3583.

[48] M. Naser-Moghadasi, Z. Mansouri, S. Sharma, F. B. Zarrabi & Bal S. Virdee, « Low SAR PIFA Antenna for Wideband Applications », IETE Journal of Research. DOI: 10.1080/03772063.2015.1135300. Published online: 29 Feb 2016.

[49] K. S. Sultan, H. H. Abdullah, E. A. Abdallah, and E. A. Hashish, « Low SAR, Compact and Multiband Antenna », Electronics Research Institute, Dokki, Giza, Egypt. Faculty of Engineering, Cairo University, Giza, Egypt. PIERS Proceedings, Taipei, March 25–28, 2013. Progress In Electromagnetics Research Symposium Proceedings, Taipei, March 25–28, 2013.

[50] Mr. K. T. Kaharpardeshi, Prof. S. U. Ullah, Prof. S. Zafar, « Dipole Phased-Array Antenna above circular patched EBG substrate with Reduced Specific Absorption Rate for Fourth Generation Mobile Phone Applications », Patel Institute of Technology, Bhopal. International Journal of Engineering Research & Technology (IJERT),Vol. 2 Issue 11, November – 2013. ISSN: 2278-0181.

[51] C. S. Shin, D. G. Choi, N. Kim, J. I. Choi, « Internal Monopole Antenna Design for Multi-band Operation and SAR Analysis », Chungbuk Na'l University, Korea. Progress In Electromagnetics Research Symposium 2005, Hangzhou, China, August 22-26.

[52] M. R. I. Faruque, M. T. Islam, N. Misran, « A New Design of Split Ring Resonators for Electromagnetic (EM) absorption Reduction in Human Head », Institute of Space Science, Department of electrical, Electronic and systems Engineering, Faculty of Engineering & Built Environment, Universiti Kebangsaan Malaysia, 43600 UKM, Bangi, Selangor D. E., Malaysia. Journal of Microelectronics, Electronic Components and Materials Vol. 42, No. 1(2012), 18-22.

[53] C. P.Nyakyi, S. I. Mrutu, A. Sam, J. Anatory, « Safety Zone Determination For Wireless Cellular Tower - A Case Study From Tanzania », IJRET: International Journal of Research in Engineering and Technology eISSN: 2319-1163 | pISSN: 2321-730. Volume: 02 Issue: 09 | Sep-2013, Available @ http://www.ijret.org.

[54] S. Hawar, S. Al-Bazzaz, «Theoretical Estimation of Power Density Levels around Mobile Telephone Base Stations », Faculty of Science and Engineering, University of Science and Technology, Sana'a, Yemen. Journal of Science & Technology, Vol. (13), No.(2), 2008, JST 3.

[55] International Std. IEC 62209-1:2005 Ed. 1.0, «Human exposure to radio frequency fields from hand-held and body-mounted wireless communication devices – Human models, instrumentation and procedures – Part 1: Procedure to determine the specific absorption rate (SAR) for hand-held devices used in close proximity to the ear (frequency range of 300 MHz to 3 GHz) », IEC, Geneva, Switzerland, February 2005, 215 p.

[56] R. Augustine, «Electromagnetic modelling of human tissues and its application on the interaction between antenna and human body in the BAN context », Universit´e Paris-Est, 2009. English, 9 July 2010.

[57] "SPEAG," DASY5, [Online]. Available: , «http://www.speag.com/products/dasy/dasy-systems/ », [Accessed 10 January 2015].

[58] C. C. Gordon, T. Churchill, C. E. Clauser, B. Bradtmiller, J.T. McConville, I. Tebbetts and R. A. Walker, «1988 Anthropometric Survey of U.S. Army Personnel: Methods and Summary

Statistics, Technical Report NATICK/TR89/044 », U.S. Army Natick Research, Development and Engineering Center, Natick, Massachusetts, USA, 1989, 335 p.

[59] R. F. Harrington, «Field computation by moment methods », New York, USA, 1968, The Macmillan Company, 229 p.

[60] J. L. Volakis, A. Chatterjee and L. C. Kempel, «Finite Element Method for Electromagnetics: Antennas, Microwave Circuits, and Scattering Applications », New York, USA, 1998, IEEE Press, 368 p.

[61] A. Taflove and S. C. Hagness, «Computational Electrodynamics: The FiniteDifference Time-Domain Method », 3rd edition, Norwood, USA, 2005, Artech House, 1006 p.

[62] W. L. Stutzman and G.A. Thiele, «Antenna theory and design », 2nd edition, New York, USA, 1998, John Wiley & Sons, 648 p.

[63] M. T. Islam, H. Z. Abidin, M. R. I. Faruque, and N. Misran, "Analysis of materials effects on radio frequency electromagnetic fields in human head," Progress In Electromagnetics Research, Vol. 128, 121-136, 2012. 48.

[64] Gabriel, C, «Compilation of the Dielectric Properties of Body Tissues at RF and Microwave Frequencies », Brooks Air Force Technical Report, AL/OE-TR-1996-0037, 1996.

[65] S. A. Abdulrazzaq, J. S. Aziz, «SAR Simulation in Human Head Exposed to RF Signals and Safety Precautions College of Engineering », Alnahrain University, Baghdad, Iraq, Computer Engineering Department, Electronics and Communication Engineering Department. September 2013 | Vol 3, Issue 9, 334-340.

[66] K. Hirasawa and M. Haneishi, «Analysis, Design, and Measurement of Small and Low-Profile Antennas », Artech House, Boston, 1992.

[67] «https://fr.slideshare.net/TANJIRALAM/planar-inverted-f-antennapifa».

[68] S. Saini, S. Singh, N. kumar, «A Review of Various Planar Inverted F Antenna (PIFA) Structures for Wireless Applications », Dept. of ECE, Guru Nanak Dev University, Regional Campus, Gurdaspur, Punjab, India. Int. Journal of Electrical & Electronics Engg. Vol. 2, Spl. Issue 1 (2015), e-ISSN: 1694-2310 | p-ISSN: 1694-2426.

[69] H. T. Chattha, Y. Huang, M. K. Ishfaq, S. J. Boyes, «A Comprehensive Parametric Study of Planar Inverted-F Antenna », Wireless Engineering and Technology, 2012, 3, 1-11. http://dx.doi.org/10.4236/wet.2012.31001.Published Online January 2012 (http://www.SciRP.org/journal/wet).

[70] «http://www.antenna-theory.com/antennas/patches/pifa.php».

[71] H. F. Chen, M. Yi Lin, and K-H.Lin, « A V-shape Edge-Groove Design for a Finite Ground Plane to Reduce Pattern Ripples of a Monopole », IEEE antennas and wireless propagation letters, vol. 7, 2008.

[72] C. A. Balanis, Antenna Theory, « Analysis and Design », 3rd ed. New York: Wiley, 2005.

[73] R. S. Elliott, « On the Theory of Corrugated Plane Surfaces », IRE Trans. Antennas Propagat., Vol. AP-2, No. 2, pp. 71–81, April 1954.

[74] C. A. Mentzer and L. Peters, Jr. , « Properties of cutoff corrugated surfaces for corrugated horn design », IEEE Trans. Antennas Propagat., vol. AP-22, no. 2, pp. 191–196, Mar. 1974.

[75] A. Kaur, H. Malik, A. Lather and V.K.Lamba, « Effect of Communication Frequency on Specific Absorption Rate of Electromagnetic Radiations In Human Body », International Journal of Soft Computing and Engineering (IJSCE), Volume-2, Issue-4, September, 2012.

[76] «Test Plan for Mobile Station over the Air Performance, Method of Measurement for Radiated RF Power and Receiver Performance, CTIA - The Wireless Association », January 2011.

[77] MMF, GSMA, « RF safety at base station sites », July 2008.

[78] «website: https://www.quora.com/Which-type-of-antennas-are-used-at-mobile-towers ».

[79] «website: http://www.radartutorial.eu/

[80] M. Rahnema, « UMTS Network Planning, Optimization, and Inter-Operation with GSM. Singapore », John Wiley & Sons (Asia) Pte Ltd, 2007.

[81] FORSK SARL, « Atoll User Manual Radio », 2015.

[82] E. Damosso, « European cooperation in the field of scientific and technical research COST telecommunications COST Action 231. 1999 ».

[83] C. a. Balanis, «Antenna Theory: Analysis and Design », vol. 28, no. 3. 2012.

[84] J. L. Volakis, «Antenna Engineering Handbook », Fourth Edition. McGraw-Hill Education, 2007.

Contribution to the study and minimization of the impact of electromagnetic waves on the human body. Application in the field of mobile telephony.

Abstract: In this thesis, we propose new types of mobile handset PIFA antenna design to reduce the specific absorption rate (SAR) in human head. Three antennas were considered: a single band PIFA operating at 1.8 GHz, a dual band PIFA operating at 900 MHz and 1.8 GHz, and a Tri-band PIFA operating at 900MHz, GSM 1800MHz, and 2400MHz. Surface current density along the ground plane was decreased by reducing the near electric field radiation coming from the radiating antenna to the human head, which in turns leads to a reduction in current density along human head as well as the SAR. This SAR reduction is accomplished by inserting several edges treatment such as U-shape at each corner of the ground plane of antenna. In this scenario, we studied three types: first one, when U-edges are made of PEC, we get SAR reduction about 78.6%. Second one is a liquid type that is considered as more advanced type. For this type, two antennas are considered: a single band PIFA operating at 1.8 GHz, and a dual band PIFA operating at 900 MHz and 1.8 GHz. In this scenario, two cases were studied: first one when the U-edge is made of water, we noticed that the peak SAR value averaged over 10 g mass tissue was reduced to 73.52% in the case of single band PIFA, whereas the peak SAR was reduced to 88.78% and 90.31% in case of dual band. Second case, when U-edge filled with water, this enhanced structure was presented to overcome the manufacturing limitations of the first case design. Simulation results showed a better performance in terms of reflection coefficient and radiation pattern for both single-band and dual-band antennas. The results of SAR were also similar to the first case structure design for the single-band antenna. However, the SAR was slightly higher for the dual-band antenna, but it still remains very low (1.6 W/Kg at 900 MHz and 0.6 W/Kg at 1800 MHz). After that, for preserving the height of antenna, and making it more realistic to be applied, another type was done by inserting U-edges above each corner of the ground plane. In this case, we get SAR reduction as follows: 74.5% at GSM1800MHz in case of single band, and about 64.37%, 79.92%, and 54.71% at GSM900MHz, GSM1800MHz, and 2400 MHz in case of Tri-band averaged over 10g mass tissue.

On the other hand, this thesis presents a modern and unprecedented safety antenna that transmits from the base station to the mobile user being operated at the GSM-900 band. The main objective of this study is to provide a constant field strength or a uniform coverage over a certain surface area, for preventing human health from several hazardous biological effects, and this strongly depends on the studied site (e.g. if it is densely urban, rural, open area, etc.). Our proposed design is synthesized using S.A.R.A (Synthesis of Array of Antenna) software. Besides, Atoll GSM planning tool is used

to ensure the signal coverage and power strength for the safety antenna, and CST (Computer Simulation Technology) software for simulating the proposed antenna.